CONSTRUCTION OF A NEUTRON SPECTROMETER AND DETERMINATION OF BEAMPORT SPECTRA OF THE KANSAS STATE UNIVERSITY TRIGA MARK II NUCLEAR REACTOR

by

JAMES WARREN ROWLAND, JR.

B. S., Kansas State University, 1964

A MASTER'S THESIS

submitted in partial fulfillment of the

requirements for the degree

MASTER OF SCIENCE

Department of Nuclear Engineering

KANSAS STATE UNIVERSITY
Manhattan, Kansas

1967

Approved by:

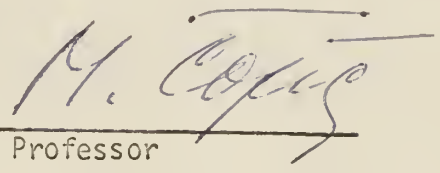

Major Professor

T
1967
P65
c 2
Document

TABLE OF CONTENTS

LIST OF TABLES

LIST OF FIGURES

NOMENCLATURE

A_1	Unshielded radiating area
A_2	Cadmium shielded radiating area
C(v)	Conversion factor between measured countrate and experimental neutron current
d	Interplanar spacing in crystal lattice
D	Empirical constant
E	Neutron energy
E_{ff}	Data channel detector efficiency
F	Structure factor for diffracting crystal
G	Geometric interception factor
h	Planck's constant
H	Empirical constant
j(v)	Neutron current as a function of velocity (n/sec)
k	Empirical constant
K_1	Empirical constant
K_2	Empirical constant
L	Length of collimator
m	Neutron mass
M_i	Monitor channel counts at position i
n	Integer signifying order of diffraction
N_c	Number of unit cells per unit volume of diffracting crystal
N_n	Nuclei per unit volume of absorber

$n_o(v)$	Observed countrate at any given setting of the detector
n_T	Attenuated neutron beam countrate
R	Cadmium cut-off correction factor
R^θ	Integrated reflectivity
R_m	Measured countrate from data channel
R_t	Resolving time of data channel counting system
S	Width of diffraction crystal
t	Thickness of neutron detecting medium
t_{cd}	Cadmium thickness of collimator slits
t_s	Absorber thickness
t_o	Thickness of diffracting crystal
v	Neutron velocity
v_c	Empirical constant
v_o	Most probable neutron velocity of the Maxwellian velocity distribution
W	Width of collimator opening
η	Mosaic spread
θ	Diffraction angle
$\Delta\theta$	Angular width of diffracted beam
$\delta\theta_T$	Total angular spread of neutron beam incident upon diffraction crystal
λ	Neutron wavelength
λ_c	Bragg cut-off wavelength
μ	Macroscopic absorption cross section for the diffraction crystal

σ	Microscopic total neutron cross section for absorber.
Σ_a	Macroscopic absorption cross section for neutron detecting medium
Σ_c	Macroscopic total neutron cross section for cadmium
τ_i	Time taken to obtain M_i monitor counts
FWHM	Full width half maximum

1.0 INTRODUCTION

Neutron diffraction was first demonstrated in 1936 using a paraffin moderated RaBe neutron source and magnesium oxide crystals. Because of the low source strength, no quantitative information was obtained. Neutron diffraction had to await the development of nuclear reactors and their high intensity thermal neutron beams before becoming a valuable research tool.

The first neutron spectrometer (1, 2) was constructed at Argonne National Laboratory in 1945. The range of this early machine was 0.04 eV to 65 eV. Since that time, the design of neutron spectrometers has undergone many changes. Many of the modern instruments have three axes. They are thus able to bombard a sample with a monochromatic neutron beam and then analyze the diffraction pattern obtained for any given energy. Some (3) of these instruments are also able to apply a magnetic field to the sample and to vary its temperature from near absolute zero to over 2000°C. Naturally, data is obtained completely automatically.

In the ensuing years since 1945, the lower energy limit (4) of the instrument has been decreased to around .00062 eV. This has been done through the use of special neutron filters to reduce higher order contamination of the incident beam and by the use of special crystals and liquid hydrogen moderating chambers.

Little success has been achieved in extending the upper limit, however. As the upper limit is approached, the resolution of the instrument greatly decreases and the diffracted beam intensity becomes very weak.

Generally, a neutron chopper is preferred for measurements of neutrons having energies in excess of 10 eV.

The neutron spectrometer has several advantages over its main competitor, the neutron chopper. The neutron spectrometer costs considerably less, is much easier to operate, requires less floor space, and is much less dangerous in operation.* The chopper, however, covers a much wider energy range although drastic changes in energy usually necessitate changing rotors. Also, the duty cycle of a chopper tends to be very low, thereby reducing the average intensity of the chopped neutron beam.

In the past several years, some of the best features of the chopper and the neutron spectrometer have been combined. A small chopper (5) is often introduced into the neutron beam prior to the diffraction crystal. The resolution of the chopper is purposely made very poor in order to provide a high duty cycle. Its function, then, is to provide a means of removing the faster neutrons from the diffracted beam in order to reduce its harmonic content. Sometimes, even two phased choppers are used for this purpose. When operated for this purpose, a chopper is usually referred to as a mechanical monochromator.

For certain types (7) of experiments, neutron diffraction methods are preferable to those of x-ray diffraction. The scattering cross sections for x-rays are proportional to the atomic number of the atom doing the scattering. Therefore, this cross section is low for the light elements such as hydrogen and carbon. Also, there is little variation between two atoms having nearly the same atomic number. Since neutrons are scattered

*It has been noted (6) that the energy stored in the spinning rotor of a fast chopper may be as high as 10^5 foot-pounds.

primarily from the nucleus, the neutron scattering cross section may vary considerably between different isotopes of the same element. Thus, neutron diffraction is an important tool in structure studies of materials containing either the very light elements, or of materials containing elements with very close atomic numbers.

The other type of experiment is the study of magnetic materials. Since the neutron has a magnetic moment, it is capable of providing information about the atomic changes that occur when materials are magnetized.

Of course the most obvious use for a neutron spectrometer is to determine the neutron spectrum emerging from the various experimental facilities at a nuclear reactor. One may then study the effect of changing the reactor core configurations upon the emergent neutron spectrum. This information may then be used to allow the neutron spectrum to be somewhat tailored to suit other types of experiments.

Another use of the neutron spectrometer is in the determination of neutron cross sections as a function of energy. For this type of measurement, a correlation is made between a spectrum taken with the sample in the diffracted beam and one taken without the sample.

The neutron spectrometer described later in this work was constructed with the possibility that it could be used as a piece of experimental apparatus in an undergraduate laboratory course at the senior level. The following theory has been written with this application in mind. In addition, complete instructions have been included to allow proper care and alignment of the instrument.

2.0 THEORY

2.1 Basic Concepts

A neutron spectrometer is the neutron analogue of the familiar x-ray spectrometer. Each instrument has a source of radiation, a diffracting crystal, and a detector. The main difference in the outward appearance of the two types of spectrometers is one of size. The common x-ray spectrometer may usually be placed upon a table three feet square and weighs less than 500 pounds (not counting the necessary electronic equipment). A typical neutron spectrometer may utilize a ten foot square and weigh many thousands of pounds. The important elements of a neutron spectrometer are shown in Figure 1.

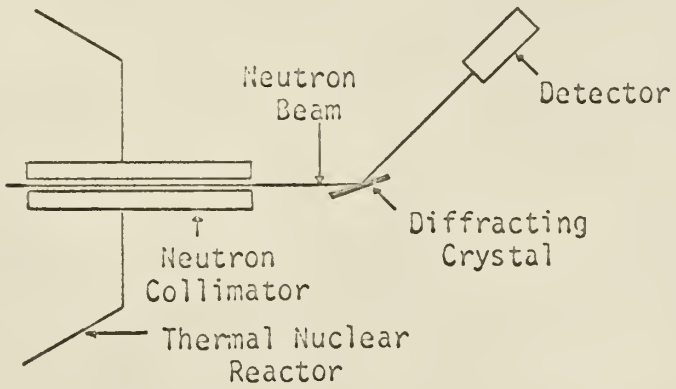

Fig. 1. Schematic diagram of a neutron spectrometer

Every portion of the system indicated in Fig. 1 which either comes in contact with or generates the neutron beam that emerges from the

collimator will have an effect upon all measurements taken with the system. In order to better understand the entire process, let us first look at the phenomena of neutron diffraction.

For nearly four decades it has been known that under appropriate circumstances behavior of the elementary nuclear particles could be predicted by assuming that they were associated with a wave having a wavelength

$$\lambda = \frac{h}{mv} \tag{1}$$

where λ is the particle wavelength,

h is Plank's constant,

m is the particle mass, and

v is the particle velocity.

From this point on, it will be assumed that equation 1 is a valid description of the neutron during the process of neutron diffraction.

Fig. 2 shows the relationship between the neutron velocity, wavelength, and kinetic energy, E, where the latter is given by equation 2,

$$E = 1/2\ mv^2. \tag{2}$$

It is instructive to observe the ranges of the various quantities plotted in Fig. 2. Neutrons having the energies indicated are found in great abundance within the core of thermal nuclear reactors. Furthermore, the corresponding wavelengths are within the order of magnitude of interplanar spacings of common crystals. Hence, suitable neutron sources and diffracting materials are available.

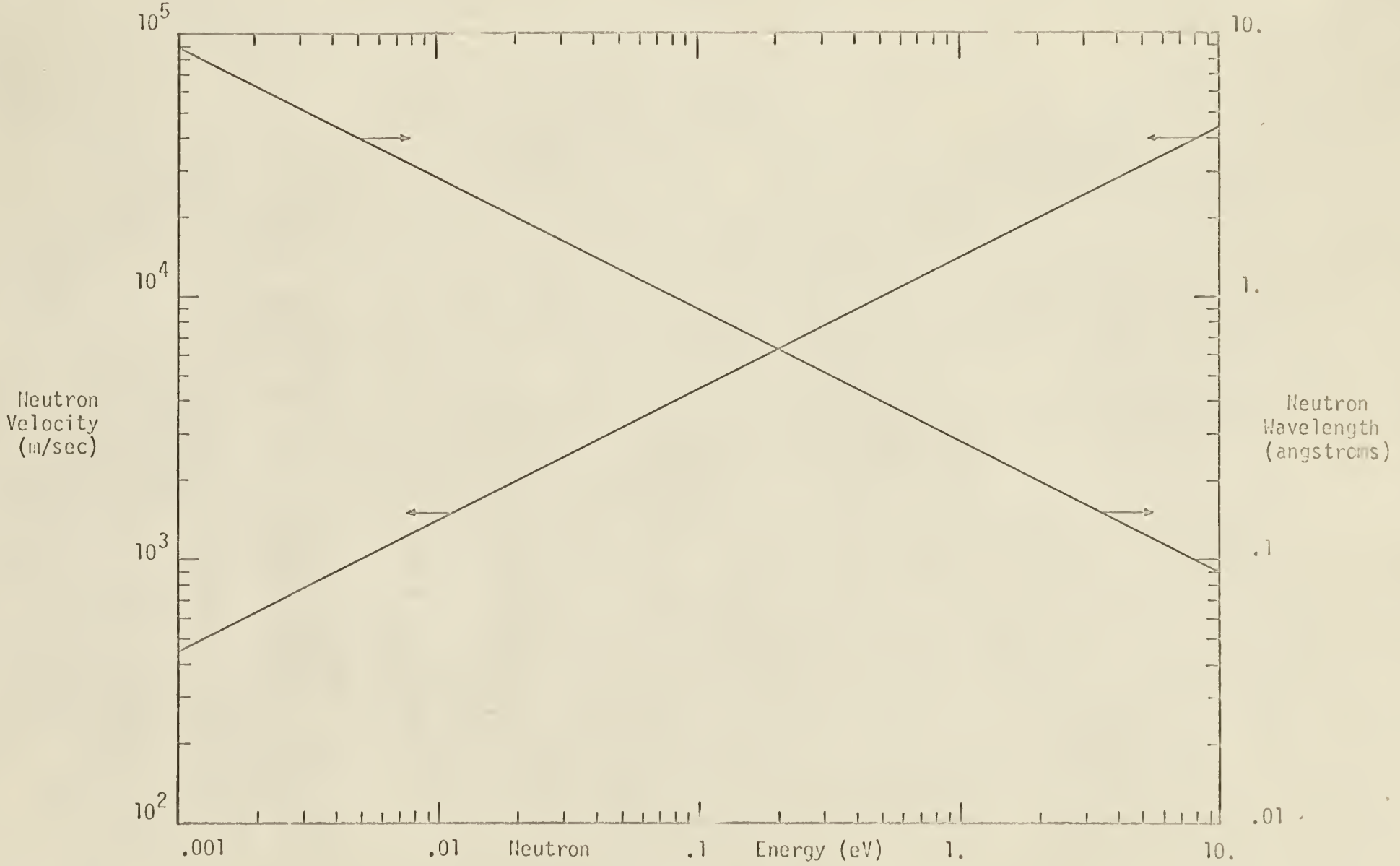

Fig. 2. Neutron velocity and wavelength vs. energy

2.2 Derivation of Bragg Law

Consider a perfect crystal (8) placed in a parallel beam of monochromatic neutrons. The angle between the crystal plane and the neutron beam will be designated θ. The interplanar spacing will be represented by d (see Fig. 3). Consider two parallel waves incident upon the crystal planes at angle θ. The condition necessary for con-

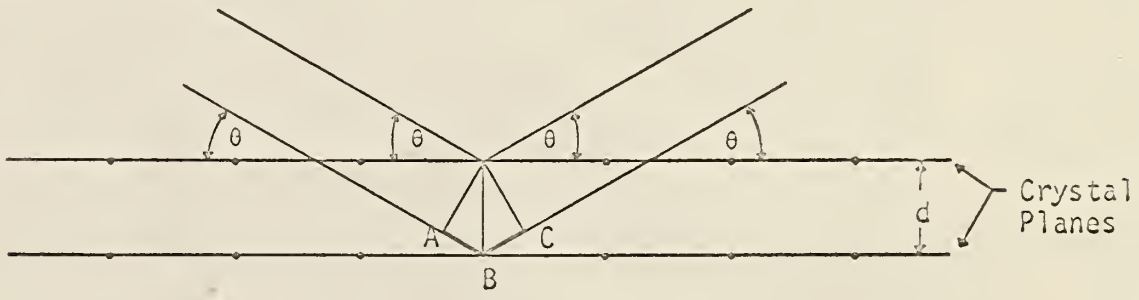

Fig. 3. Waves diffracted from crystal planes

structive interference to occur after diffraction is given by

$$n\lambda = \overline{AB} + \overline{BC} \qquad (3)$$

where n is an integer (1,2,3,...,n). From geometrical considerations (Fig. 3), it is seen that

$$\overline{AB} = \overline{BC} = d \sin\theta. \qquad (4)$$

Substituting equation 4 into equation 3, the familiar Bragg diffraction law, equation 5, is obtained:

$$n\lambda = 2d \sin\theta. \qquad (5)$$

Scattering which obeys equation 5 is termed "Bragg scattering".

2.3 Results of Different Types of Scattering

At this point, mention should be made of the various types of scattering which will be of interest. All of the available information about the spectrum will be obtained from the coherent elastic scattering. Unfortunately, incoherent elastic scattering and inelastic scattering will also occur. For incoherent elastic scattering, it is well known that small angle scattering is much more probable than large angle scattering. On the other hand, inelastic scattering is nearly isotropic for neutrons having an energy around one eV or below. In this energy range, most of the commonly used diffraction crystals have a relatively low absorption cross section. Thus, the intensity of this component of the background will be roughly proportional to the volume of the crystal which is intercepted by the neutron beam. Naturally, this volume will increase as the diffraction angle decreases up to the point where the entire crystal is in the neutron beam. From this point on, absorption may cause a slight decrease.

As a result of these two effects, one may expect the background to be a function both of angle and of the incident neutron spectrum. For large diffraction angles, the background should be relatively constant. For small diffraction angles, however, the background may be expected to exhibit a strong angular dependence.

One further comment should be made about coherent elastic scattering. In this type of interaction, the neutron is interacting with an atom which is tightly bound in a crystal lattice. Therefore, the neutron effectively interacts with the entire crystal. As a result of the mass ratio between the crystal and the neutron, the neutron loses virtually no energy in the process of diffraction.

2.4 Collimator Effects on Resolution

The assumption of a monoenergetic parallel beam of neutrons, used in deriving equation 5, is not really justified in neutron diffraction work. Instead, the neutron beam is usually collimated to a divergence of somewhat less than one degree. Also, the velocity distribution of a thermal neutron emergent from a nuclear reactor is typically (9, 10) described by a modified Maxwellian distribution function joined to a 1/E tail.

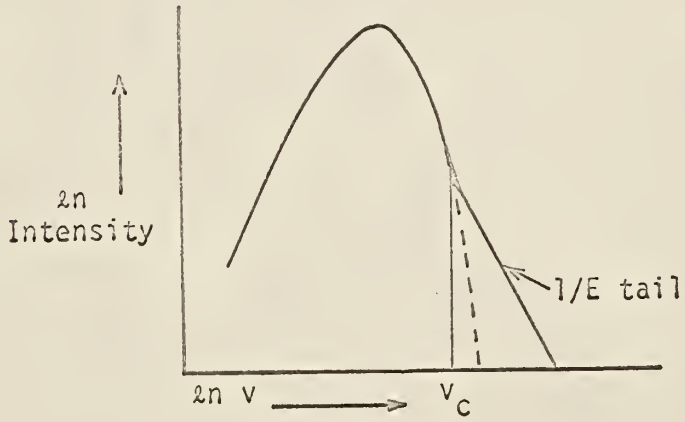

Fig. 4. Typical thermal leakage spectrum from a nuclear reactor

Since measurements will be taken of a leakage spectrum, the neutron current density, $j(v)$, in the emergent beam may be represented by

$$j(v) = \begin{cases} K_1 v^3 e^{-v^2/v_o^2} & \text{for } v<v_c \\ K_2 v^{-1} & \text{for } v>v_c \end{cases} \tag{6}$$

where K_1 and K_2 are constants, v_o is the most probable neutron velocity (in the sense of a Maxwellian distribution), and v_c is the point at which the two functions are joined to best fit the experimental data.

To make a correction for the finite divergence of the incident neutron beam, consider Fig. 5. Neutrons from a point source, P, may strike the

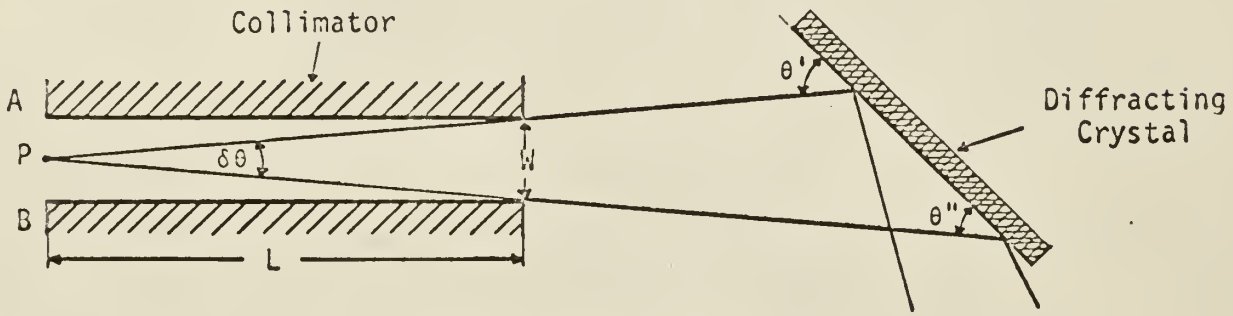

Fig. 5. Effect of finite divergence of incident neutron beam

crystal surface at any angle between θ' and θ''. If $L>>W$, then

$$\delta\theta = (\theta' - \theta'') = W/L. \tag{7}$$

However, the actual neutron source at the entrance to the collimator is better described as a plane source. The total spread, $\delta\theta_T$, of the inci-

dent angle of the neutron beam upon the crystal is then given by

$$\delta\theta_T = \frac{2W}{L} . \tag{8}$$

This may easily be seen by following point P as it travels from point A to point B across the end of the collimator.

To convert equation 8 to a more suitable form, differentiate equation 5 to obtain

$$n\delta\lambda = 2d \cos\theta \, \delta\theta . \tag{9}$$

Equation 10 is then obtained by substituting equation 8 into equation 9:

$$\delta\lambda = \frac{4dW}{nL} \cos\theta . \tag{10}$$

Since most of the work done in this paper is in terms of velocity or energy, equation 1 is differentiated and substituted into equation 10 with the following result:

$$\delta v = \frac{4dWmv^2}{nhL} \cos\theta . \tag{11}$$

Equation 11 yields the velocity spread introduced into the diffracted beam by the finite divergence of the incident neutron beam. It should be noticed that the velocity spread in equation 11 is not constant but, indeed, depends upon the angle of diffraction.

2.5 Crystal Effects

2.5.1 Mosaic Spread

The next element of the system to be considered is the diffraction

crystal. In the derivation of equation 5, a perfect crystal was assumed. Unfortunately, all large single crystals are composed of a large number of small perfect crystals. These are usually termed crystallites. Naturally, to produce a large single crystal, these crystallites must have their corresponding crystal planes highly oriented. The degree of their orientation is usually considered (11) in the following manner. Erect a line perpendicular to a given crystal plane in each crystallite and find the deviation of each of these normals from the average normal. Plot this deviation against its frequency of occurrence. A roughly Gaussian curve is thereby obtained. The FWHM of this curve is given the name "mosaic spread". As a result of this type of crystalline structure, diffraction will occur over a narrow band of angles, even with a perfectly parallel monochromatic incident neutron beam. This allows a curve of the diffracted beam intensity versus diffraction angle to be obtained. The area underneath this curve is designated the "integrated reflectivity". It is a measure of the number of neutrons having a given energy which are diffracted from the crystal. Bacon (12) gives the following relation for the integrated reflectivity, R^{θ}:

$$R^{\theta} = \int_{-\infty}^{\infty} \frac{a\,d\Delta}{(1+a) + (1+2a)^{1/2} \coth A(1+2a)^{1/2}}, \qquad (12)$$

where $A \equiv \mu t_o / \sin\theta$,

$$a \equiv \frac{Qe^{-\Delta^2/2\eta^2}}{\mu\eta\sqrt{2\pi}},$$

$Q \equiv \lambda^3 N_c^2 F^2 / \sin 2\theta$,

μ is the macroscopic absorption cross section for the crystal,

t_o is the crystal thickness,

F is the structure factor of the unit cell,

N_c is the number of unit cells per unit volume, and

η is the mosaic spread of the crystal.

This equation is valid for the reflection case of an imperfect crystal having finite absorption. In order to evaluate equation 12 numerically, the following transformations have been made: let

$$U = \frac{\Delta}{\eta\sqrt{2}}$$

$$G_s = A(1+2a)^{1/2}$$

$$V = \frac{\Omega}{\mu\eta\sqrt{2\pi}},$$

then equation 12 becomes

$$R^{\theta} = 2\sqrt{2}\eta \int_0^{+\infty} \frac{Ve^{-u^2}\,du}{(1+Ve^{-u^2}) + (1+2Ve^{-u^2})^{1/2}\coth G_s}. \qquad (13)$$

Let

$$T = 1+2Ve^{-u^2},$$

then by rearrangement,

$$U = 1/2\ \ln\left(\frac{2V}{T-1}\right).$$

Equation 13 then becomes

$$R^{\theta} = \frac{-\sqrt{2}\eta}{2} \int_{1+2V}^{1} \frac{dT}{\{1/2\ \ln(\frac{2V}{T-1})\}\{(\frac{T+1}{2})\} + T^{1/2}\coth G_s}. \qquad (14)$$

But, $G = AT^{1/2}$, leaving

$$R^{\theta} = 2\sqrt{2}\, n \int_{1}^{1+2V} \frac{(e^{2AT^{1/2}} - 1)\, dT}{(T+1)\,(e^{2AT^{1/2}} - 1)\, \ell n(\frac{2V}{T-1}) + 4T^{1/2}\,(e^{2AT^{1/2}} + 1)}. \quad (15)$$

With benefit of hindsight, the following relation will be stated:

$$\frac{R^{\theta}}{\sin\theta} = f(\theta), \quad (16)$$

where

$$f(\theta) = D + H\theta^{k} \quad (16a)$$

and D, H, and k are empirically determined constants.

In the preceding discussions, it has been shown that the diffracted neutron beam will not be monoenergetic, but will instead consist of a range of energies, δE, about some E. The practical result of all of this will be to raise the diffracted beam intensity, but to reduce the beam purity.

It has been mentioned previously that the intensity and the divergence of the diffracted beam will depend upon two things. These are the mosaic spread of the diffracting crystal and the divergence of the incident neutron beam. Egelstaff (13) gives the following equation for the angular width of a diffracted beam:

$$\Delta\theta = \left[\eta^2 + \frac{1}{2}\,\delta\theta_T^2\right]^{1/2}. \quad (17)$$

He also suggests that for a diffracted beam of given divergence, the maximum intensity may be obtained by adjusting the collimation of the neutron

beam until its total angular spread, $\delta\theta_T$, matches the mosaic spread of the crystal.

2.5.2 Beam Interception

The last important characteristic of the crystal interaction is entirely one of geometry. As a result of the dimensions of the incident beam and the diffraction crystal, it is likely that for small angles of incidence, the crystal will not intercept the entire beam. Therefore, a geometric interception factor, G, will be defined as follows:

$$G = \begin{cases} 1 \text{ if } \sin\theta \geq W/S \\ \left(\frac{S \sin\theta}{W}\right) \text{ if } \sin\theta \leq W/S, \end{cases} \tag{18}$$

where S is the width of the diffraction crystal.

2.6 Neutron Detector

The final element of the system to be considered is the neutron detector. The most common detector used in this work is a large, high pressure BF_3 probe. Its efficiency, E_{ff}, may be rather easily calculated (14) by assuming that if a neutron is absorbed in the detecting medium, a signal will be obtained. The resulting equation is simply

$$E_{ff} = 1 - \exp(-\Sigma_a t), \tag{19}$$

where Σ_a is the macroscopic absorption cross section of the detecting medium and t is the thickness of the detecting medium through which the neutrons may pass.

2.7 Theoretical Correction Factor

Now that all of the correction factors have been determined, we are able to calculate a theoretical correction factor, C(v), for a neutron spectrometer where C(v) is defined by equation 20:

$$j(v) = C(v)\, n_o(v), \tag{20}$$

where $n_o(v)$ is the observed countrate at any given setting of the instrument, and j(v) is the corresponding experimental neutron current. C(v) is given by the proper combination of equations 11, 16, 18, and 19. Thus, we have

$$C(v) = \frac{nL}{2\, Wv\, \cos\theta}\, f(\theta)\, G(1 - e^{-\Sigma_a t}) \tag{21}$$

2.8 Cross Section Determination

The determination of a neutron cross section is, in theory, a relatively simple matter. When a sample is placed in a neutron beam, (15,16) the new beam intensity, n_T, is given by

$$n_T = n_o e^{-N_n \sigma t_s}, \tag{22}$$

where n_o is the unattenuated countrate, N_n is the number of nuclei per unit volume of the sample, σ is the microscopic neutron cross section, and t_s is the thickness of the sample. Equation 22 may be written in the somewhat more convenient form

$$\sigma = \frac{1}{N_n t_s} \ell n\left(\frac{n_o}{n_T}\right) . \tag{23}$$

Thus, the velocity dependence of σ may be readily determined. Naturally, the particular cross section measured depends upon the geometry of the experiment. Typically, the total cross section will be measured in a "good geometry" experiment.

With the exception of specially prepared specimens, most crystalline materials consist of a great number of randomly oriented microcrystals. If a suitable sample is placed in a collimated neutron beam having a continuous spectrum, diffraction may occur from each microcrystal according to equation 5. Equation 5, however, predicts a maximum wavelength, which may be scattered for any given set of crystal planes. Under the limiting conditions of maximum wavelength, equation 5 becomes

$$\lambda_c = 2d \tag{24}$$

and is sometimes known as the Bragg cutoff formula.

Thus, it is apparent that neutrons having a shorter wavelength than given in equation 24 will undergo more scattering than those having longer wavelengths. Hence, one expects a sharp change in the scattering cross section at certain energies. This effect is very pronounced in a number of materials, as is shown in Fig. 6.

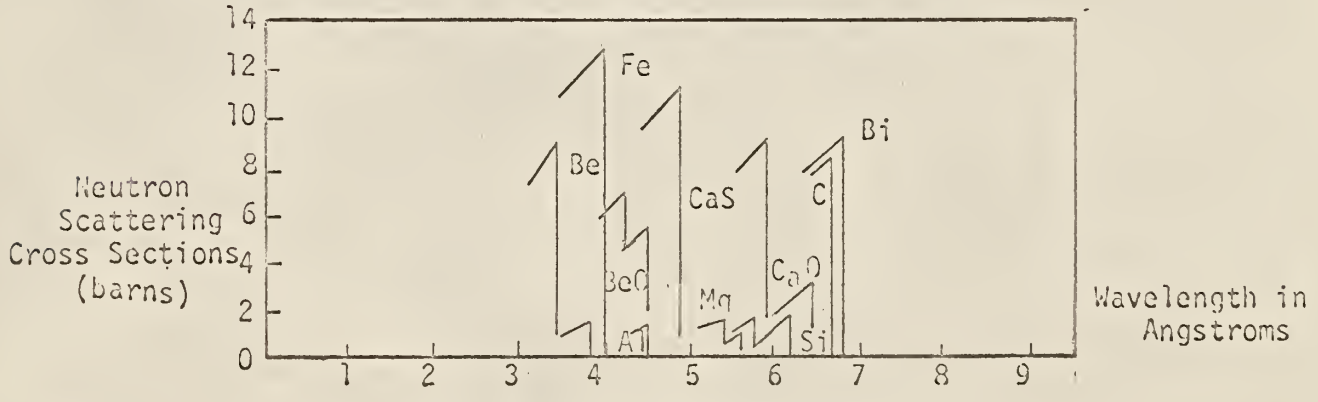

Fig. 6. Bragg cutoff wavelengths of different materials (17)

3.0 EXPERIMENTAL

3.1 Description of the Reactor

The Kansas State University TRIGA Mark II (KSUTMII) nuclear reactor is a light water cooled, graphite reflected reactor. The fuel consists of a uranium-zirconium hydride alloy with a 20% enrichment in U-235. Because of the nature of the hydrogen bonding in the fuel, nearly all of the moderation for neutron energies below .13 eV occurs in the cooling water surrounding the fuel elements. Above that energy, moderation may take place in either the fuel or the cooling water. At the present time, the maximum licensed power level is 100 kw. The varied experimental facilities are indicated in Fig. 7. They include four beamports which are designated by the direction in which they face, i.e., S.E., N.E., N.W., and S.W.

The S.E. beamport looks at the graphite reflector tangentially to the reactor core. Therefore, all neutrons and core gammas emergent from this port must have been scattered at least once. After this first scattering, most of them must still pass through a large thickness of graphite before entering the beam tube. Thus, this port is used for experiments requiring a well-moderated beam of neutrons and a high neutron to gamma ratio.

The N.E. beamport looks directly at the outside of the reactor core through a hole in the graphite reflector. This port, then, will yield a relatively high flux of epithermal and fast neutrons together with a high gamma dose rate.

The N.W. and S.W. ports are identical except for their location. Like

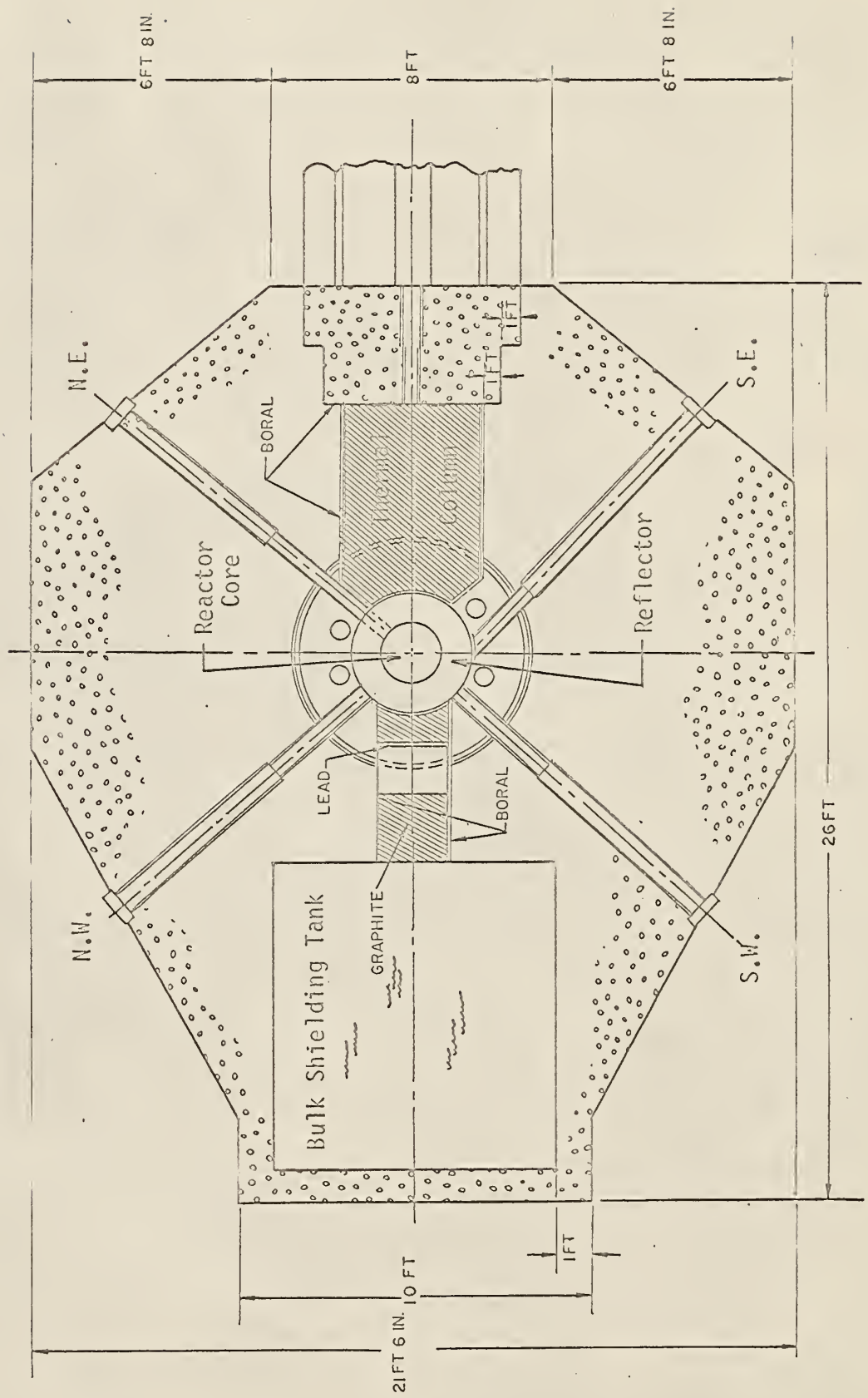

Fig. 7. Experimental facilities of the KSUTMII nuclear reactor

the N.E. port, they look radially at the outside of the reflector. However, they are not aligned with any hole in the reflector. Therefore, all neutrons emerging from these ports must have passed through at least 12 inches of graphite.

Table I gives the best available estimate of the relative neutron fluxes and gamma dose rates at selected points in the reactor.

Table I. Radiation Fields at Selected Points in Reactor for 100 kw Power Level (18)

Position	Neutron (n/cm^2-sec)		Gamma (rads/sec)
	Fast (>10 KeV)	Thermal (<.21 eV)	
N.E. port next to core	8.0×10^{11}	8.0×10^{11}	4.0×10^{3}
Reactor pool outside reflector	2.7×10^{10}	2.7×10^{11}	1.8×10^{2}

All of the beam tubes terminate at the outer edge of the reflector. Because of manufacturing and constructional tolerances, there is approximately 1/2 inch clearance between the ends of the beam tubes and the outer surface of the reflector. The space in between these two surfaces is filled with aluminum shims which are curved on one side to match the curvature of the reflector housing. Because the reflector is canned in 1/2 inch thick aluminum and the ends of the beam tubes are about 5/32 inch thick, neutrons must penetrate a substantial amount of aluminum before they enter the beam tube. Since the mean free path for thermal neutrons in aluminum is about two inches, one may expect

a certain perturbation in the thermal neutron spectrum corresponding to the variation in the aluminum cross section. The exact magnitude of the perturbation is, however, very difficult to predict.

Fig. 8 shows the standard fuel loading. This particular loading is designated number 6. Note that there are four fuel elements in the F ring. These fuel elements may be placed in any convenient location in this ring. Also, up to six of the graphite reflector elements may be removed and still maintain enough reactivity to attain a power level of 100 kw, provided that no extraneous poisons are inserted into the core. Figures 9, 10, and 11 show fuel loadings which have been modified to achieve certain desired results. All comparisons made in the following descriptions of the modified fuel loadings will be with respect to the standard fuel loading.

In Fig. 9, the four fuel elements in the F ring have been placed in a position close to the tangential port in order to increase the neutron flux from this port. This loading is designated 6'.*

Fig. 10 indicates a fuel loading, 6" which will increase the fast and epithermal neutron fluxes from the N.E. port. Note that this loading permits a minimum of water between the fuel and the reflector housing. This is very important because of the moderating properties of water.

Fig. 11 indicates a fuel loading, 6"', which will increase the thermalization of the neutron beam from the N.E. port. Note that the essential change is that the graphite reflector elements have been replaced by a much more effective moderator, water.

---

*The designation given to the different fuel loadings is that given by the reactor supervisor and entered into the reactor log book.

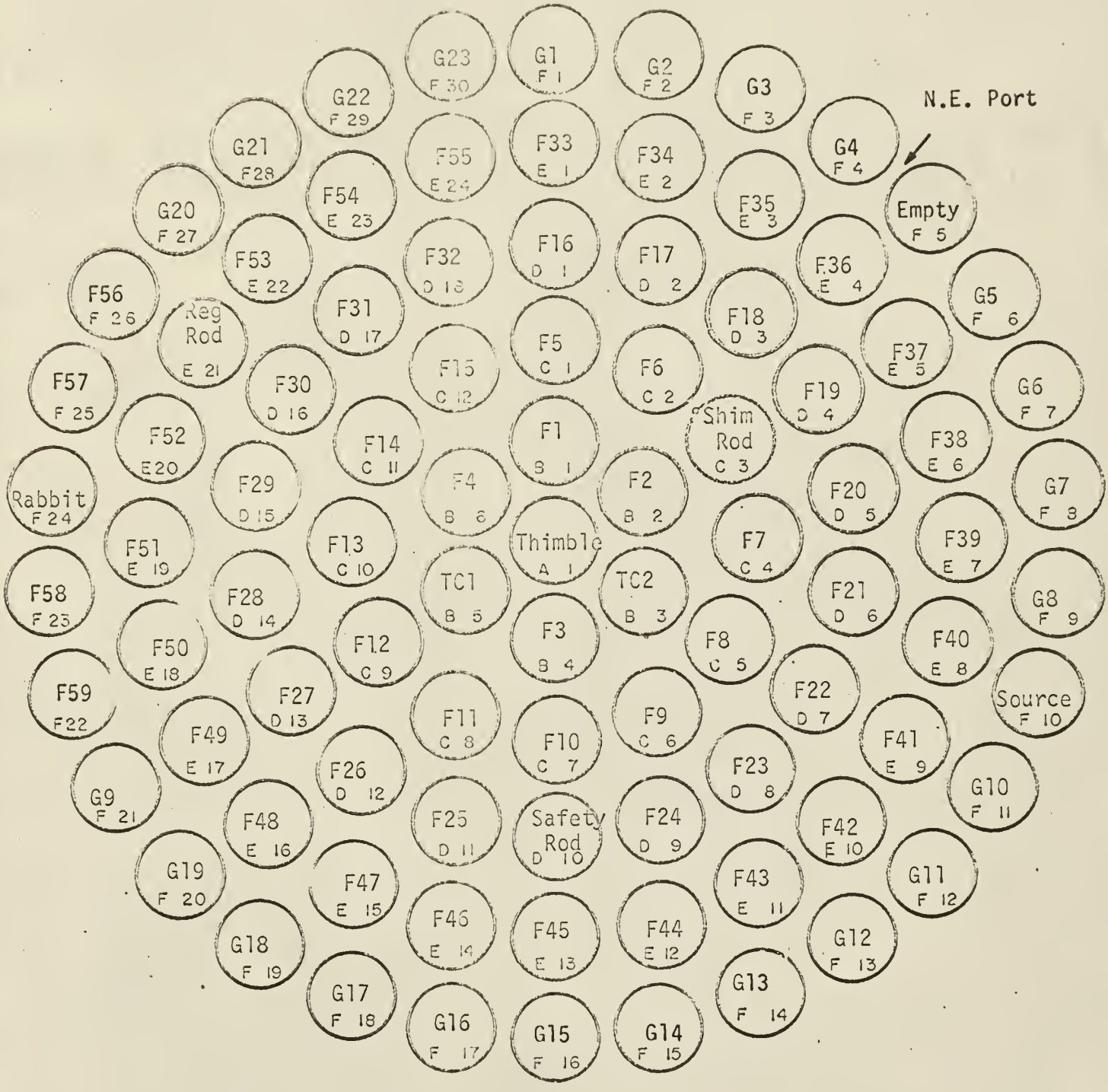

Core Loading Diagram

F Fuel Element
TC Instrumented Fuel Element
G Graphite Reflector Element

Fig. 8. 6 core load

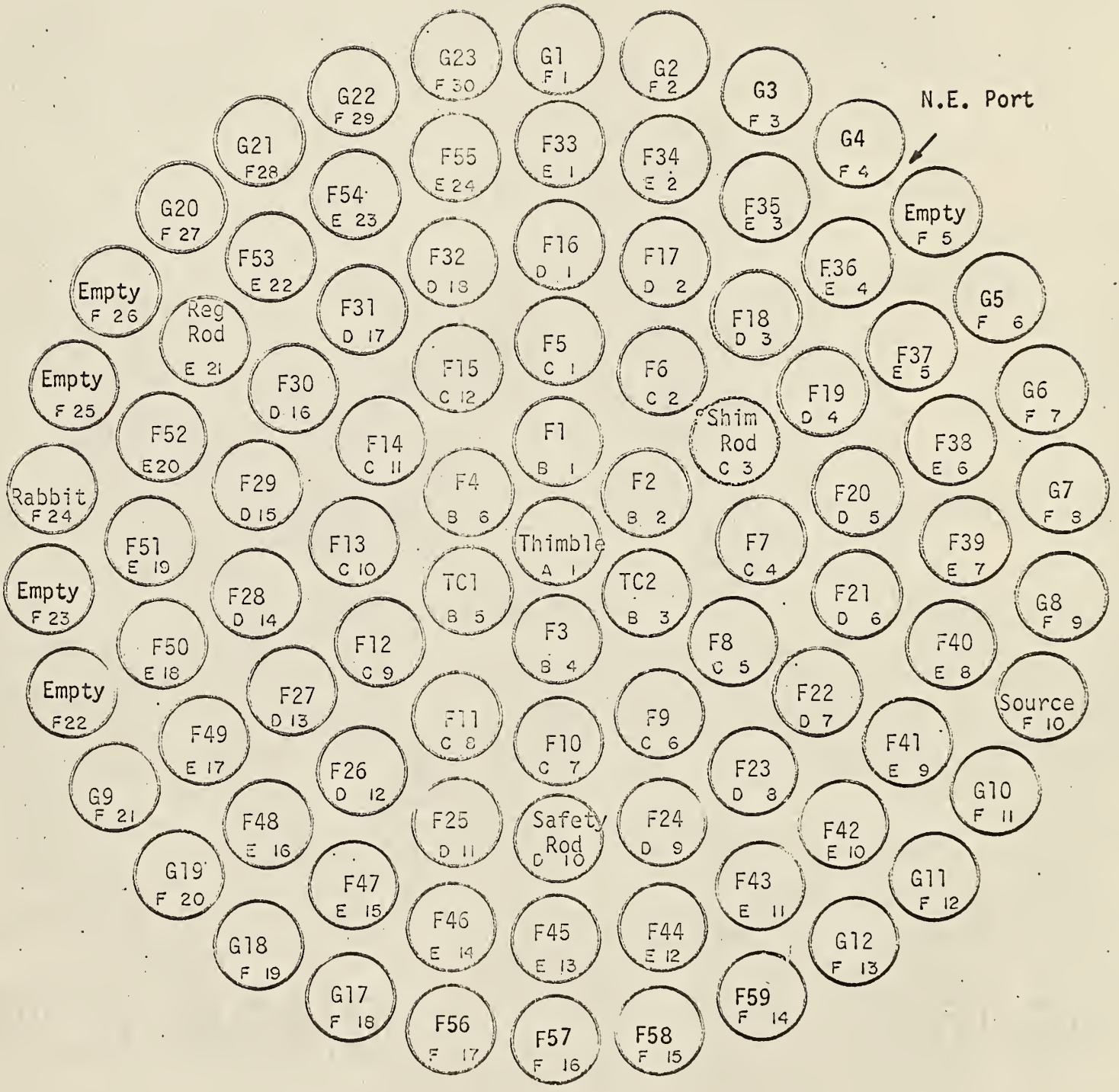

Core Loading Diagram

F Fuel Element
TC Instrumented Fuel Element
G Graphite Reflector Element

Fig. 9. 6' core load

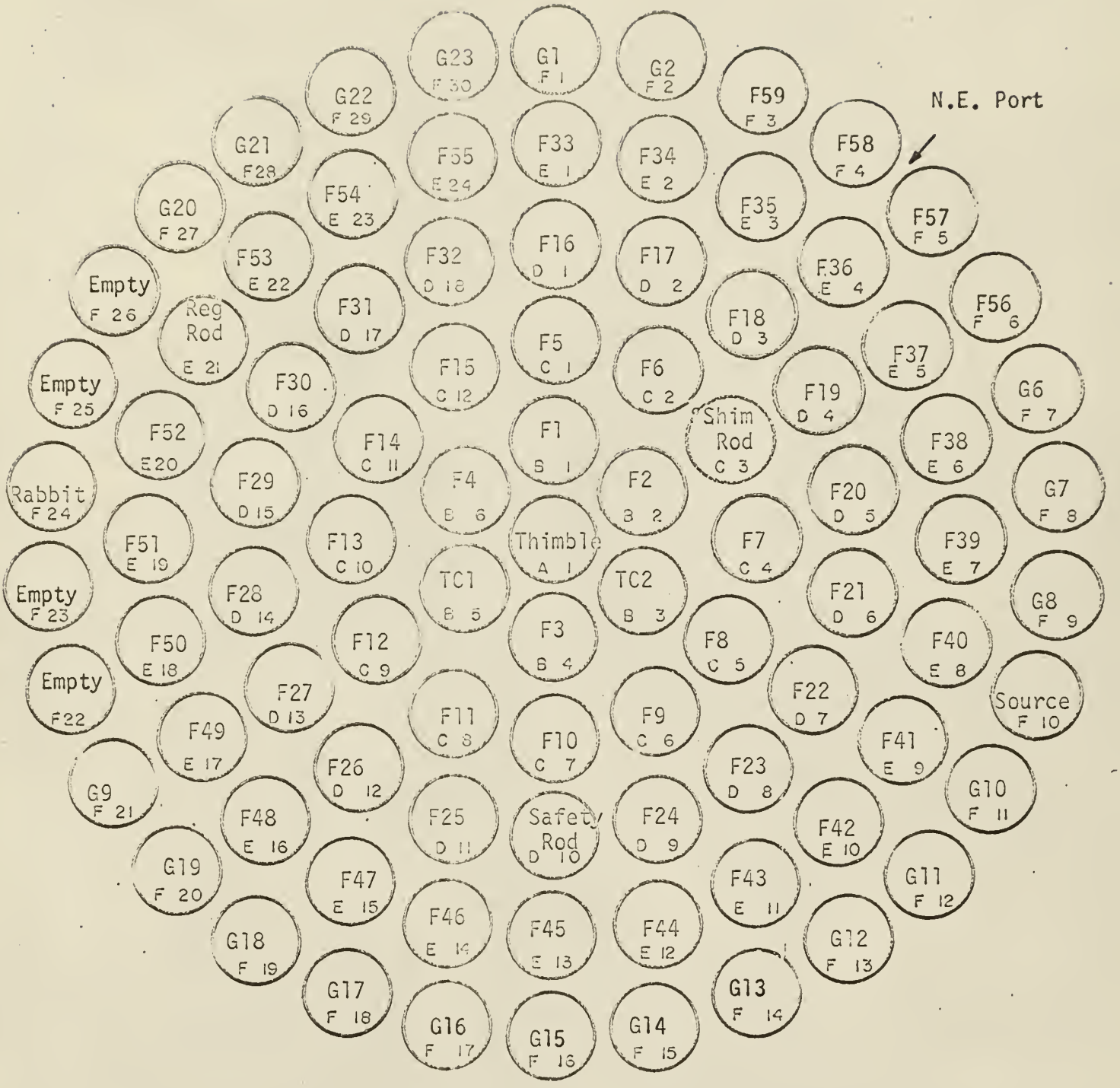

Core Loading Diagram

F Fuel Element
TC Instrumented Fuel Element
G Graphite Reflector Element

Fig. 10. 6" core load.

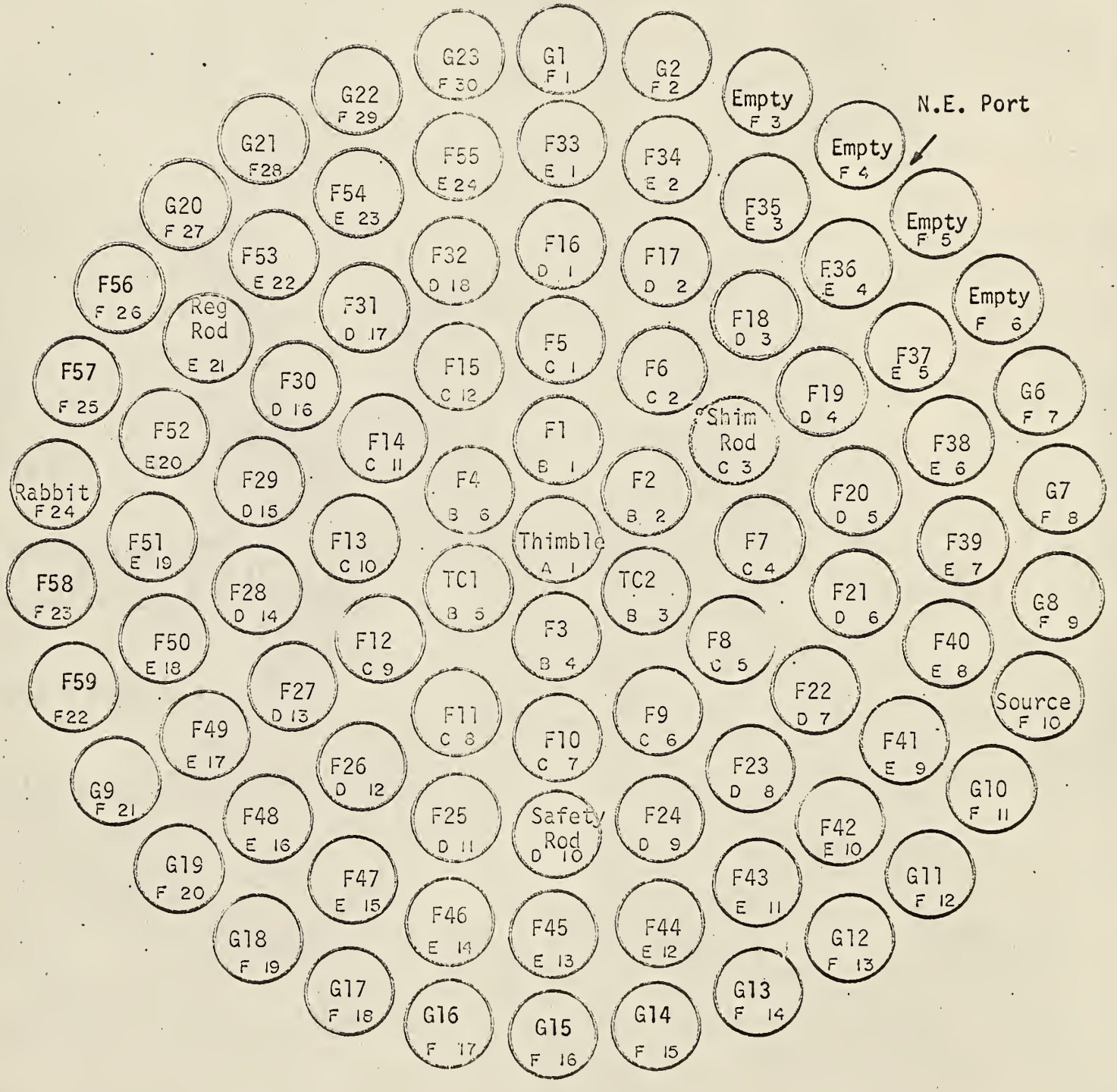

Core Loading Diagram

F Fuel Element
TC Instrumented Fuel Element
G Graphite Reflector Element

Fig. 11. 6"' core load

3.2 Description of the Collimator

The radiation beam emergent from a completely open beam tube is much too hazardous and unwieldy for most experiments. As a result, collimators are used to reduce the radiation beam to more manageable dimensions and to provide a means of reducing its angular divergence. The collimator must therefore fill the beam tube for a distance of several feet. The only opening* will be a suitably sized hole through which a radiation beam of the desired cross section is allowed to pass. Because of the sizable gamma and fast neutron dose rates present near reactor cores, most collimators contain sizable quantities of lead, steel and concrete. As a result, the typical collimator is a rather large, heavy device.

Since no collimator was available for the KSUTMII, one had to be constructed. The design requirements were as follows:

1. The collimator must fit in all four beam tubes and allow the safety shutter to be completely closed and the outer door to be sealed and locked,
2. Shielding plugs must be provided so that the reactor may be run at 100 kw with the collimator in any beam tube and still not produce a radiation hazard when the collimator is not in use,

---

*Other openings for instrumentation, etc., are sometimes present, but they are usually stepped in some manner to avoid a radiation hazard.

3. The collimator must provide good collimation for fast neutrons, thermal neutrons, and gamma rays,
4. The collimator must not present a storage problem because of neutron activation of materials having long half lives,
5. The collimator must provide an air seal when in place so as to prevent hazardous quantities of radioactive gases from venting from the beam tube into the reactor bay, and
6. The collimator must be constructed from inexpensive and available materials so far as possible.

In order to determine a size for the proposed collimator, it was first necessary to check the dimensions of all beamports. The diameters were found in an appropriate publication (19), but no reference could be found which gave the linear dimensions. Thus, all of the beam tube plugs had to be removed and the beam tubes measured.*

The internal dimensions of the hole through the collimator were set by the size of the diffraction crystal and the size of the available lining tube.

At that time, the maximum power level for which experimental dose rate measurements from an open beamport were available was three watts. Thus, a series of measurements* was prepared for different power levels at the S.E., N.E., and N.W. ports. The N.W. port was chosen in preference to the S.W. port because of the arrangement of equipment within the reactor bay. After these data had been evaluated and more confidence gained in the measuring techniques, the N.E. port was completely opened and the reactor was

---

*See Appendix A for a summary of these measurements.

operated at higher power levels to determine the magnitude* of the scattered radiation at various points around the reactor bay.

The aforementioned series of measurements yielded enough data to enable the collimator to be designed and constructed. Fig. 12 shows the internal construction of the collimator while Fig. 13 is a photograph of the actual collimator and its associated equipment.

To simplify geometrical considerations, it was decided to construct the collimator to produce a radiation beam having a rectangular cross section. A suitable tube and sizable quantities of lead and polyethylene were obtained from government surplus. Simple calculations indicated that nearly 10 inches of lead would be required to reduce core gammas and capture gammas to the desired dose rate. The lead was cast into five two-inch discs in order to better distribute the weight and to conform to the "removal cross section" concept. The lead discs were separated by borated paraffin which was cast in place.

Cadmium and polyethylene discs were placed on the inside end of the collimator to thermalize intermediate and some fast neutrons and to prevent the thermal neutrons from activating the impurities in the lead. Although these impurities may become highly radioactive** under neutron bombardment, they appear to be nearly pure beta emitters with a fairly short half life. Because of the low neutron flux in which the collimator is placed and the amount of self-shielding provided in the collimator design, it was decided

---

*See Appendix A for a summary of these measurements.

**See Appendix B.

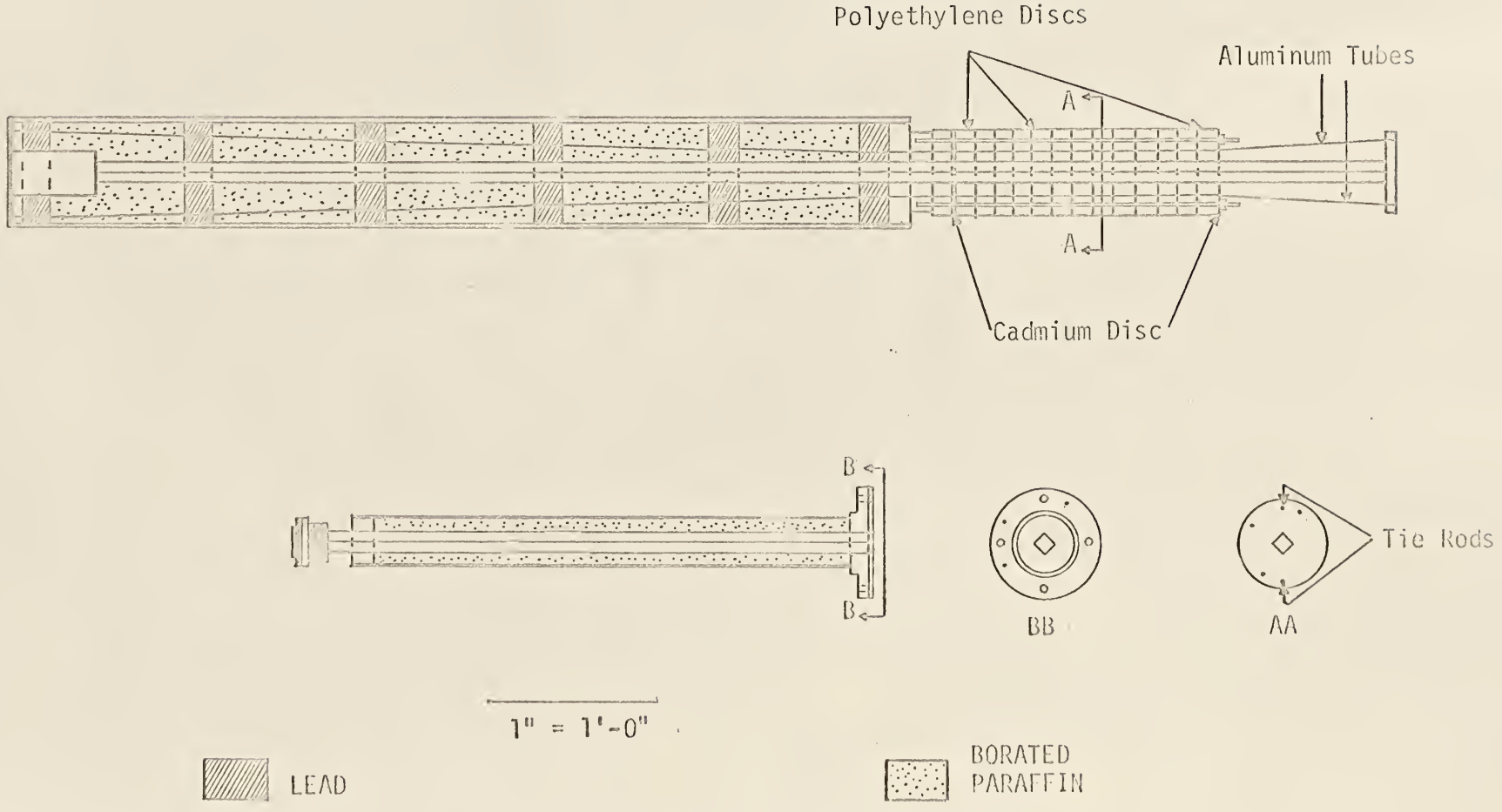

Fig. 12. Internal construction of the collimator

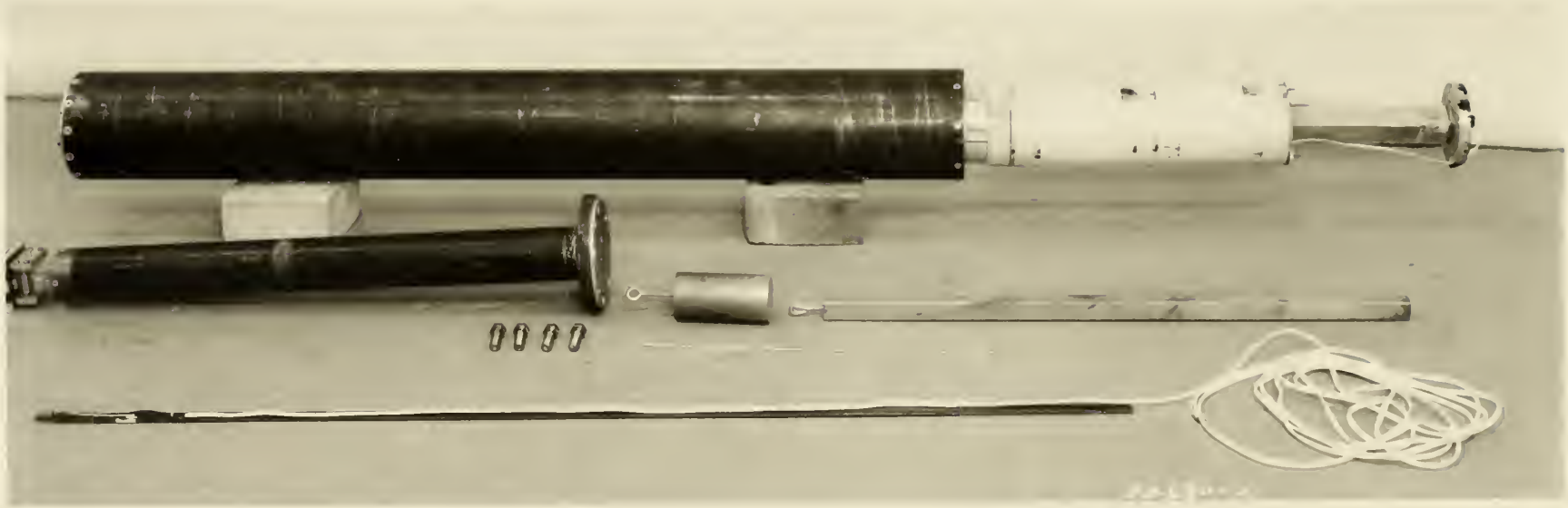

Fig. 13. Collimator and associated equipment

that these impurities would cause no storage problems. Also, an additional amount of boric acid was placed against each face of the lead discs during construction of the collimator as an added precaution.

As is obvious from Figures 12 and 13, the collimator consists of two major parts. The larger part fits into the beam tube and may contain the shielding plugs. The smaller part is an extension to provide better collimation for thermal neutrons. It also serves as a handle with which to insert and to extract the collimator from the beam tubes. When this extension (snout) is removed, the beam port safety shutter and outer door may be completely closed with the main body of the collimator remaining in the beam tube. The shielding plugs fit tightly enough to serve the same purpose if the snout is removed.

One special precaution should be observed when moving the collimator. The square tube along the longitudinal axis of the collimator is a magnesium-aluminum alloy. All welded joints along this piece are fragile and should be bumped as little as possible. Special care should be taken when inserting the collimator into a beam tube.

Three tubes were run through the length of the collimator to allow future expansion. They may be used for such things as instrumentation cables and refrigerants.

3.3 Description of the Neutron Spectrometer

To insure adequate counting statistics, the cross-sectional area of the neutron beam being diffracted is fairly large, typically on the order

of a few square inches. In order for the detector to intercept the diffracted beam, it usually has a cross section of at least the same dimensions. Since BF_3 detectors are generally used because of their ease of operation and their excellent gamma rejection, the detector must be nearly 20 inches long in order to achieve the desired efficiency for end-on counting. Because of its large size, the detector must be efficiently shielded to eliminate any room scattering contributions to the background. This shield, then, will weigh several hundred pounds.

To obtain good angular resolution with such a large neutron beam, the detector is often placed some distance from the diffracting crystal. Thus, a good neutron spectrometer must be capable of accurately supporting a long arm with a heavy weight on the far end. This is the reason for the large size of such instruments.

The design of the KSU neutron spectrometer was determined by the following considerations:

1. Available neutron flux at the exit of the collimator,
2. Cost,
3. Usable at the S.E., N.E., and N.W. beam ports,
4. Accuracy,
5. Ease of operation,
6. Energy range covered and purity of the diffracted beam, and
7. Further possibility of expansion of the capabilities of the instrument.

Preliminary measurements of the neutron flux emergent from the beamport collimator at the S.E. port yielded a value for the neutron flux at the position of the detector of 10 n/cm^2-sec/watt. It was thus concluded that

a neutron spectrometer could be constructed which could give meaningful measurements.

Exclusive of labor costs, the neutron spectrometer and the collimator were constructed for approximately $1500. Much use was made of surplus material, but such things as precision gears and diffracting crystals had to be obtained through normal commercial channels.

The maximum length of the detector arm was determined by the space between the reactor shielding and the shielding wall for the neutron generator located near the N.E. beam port. This is a distance of 12 feet. The height of the diffracting crystal was determined by the distance of the center of the beam ports above the reactor bay floor. This was a major design consideration as the distance is only 36 inches.

Accuracy proved to be the major problem. Although the detector could be positioned within 1/20 of a degree of the desired setting, reproducible results could not be obtained. Early measurements indicated that movement of the arm produced enough internal strain to tilt the crystal. The main support ring was investigated and found to have a saddle-shaped surface. This surface was then finished to a tolerance of ±.002". The main bearings and the gearbox mountings were redesigned. These steps helped to correct the problems but did not entirely eliminate them. At this time a more sensitive optical method of checking the internal alignment was devised.

An optical level was placed about 15 feet from the crystal holder. A small light bulb was fastened on the outside end of the detector shield and a front-surfaced mirror placed in the crystal mounting. The crystal table was rotated until the light was observed to be centered on the cross hair

Fig. 14. Side view of neutron spectrometer

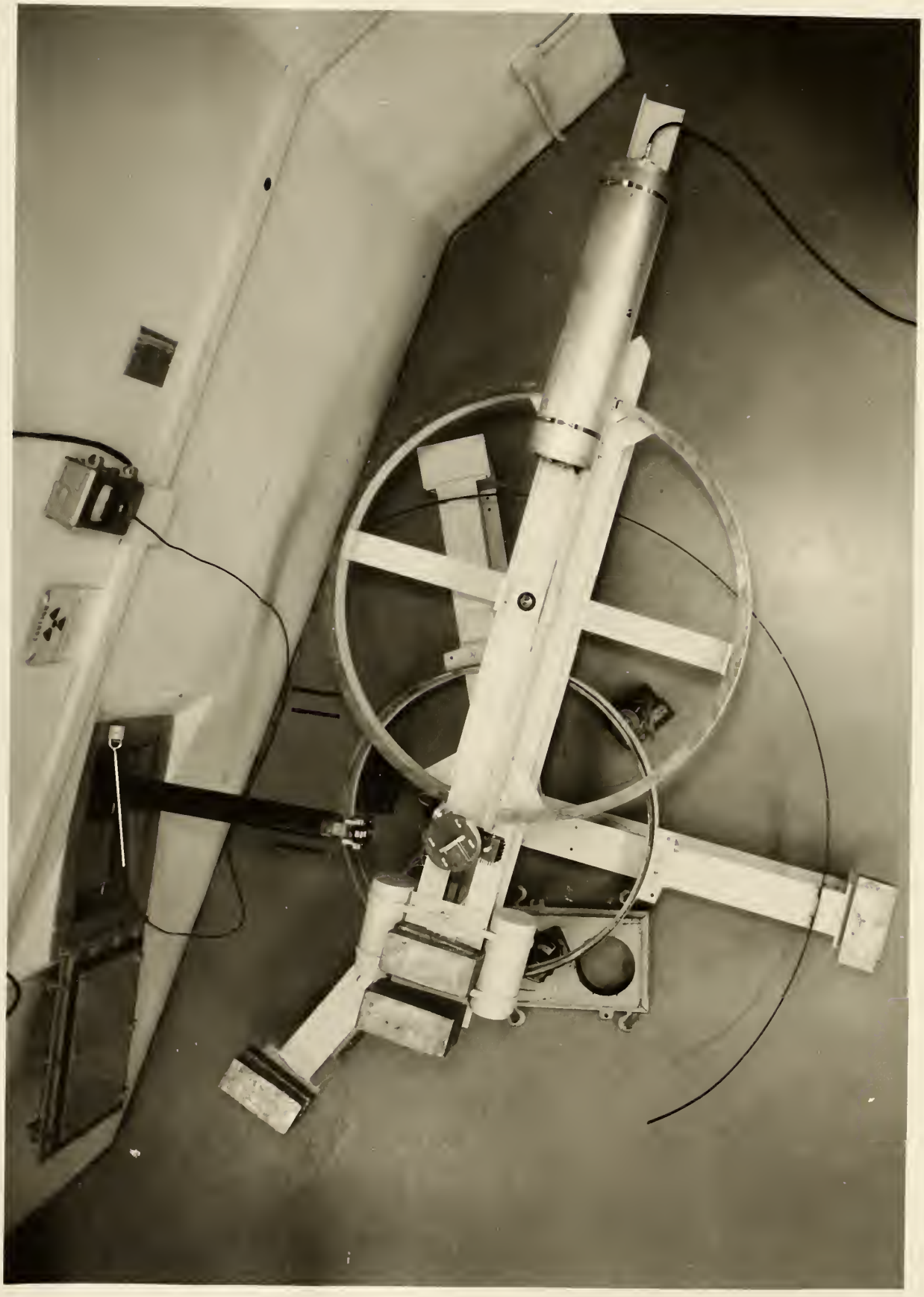

Fig. 15. Top view of neutron spectrometer

scratched on the front surface of the mirror. The arm was then rotated through an angle of approximately 100 degrees (the operating range of the instrument) and the apparent displacement of the light noted.

This optical method allowed the causes of the irregular behavior of the crystal to be finally determined. They were found to be a movement of the crystal table caused by some electrical leads, and deflections of the support ring under the weight of the main arm and its associated counterweights. The use of more flexible wires and the placement of hydraulic jacks at strategic points under the support ring cured these remaining difficulties.

The gearbox provides the necessary 2:1 reduction in angular displacement between the detector and the diffracting crystal. A photograph of the gearbox and the crystal table assembly is shown in Fig. 16. The gearbox is fastened to the upper main arm bearing by three 10-24 cap screws. These screws are easily visible on the bottom shelf of the gearbox. Before removing these screws, it is first necessary to loosen the bottom left gear. After doing this, the three screws may be removed. The entire gearbox and crystal table assembly may then be removed by lifting them straight up. If only the crystal table assembly is to be removed, it is necessary to loosen only the gear in the upper left of the gearbox. The entire crystal table assembly may then be removed by lifting it straight up.

The manner in which the gearbox achieves its 2:1 reduction is not entirely obvious from Fig. 16. Although the gearbox itself is fastened to the upper main arm bearing, the small gear in the lower left of the gearbox is attached to a pin. This pin is press fitted into the main shaft which, in turn, is firmly attached to the base of the instrument. Thus, this gear remains stationary and the entire gearbox rotates around it. The pin ends just below

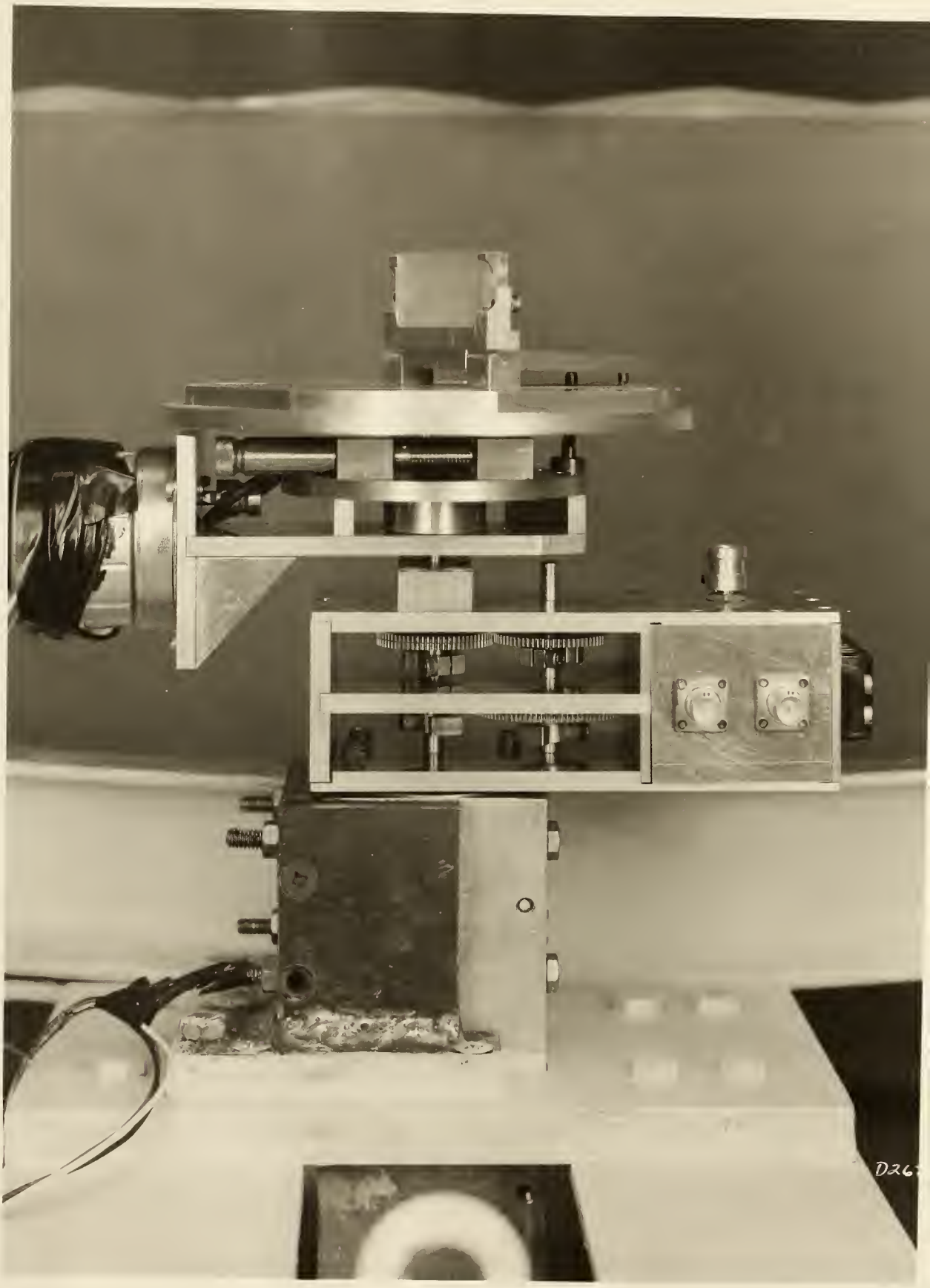

Fig. 16. Gearbox and crystal table assembly

the middle shelf in the gearbox. The shaft supporting the crystal table assembly then rests on the top of the pin for vertical support. The shaft on the right side of the gearbox is solid and only transmits the motion between the lower and upper sets of gears. Since the ratio of the two gears in the top is 1:1, the desired overall ratio is achieved.

Because of the type of experiments which were to be performed, as well as constructional problems, it was decided not to construct a massive shield around the diffraction crystal. Instead, an external beam catcher was to be used. Also, it was felt that this approach would help to reduce the background for small diffraction angles. Later measurements of both the scattered radiation within the reactor bay and of the collimated beam indicated that no particular radiation safety problems would be presented by this decision.

It was felt that automation of the entire instrument would be too costly and add greatly to the undertaking. Therefore, only the adjustment which provided rotation of the crystal about the vertical axis was equipped with a motor drive. This was done mainly because of the fineness of the adjustment. The reversible motor is manually controlled with a three-position, center-off, switch. The motor is coupled to the adjustment thumb-screw with a suitably sized O-ring.

Two other adjustments are provided for the crystal. They allow rotation about a horizontal axis as well as translation of the entire crystal. Complete instructions for the alignment of the neutron spectrometer are provided in the following section.

In order to minimize the effects of fluctuation in the reactor power,

a monitor assembly was devised. Initial attempts at placing a partially shielded BF_3 probe near the collimator met with failure. The monitor probe assembly so constructed proved to be highly dependent upon the main arm position. The BF_3 probe was finally placed within a polyethylene block which was placed between two masonite spacers (see Fig. 17). The outer wooden shielding plug was removed from another beam tube and the monitor assembly was then inserted to a depth of 14 1/2 inches. Two additional polyethylene blocks were placed between the monitor probe and the inner beam plug to help thermalize some of the fast neutrons. All polyethylene blocks used were cylinders 9 inches long by 5 3/4 inches in diameter.

The electronic equipment used was connected as indicated in Fig. 18. The idea is to collect a preset number of counts from the diffracted beam (data channel). When this preset number is reached, the timer and the power monitor (monitor channel) counter are stopped. Thus, the monitor channel yields a number which is proportional to the time integral of the reactor power during the counting time.

The timer allows one to make a resolving time correction to the data channel information. No such correction for the monitor channel is necessary so long as the reactor is run at a relatively constant power. By suitable adjustment of the position of the monitor probe within the beam tube, the countrate of the monitor channel can be made to greatly exceed that of the data channel. (Care must be taken not to saturate the monitor channel scaler, however.) Thus, the statistics of the final data will be determined mainly by those of the data channel.

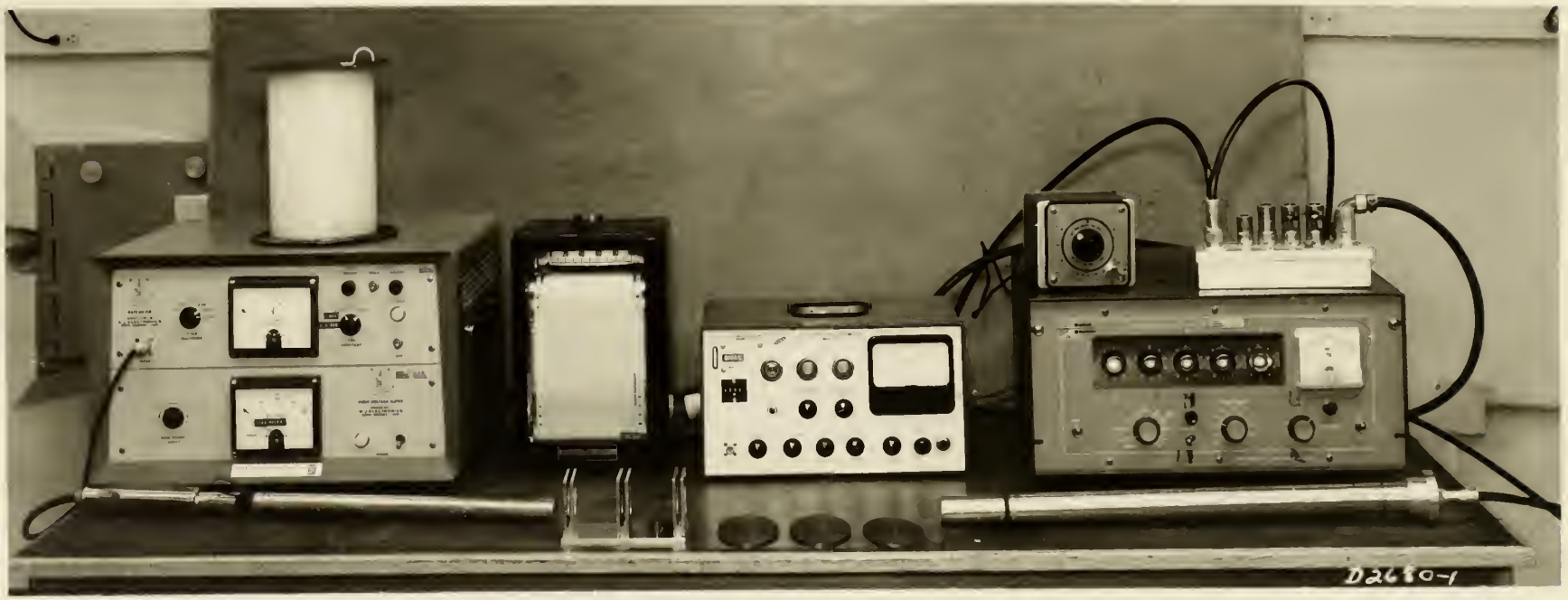

Fig. 17. Electronic equipment, monitor probe assembly, and beryllium discs and holder

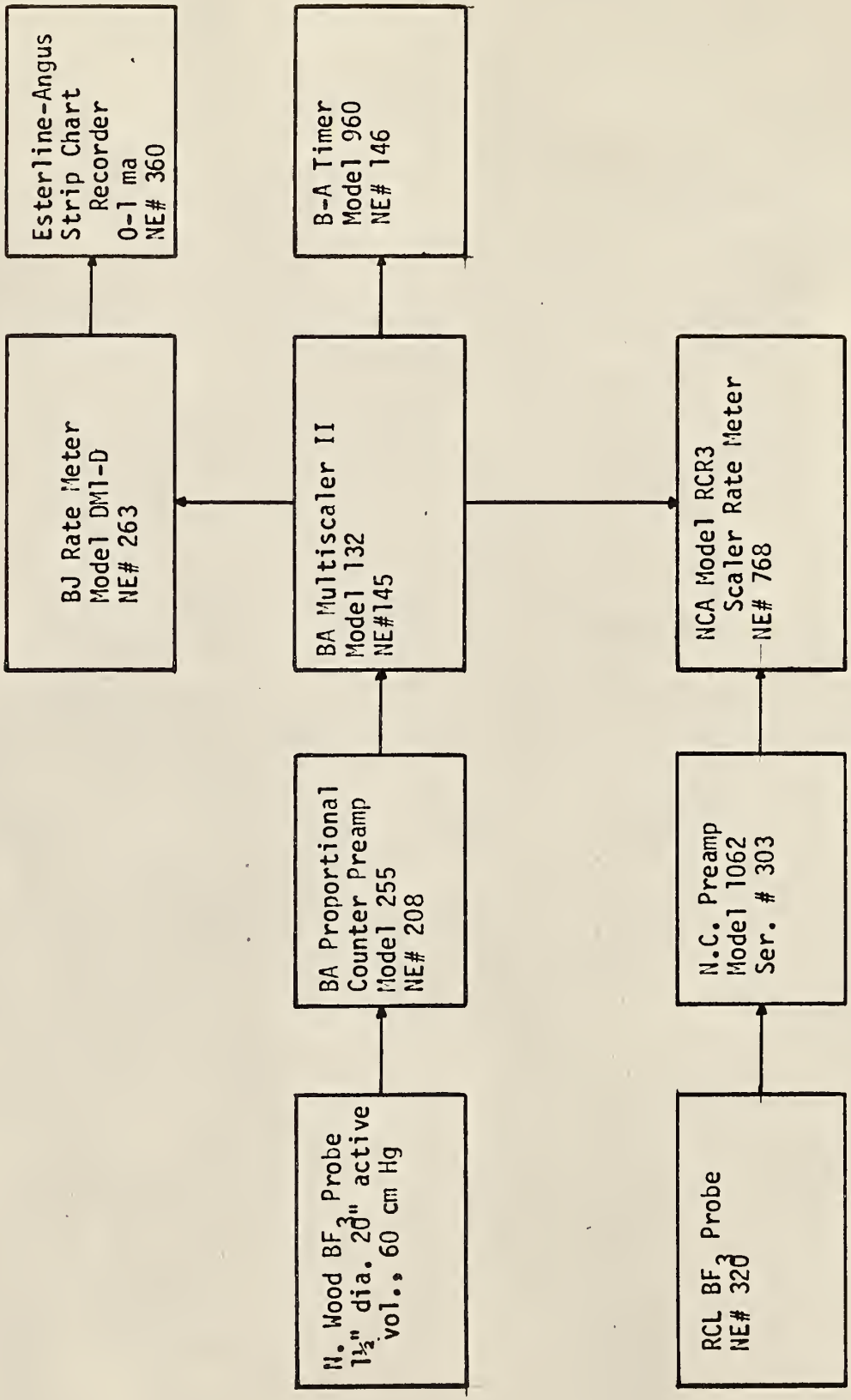

Fig. 18. Block diagram of electronics

Although it was not used in obtaining the final data, a circuit was designed to provide an analogue voltage proportional to the arm angle. The circuit diagram is shown in Fig. 19. It is a simple voltage divider circuit with a voltage regulator. This circuit was designed to be used in conjunction with a TMC GAMMA SCOPE operating in the Mossbauer mode.

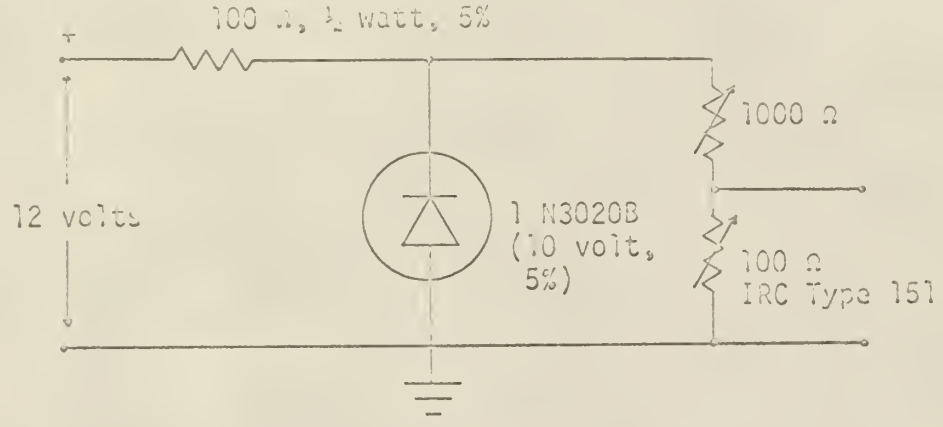

Fig. 19. Analogue position circuit

LiF crystals were selected for the diffraction grating because of their cost, availability, and suitability. The maximum size available was 2 inches by 1 inch with a thickness of 6 millimeters. Two crystals were obtained with a face cut parallel to the (111) plane and two cut parallel to the (200) plane. The (111) crystals have the advantage (20) that they are known to produce no second order diffraction pattern. They do, however, produce a sizable third order pattern. The (200) crystals have (21) a second order diffraction pattern, but they also have a smaller interplanar spacing and a smaller third order diffraction pattern than the

(111) crystals. Also, the (200) crystals have the advantage of a smaller mosaic spread and therefore, can be used to make higher resolution measurements than are possible with the (111) crystals.

3.4 Neutron Spectrometer Alignment Procedure

I. Major Adjustments

Any adjustment that is not specifically indicated in these instructions should not be made except under the direction of an experienced mechanic. Even then, the adjustment of the central shaft should be undertaken only after great deliberation. If it is moved out of alignment, it must be reset with a special jig and a dial indicator.

II. Alignment with the Reactor Shut Down

During this procedure, there should be no excuse for anyone to receive any significant radiation dose. It has been demonstrated (see the reactor beamport log) that the dose rate emerging from the beamport may be as high as 10 R/hr. (after a 100 kw run), even though the reactor is subcritical. Also, there may be a sizable amount of radioactive gas generated inside the beamport. Since both of these hazards rapidly decrease with time, they may be reduced to minor proportions by merely waiting the proper length of time.

1. Consult with the Reactor Supervisor about the past operating history of the reactor and the approved techniques for opening the beam ports.
2. Obtain suitable radiation measuring equipment, an automatic level or transit, a carpenter's level, a light source which may be inserted into the collimator, and the special front-surfaced mirror.

3. Using suitable technique, remove the beamport plugs and insert the collimator into the chosen beamport. Make the proper entries in the beamport log.
4. Place the spectrometer assembly roughly in position with the edge of the crystal table about 1" from the front of the collimator snout. Place the carpenter's level across the bottom ring and adjust the three jackscrews until the instrument is level. Do not raise the instrument any higher than necessary. (See Fig. 20)
5. Remove the snout and the internal shielding plugs from the collimator. Insert the light source until it hits the inside end of the collimator.
6. Using the automatic level or transit, move the whole spectrometer assembly until center of the crystal holder is in line with the collimator (vertical axis only). The overhead crane will be necessary for this movement.
7. Place 1 drop of oil on each bearing in the gearbox. Generously oil both main shaft bearings on the main arm.
8. Relevel the spectrometer by adjusting the three jackscrews and adjust height of the instrument until the bottom of a neutron beam from the collimator would just strike the top of the crystal table.
9. Insert the front-surfaced mirror into the crystal holder.
10. Using the transit or automatic level, rotate the spectrometer arm and make sure that the center of rotation of the crystal holder is correct. The upper crystal table may be slid back and forth to correct for any misalignment.
11. Move the light source in the collimator sufficiently close to the

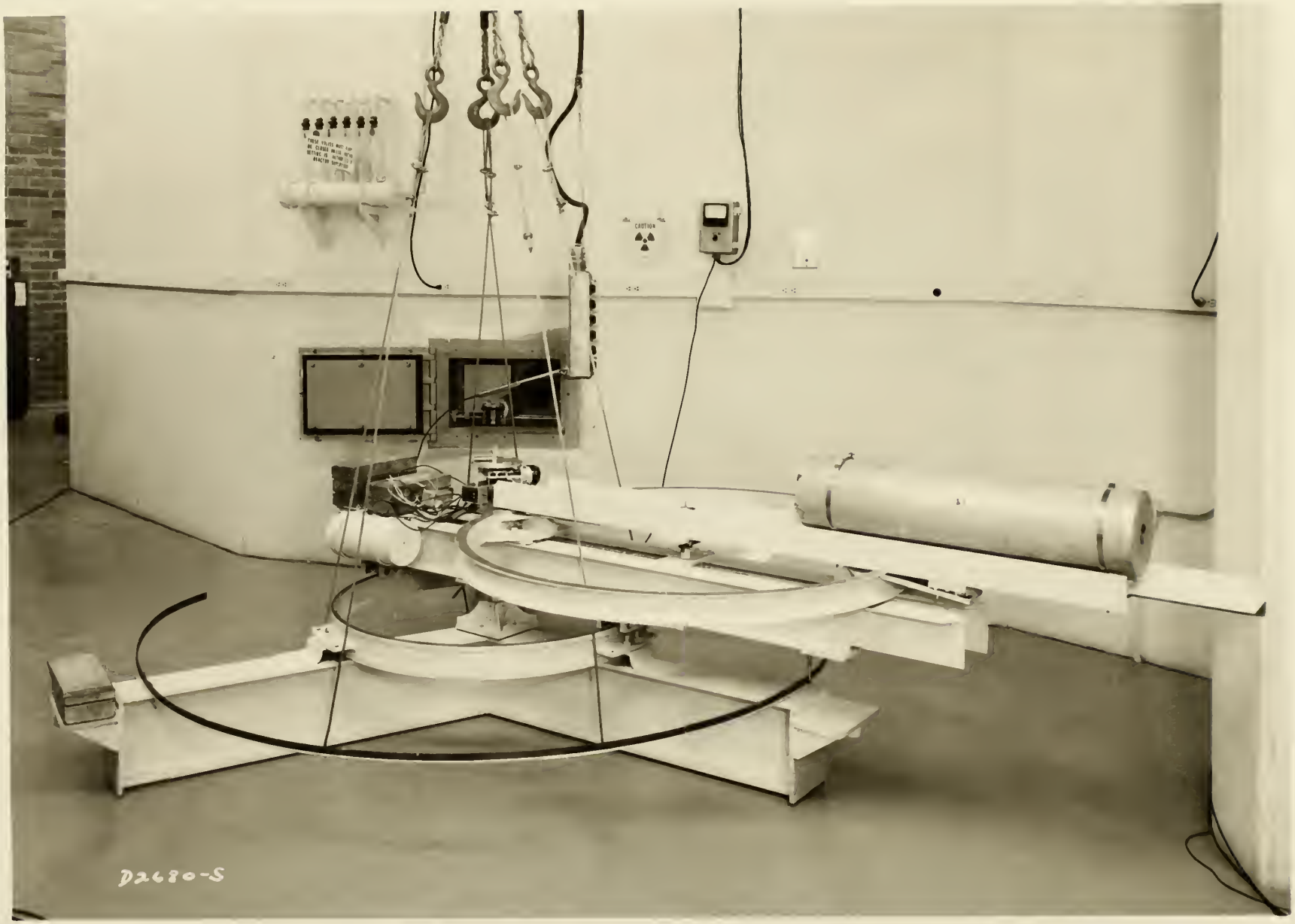

Fig. 20. Proper method of lifting spectrometer

outside so that a usable reflection from the mirror may be obtained. Place the arm at approximately a 30° angle and adjust the crystal holder until the spot of light illuminates the detector.

12. Remove the mirror from the crystal holder and the light from the collimator. Move the beam definition shields on front to produce a neutron beam ½" wide and 1" high. Make sure that the beam will strike only the crystal and only in the center. Position the beam catcher behind the spectrometer.

13. The collimator is so designed so as to enable it to be placed in any of the four beamports and have both the shutter and the outer door closed. If this is done, however, the collimator should have its own internal shielding plugs in place. With these in place, the radiation field outside the beamport will be less than 2 mr/hr. even with the reactor operating at 100 kw. Hence, if the spectrometer is to be left unattended for any length of time, the collimator should be plugged to avoid accidents. Also, remember to bring the beamport status sign up to date.

III. Neutron Alignment

1. After checking with the Reactor Supervisor, remove the shielding plugs from the collimator and attach the collimator snout. Hang the RAM probe over the snout and lock it in position with the beamport lock.

2. After allowing a suitable warmup time for the associated electronic equipment, take the reactor up to a power level of

beamport	power level	maximum expected countrate
a. tangential	100 watts	36,000 cpm
b. fast	30 watts	35,000 cpm
c. regular	100 watts	42,000 cpm

3. Without a crystal in place move the spectrometer arm until the detector is barely out of the direct neutron beam. Take a one minute count and move the arm ½ cm closer to the beam. Continue until the width of the beam has been traversed. By plotting these data, the zero point on the calibration ring may be determined.
4. Either scram the reactor or reduce the power level to one watt or less.
5. Carefully install the proper crystal in the crystal mount and then move the spectrometer arm until it makes an angle of about 30° with the emergent neutron beam.
6. Increase the reactor power to

beamport	power level
a. tangential	10 kw
b. fast	3 kw
c. regular	10 kw

7. Being very careful not to get any portion of the body in direct contact with the radiation beam, use one hand to adjust the crystal using the adjusting screws underneath the crystal table until the maximum countrate is obtained. (See Fig. 21)
8. Rotate the crystal about a vertical axis until only background is obtained. Rotate 1° more in same direction.
9. Increase reactor power to triple that indicated in step 6 above.
10. Using a ratemeter with a time constant of 1 second and a recorder, rotate the crystal table back through the peak countrate position

Fig. 21. Proper position for crystal table adjustments

until only background is being recorded. Use the motor drive feature for this part. The speed of the motor drive may be determined by timing the degree markings on the edge of the crystal table. This procedure gives the rocking curve, which is a measure of the instrument resolution.

11. Reverse the direction of rotation of the crystal table until the countrate again reaches the peak and then turn off the motor.

12. Position arm for first reading.

13. Increase reactor power to

a.	tangential port	100 kw
b.	fast port	100 kw
c.	regular port	100 kw

and request reactor operator to switch to automatic control.

14. When power level has stabilized (5 minutes) determine neutron spectrum by taking a certain number of counts for each of several different positions of the spectrometer arm.

15. Upon completion of data taking, shut down the reactor and allow it to cool until such time as it is safe to reinsert the shielding plugs into the collimator.

IV. Radiation Monitoring

During part II of these alignment instructions, the only monitoring necessary should be that of the gamma field during placement of the collimator. If proper time has been allowed for the reactor core to cool, then the radiation field should be at most 40 mr/hr gamma. From the time and the distances involved it would seem highly unlikely that an exposure of more than 40 mr would result. Indeed, 1 mr would be

more likely.

Part III will require somewhat more monitoring. III-1 through III-6 should only require an observer to make sure that the person making the adjustments stays out of the direct radiation beam. If properly performed, no one would come within one foot of the direct radiation beam. III-7 and III-8 will require that a finger dosimeter be worn. The radiation field underneath the crystal table is about 60 mr/hr (at 100 kw) and results mainly from the Cd strips on the front of the collimator. Even so, it would be unlikely that the hands would receive more than 20 mr. in the necessary time. If the hands are placed in the direct radiation beam, however, that is another story. III-9 through III-15 will not require any adjustments which will cause the operator to get closer than two feet to the direct beam. If a suitable beam catcher is used, the radiation levels in the occupied areas would probably not exceed 10 mr/hr.

4.0 RESULTS

4.1 Initial Measurements

Two initial measurements which are made with any neutron spectrometer are the rocking curve and the zero point determination. The rocking curve is then valid only so long as the collimator openings and the diffracting crystal are not changed. The zero point is valid only so long as the base of the instrument is not moved.

Typical rocking curves taken with the automatic drive on the crystal table are shown in Fig. 22. The time constant of the ratemeter was one second and the reactor power was 96 kw. These curves were obtained at the N.W. beam port at four different diffraction angles using a (111) LiF crystal. All four were taken with the crystal table rotating in the same direction and all yield a value for the FWHM of the rocking curve of 27. ± 4. minutes. Solution of equation 17 yields a result of 24 minutes. Thus, it may be assumed that the crystal and the collimator are reasonably well matched.

The slight irregularities in the curves are caused primarily by slippage in the drive belt from the motor. The relative scale factors are given for each of the curves in order for the reader to obtain an estimate of the magnitudes of both the diffracted beam and the background for the different diffraction angles. Fig. 23 shows a typical zero point determination curve. It was obtained at the S.E. beam port with a reactor power of 100 watts.

---

*These and all following measurements were taken with a ½ inch wide opening on the entrance and exit of the collimator, and a 1 inch wide opening on the front of the detector shield. All openings were defined with .020 inch thick cadmium sheet.

Position 60

Position 160

Position 110*

Arm Zero Position = 41.5

Position 210

*To convert to diffraction angle in degrees, subtract arm zero position and divide by 4.

Fig. 22. Typical rocking curves using (111) LiF crystal

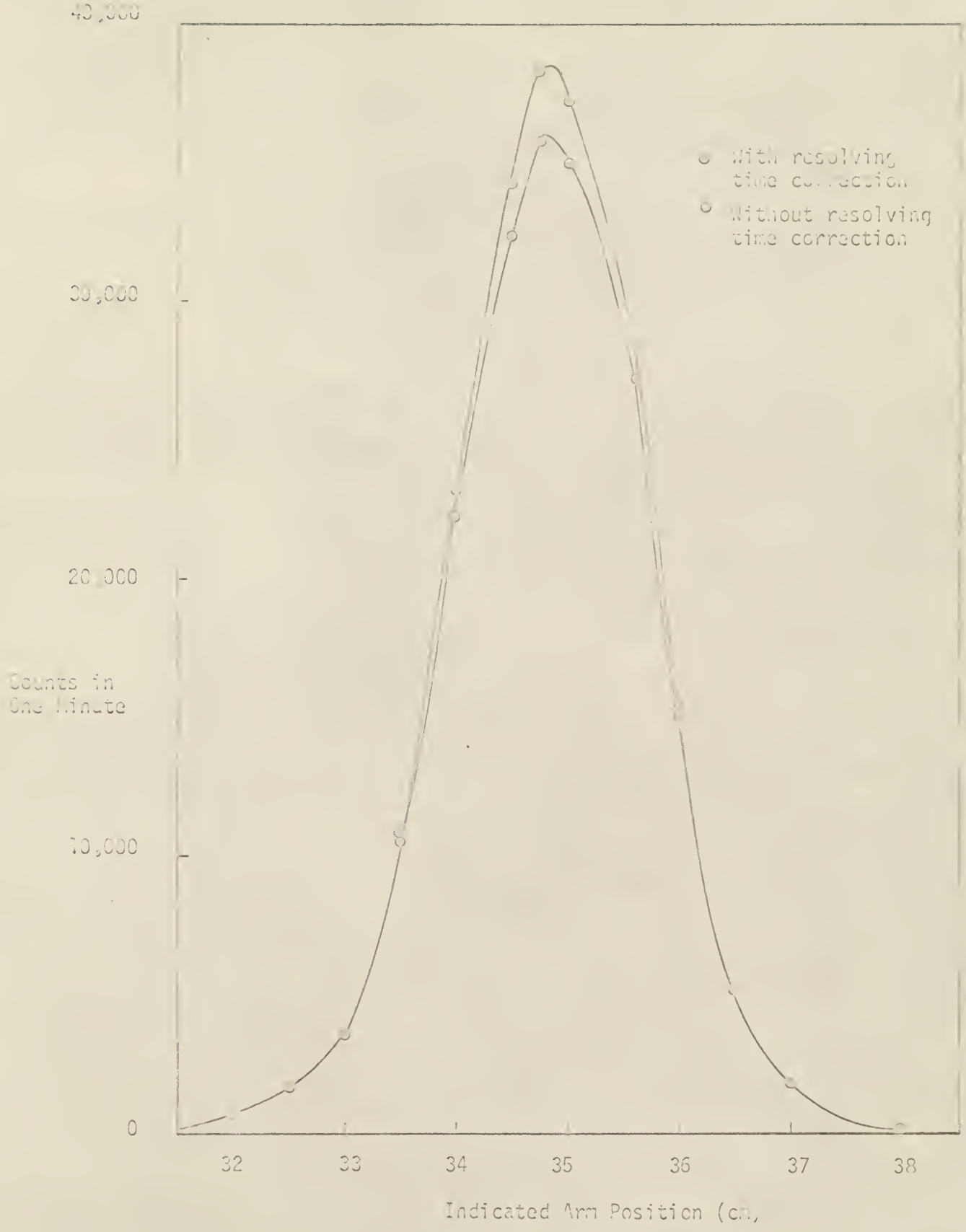

Fig. 23. Zero point determination curve

The curve is shown both with and without the standard correction* for the resolving time of the counter. Note that the only effect of this correction is to sharpen the peak of the curve and is not really necessary in order to determine the zero point location. The correction is included here only to give an idea of the order of magnitude of the correction in preparation for the determination of the neutron spectrum in section 4.3.

Another important initial measurement is the reproducibility of the results. If the results are consistent, suitable correction factors may at least be devised in order that the true answers may be obtained. If the settings of the instrument are not reproducible, the machine is nearly worthless.

The reproducibility was determined by selecting a set of five different points in the vicinity of the peak velocity. Five determinations of each set were made with each point being taken in cyclic order. Since the reactor power was fairly constant (constant resolving time correction for each different position) and the preset count on the diffracted beam was constant, only the monitor counts are listed in Table II.

---

*The resolving time for the scaler and the preamp was experimentally determined by Ihde (22) to be 108 microseconds. Since the BF_3 is operated in the proportional region, its deadtime is much smaller than the rest of the system and may be neglected. As a result, no further investigations were made along this line.

Table II. Monitor Counts for Repeated Settings of Main Arm

Run/neutron energy	.090 eV	.072 eV	.058 eV	.048 eV	.039 eV
1	98059	74674	69527	73053	78417
2	97050	74316	68981	72794	79078
3	96472	74790	69295	72105	79435
4	97035	74415	68180	72400	79428
5	97713	75325	69445	73103	79187

The data taken at .090 eV are somewhat more scattered than at the other energies. This may be attributed to the backlash in the instrument and the process of making the first setting.

4.2 Further Correction Factors

4.2.1 Cadmium Cut-off Correction

Preliminary examination of the data showed a strange peak in the vicinity of .4 eV. This peak was finally attributed to the use of cadmium for the definition of a collimated neutron beam. In the range from .1 eV to 1. eV, the total neutron cross section for cadmium decreases by nearly four orders of magnitude. A correction factor, R, was then derived in the following manner: consider an opening consisting of an unshielded area, A_1, and a cadmium shielded area, A_2. The ratio, R, of the neutrons passing through both areas is given by

$$R = \frac{A_1}{A_1 + A_2 e^{-\Sigma_c t_{cd}}} \tag{25}$$

where Σ_c is the macroscopic total neutron cross section for cadmium and t_{cc} is the thickness of the cadmium covering area A_2. Upon inspection of the total neutron cross section for cadmium, it is found that between .25 eV and .7 eV, the following is a good approximation:

$$\Sigma_c = \left(\frac{.3}{E}\right)^4. \tag{26}$$

Substitution of equation 26 into equation 25 and the introduction of the proper numerical quantities for the two areas and the cadmium thickness yields

$$R = \frac{8}{8 + 13\, e^{-\frac{.0211}{E^4}}} \tag{27}$$

A graph of this equation is shown in Fig. 24. Even though equation 26 is not valid for energies less than .25 eV or greater than .7 eV, the limiting values have nearly been reached at these extremes and so the correction factor may be applied to all energies within the range of the instrument without any loss of validity of the final answer.

The correction factor derived is thus a correction for the increase in radiating area. Although it would seem that a similar correction factor should be applied to the collimator exit, no such factor is needed. The size of the crystal is such that the effective crystal width presented to the collimated neutron beam above the cadmium cut-off energy is less than the width of the collimator opening.

It will be noted that in some of the following curves, especially Fig. 31, all of the cadmium peak has not been removed. This is attributed to

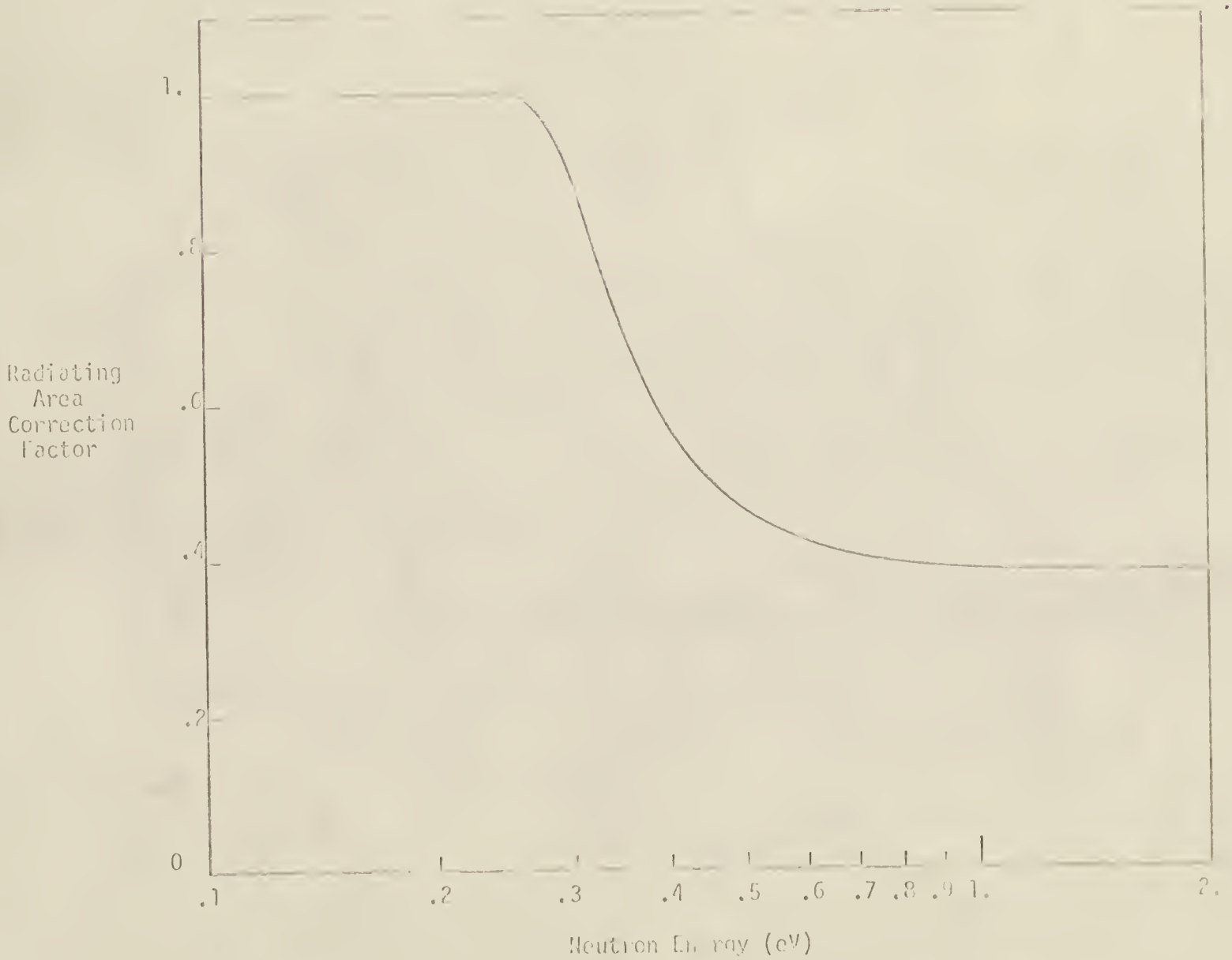

Fig. 24. Radiating area correction factor versus energy

a slight misalignment of the diffracted neutron beam. This misaligned beam then strikes the cadmium slits of the front of the detector shield. Since the amount of this misalignment was not known, no attempt was made to apply a suitable correction.

4.2.2 Resolving Time Correction Factor

After inspection of the magnitudes of the original data, it was decided to make a correction for the resolving time of the data channel. Since, for any given run, the countrate of the monitor channel was nearly constant, a constant resolving time correction factor could be obtained; however, it was not applied.

The standard correction for resolving time of a counter is given by

$$n_o = R_m(1 + R_m R_t) \tag{28}$$

where n_o is the true countrate, R_m is the measured countrate, and R_t is the resolving time. As previously mentioned, R_t was found to be 108 microseconds. In order to simplify the data collection and processing, equation 28 was somewhat modified.

If τ_1 represents the time needed to collect a given number of counts, M_c in the monitor channel, then the time, τ_i required to collect any other given number of counts, M_i, is

$$\tau_i = \frac{M_i}{M_c} \tau_1 \tag{29}$$

provided the reactor power is nearly constant. Thus, only one time need be entered for each different set of data. The maximum resolving time correction for the various spectra obtained was about 10%.

4.3 Leakage Spectrum Measurements from Various Beamports

4.3.1 S.E. Beamport

Figures 25 and 26 show the spectra obtained for fuel loadings 6 and 6' using a (111) crystal. Upon comparison of the two spectra, it may be seen* that the major effects of changing between these two core configurations is to increase the magnitude of the 1/E tail by approximately 50%. Little change is otherwise made in the curves.

Inspection of the original data indicated that the countrate at the peak of the distribution was changed by 4% with the change in core configurations. This latter figure is not entirely meaningful since adjustments were made to the crystal between these two different runs. The nature of these adjustments is such that it is very difficult to reposition the crystal so that the diffracted beam intensity is within 5% of that from a previous run.

In Figures 24 through 36, only a few of the standard deviations** are shown. Most of those shown are either in the 1/E region or close to it. The standard deviations for the remaining sections of the curves are in the neighborhood of 1-2% and are too small to indicate on the graphs. Also, the other uncertainties for the various correction factors are far in excess of those indicated in the figures. Besides the correction factors previously mentioned, it is thought that the process of off-setting the crystal for background measurements may have contributed to the error in the background for small diffraction angles.

---

*Pertinent parameters of the experimental curves are given in Table 3.

**These deviations are computed from the measured values of data channel and monitor channel for both the diffracted beam and the background.

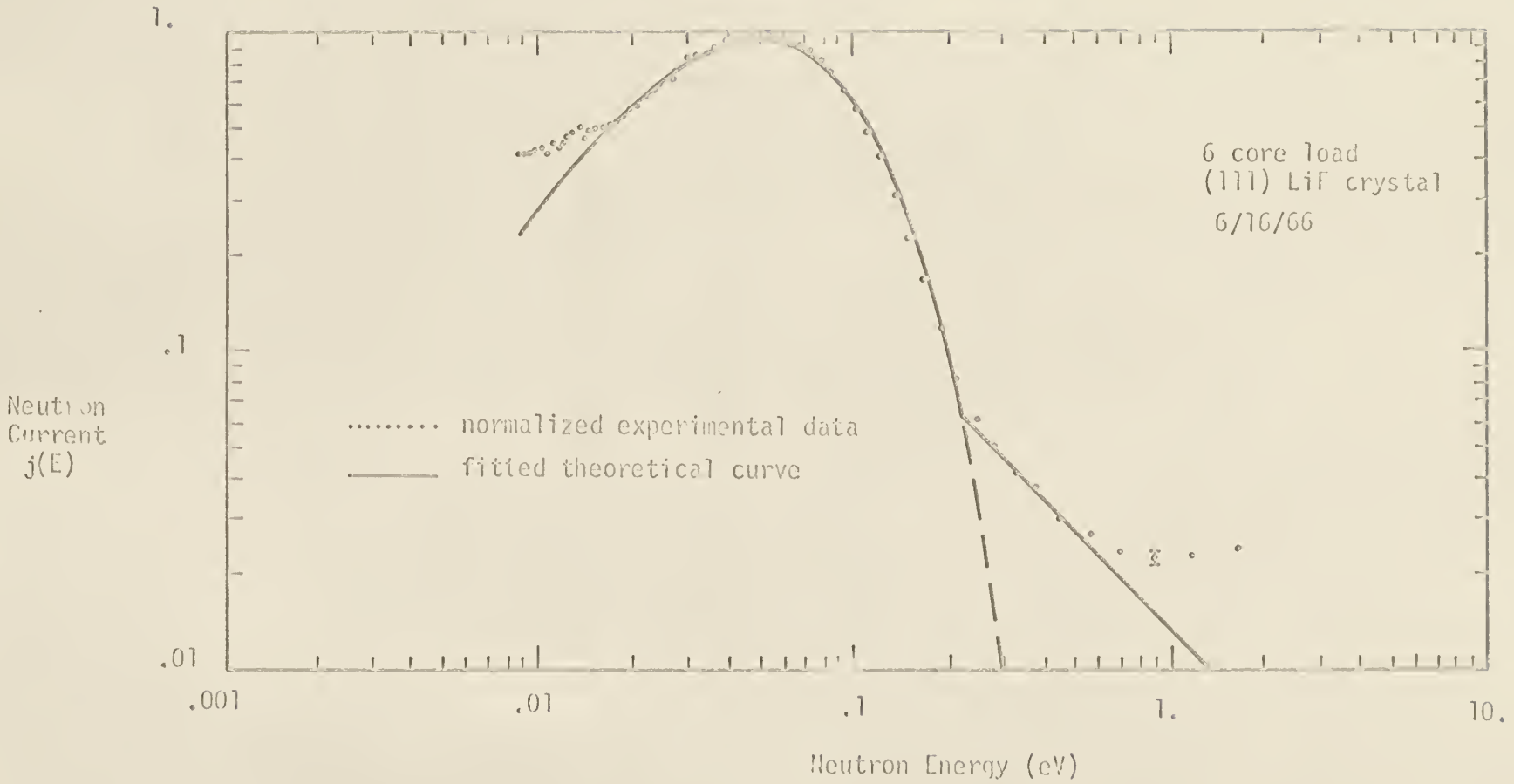

Fig. 25. Neutron spectrum fro[illegible].E. beamport

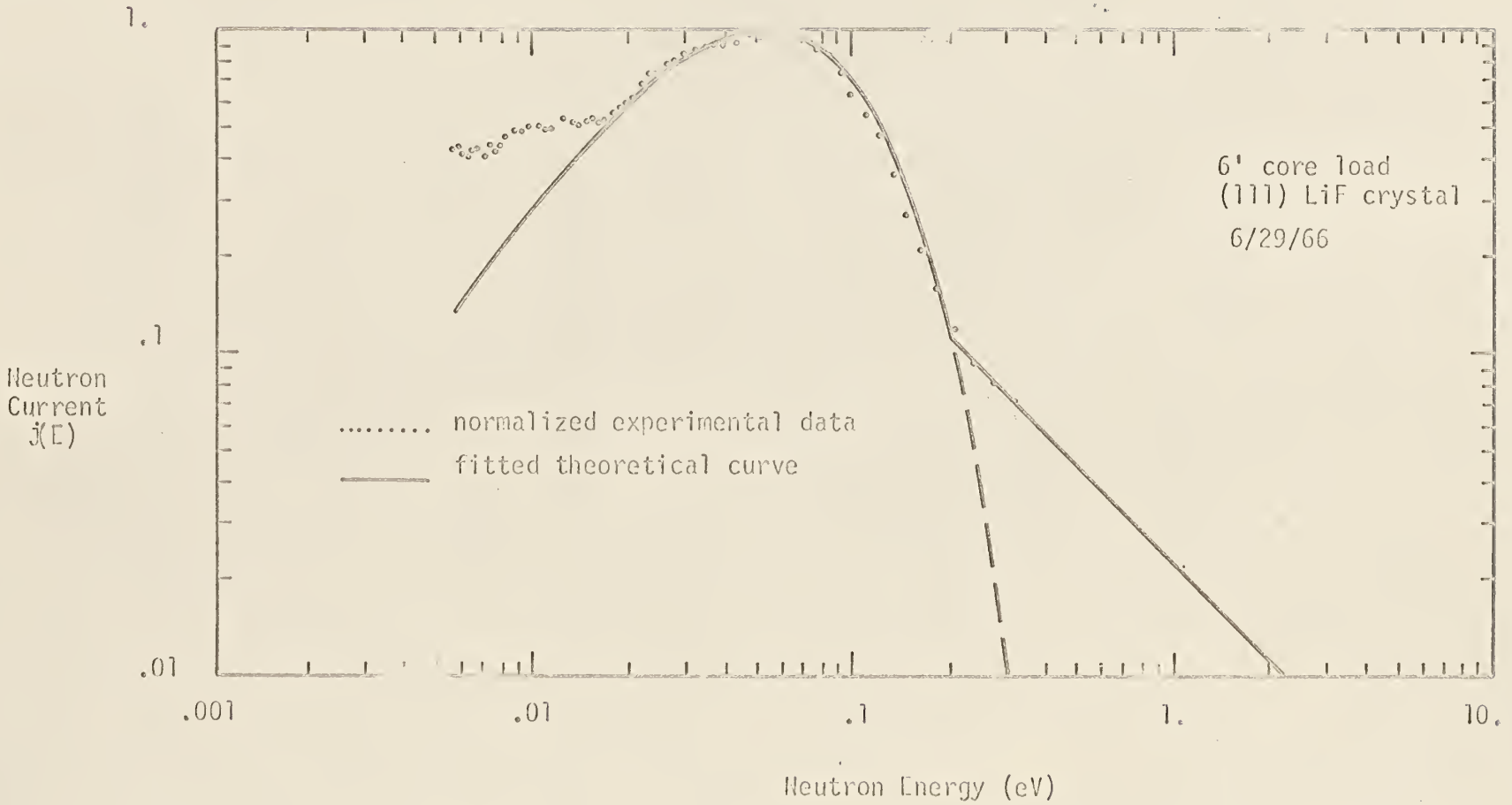

Fig. 26. Neutron spectrum from S.E. beamport

For energies lower than v_c, the theoretical curve was obtained by least-squares fitting the normalized experimental data points to equation 6. The 1/E tail is fitted using an eyeball approach since the data in this region are somewhat uncertain.

Interesting results were obtained for the spectrum (Fig. 27) taken with the (200) crystal. The fuel loading was number 6. This spectrum agrees fairly well with that shown in Fig. 24 down to .055 eV. Below that value, the two spectra diverge, with the theoretical curve lying somewhere between the two curves. No explanation can be given for the magnitude of this divergence.

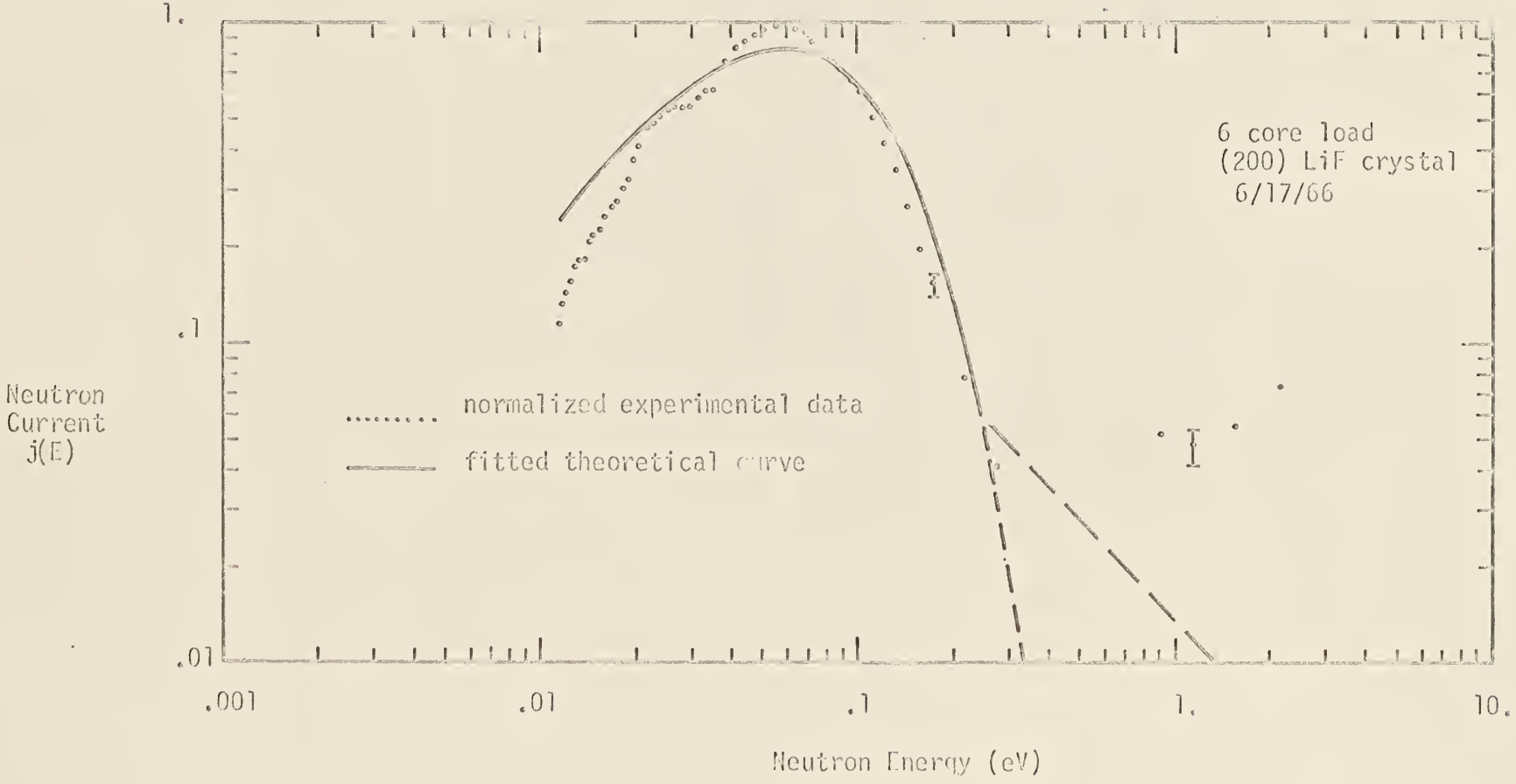

Fig. 27. Neutron spectrum from S.E. beamport

4.3.2 [illegible] Beam Port

Figures 28, 29, and 30 show the spectra obtained using f[illegible]l loadings 5, 6"', and 6", respectively. As might be expected, little difference in the spectra is observed between the first two fuel loadings. However, fuel loading 6" increases the magnitude of the 1/E tail by nearly a factor of two.

Little difference between the maximum countrates obtained for fuel loadings 6 and 6"' is noticeable. However, the maximum countrate for fuel loading 6" was more than 20% greater than that of the two others. Here, no adjustment of the crystal was made between the three runs.

Certain perturbations in the vicinity of .01 eV are much more prominent in these spectra than for the spectra from the S.E. port. As will be shown in section 4.[illegible], these perturbations are caused by the presence of a sizable thickness of aluminum in the neutron path.

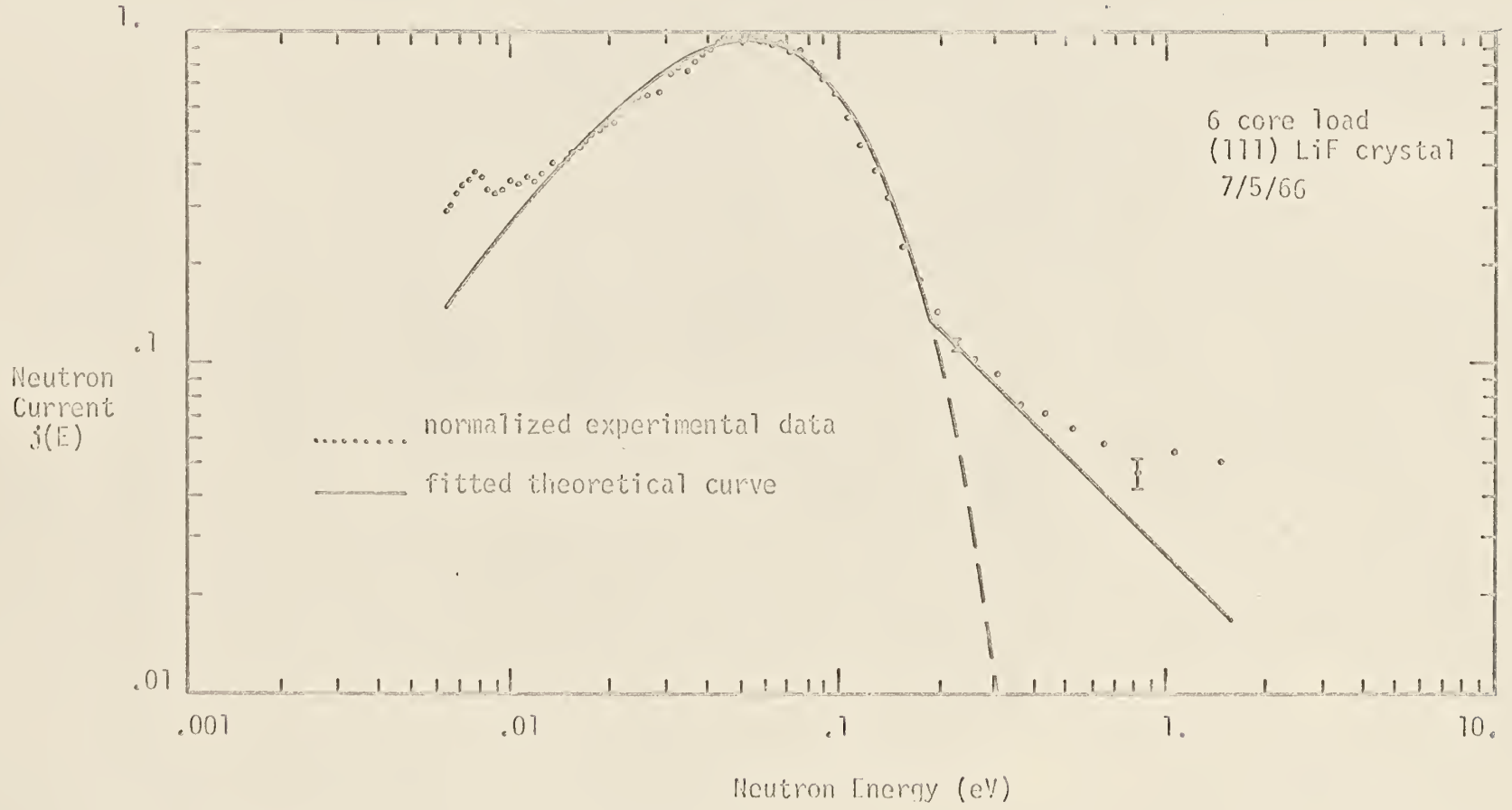

Fig. 28. Neutron spectrum from N.E. beamport

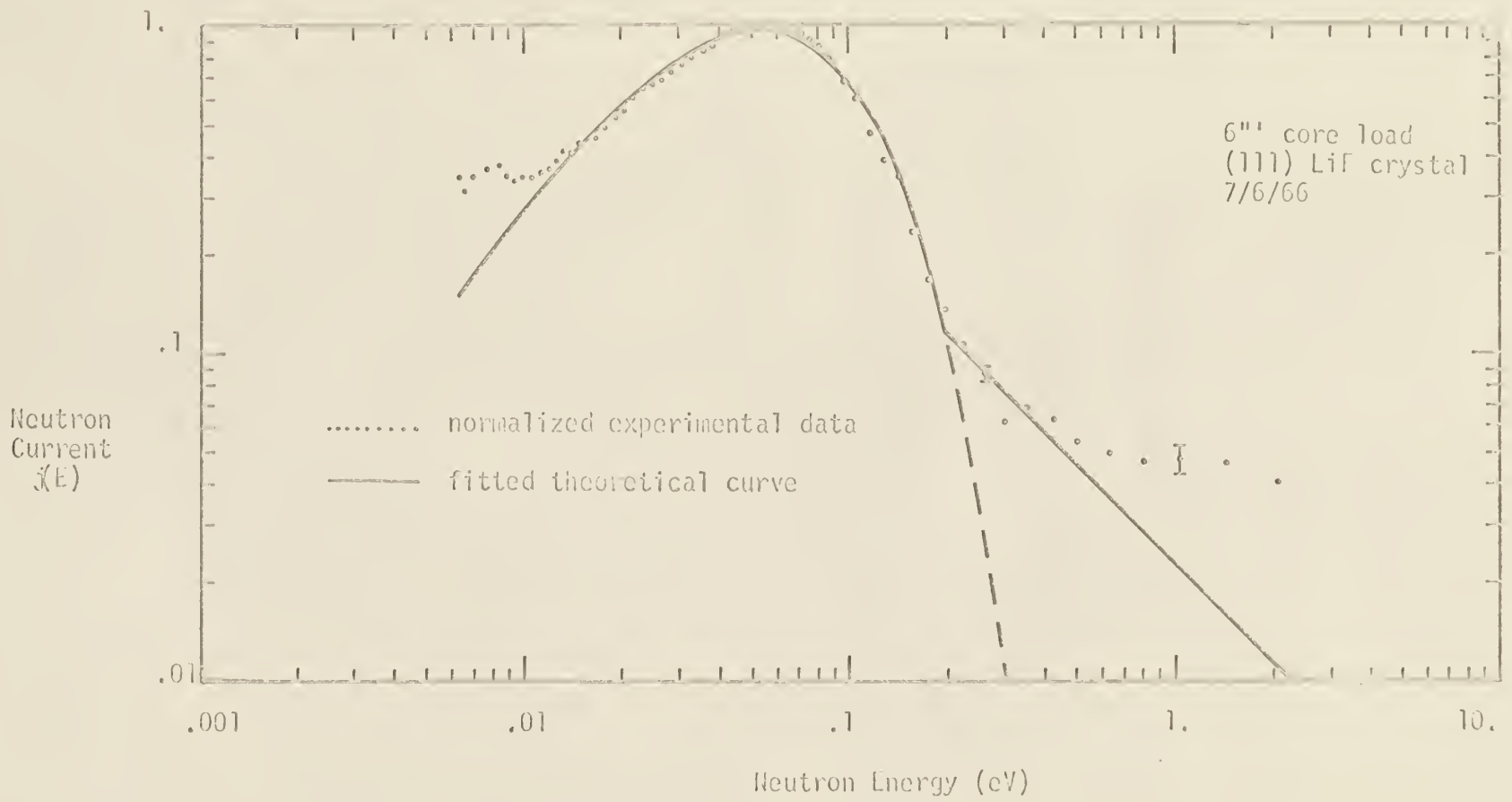

Fig. 29. Neutron spectrum f N.E. beamport

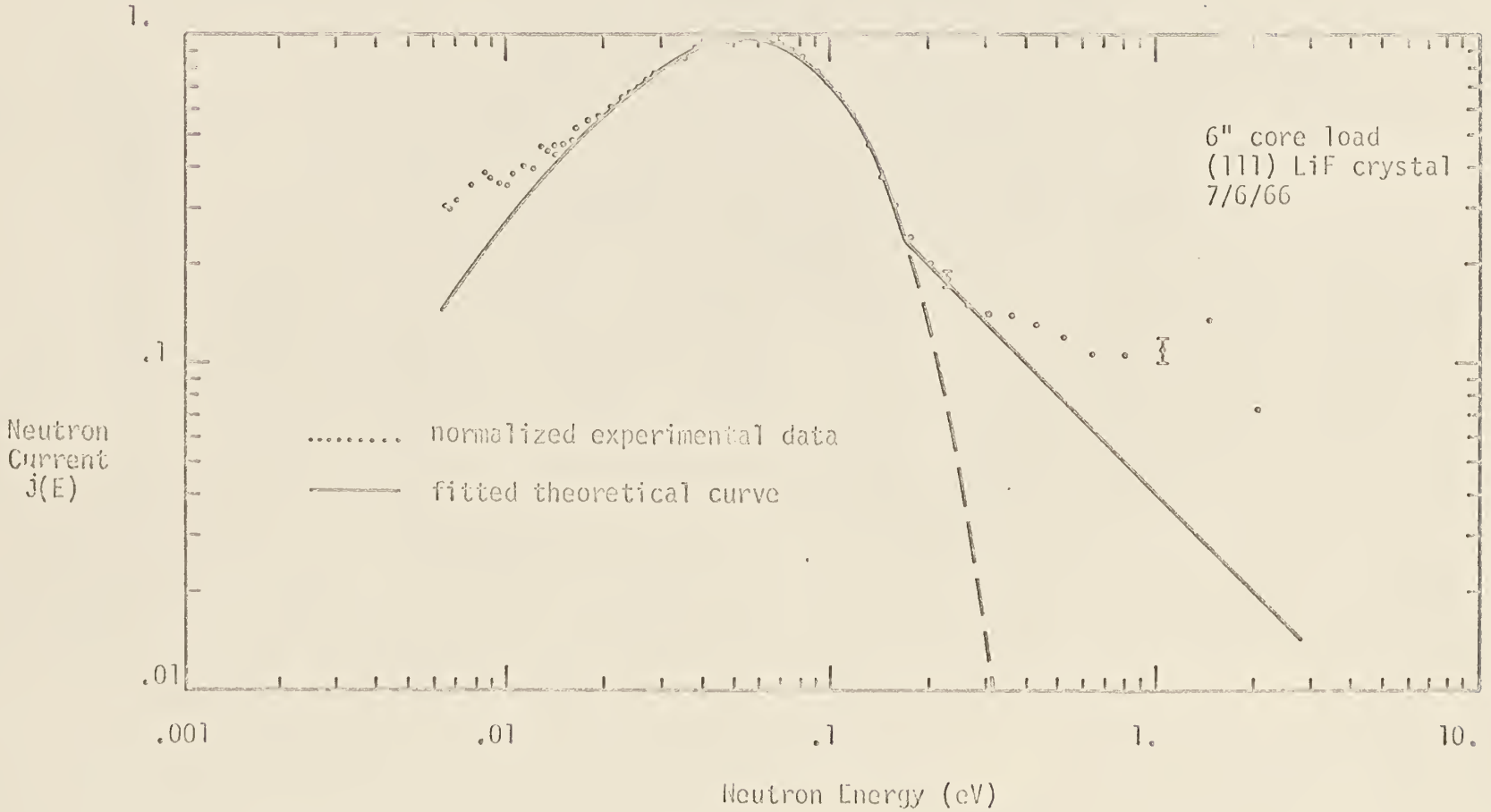

Fig. 30. Neutron spectrum from N.L. beamport

4.3.3 N.W. Beamport

Figures 31, 32 and 33 show the spectra obtained using the standard fuel loading. This series of measurements was conducted in order to determine the effectiveness of the alignment procedures. After the spectrum shown in Fig. 31 was obtained, the entire instrument was moved to the N.E. port and several spectra taken. The spectrometer was then returned to the N.W. port and realigned. The spectra shown in Figures 32 and 33 were then obtained.

Inspection of the original data indicates that the peak countrates were within about 10% of each other for the three different runs. The data in Fig. 32 are somewhat suspect. Shortly after these data were taken, the scaler on the monitor channel was found to be oscillating intermittently.

Fig. 34 shows the spectrum obtained when a piece of aluminum 2 1/8 inches thick was placed in the collimator shielding hole. The peaks (24) in the cross section around .01 and .015 eV are especially pronounced. The effect of this thickness of aluminum was to reduce the maximum countrate by a factor of two.

During the realignment procedure, it was noticed that the longitudinal axis of the collimator was not horizontal. The entire collimator was rotated in the beam tube 180 degrees to ensure that this effect was not caused by a warped collimator. Since this procedure did not correct the misalignment, it was assumed that the beam tube was at fault. No similar difficulties were experienced at either the S.E. or the N.E. port.

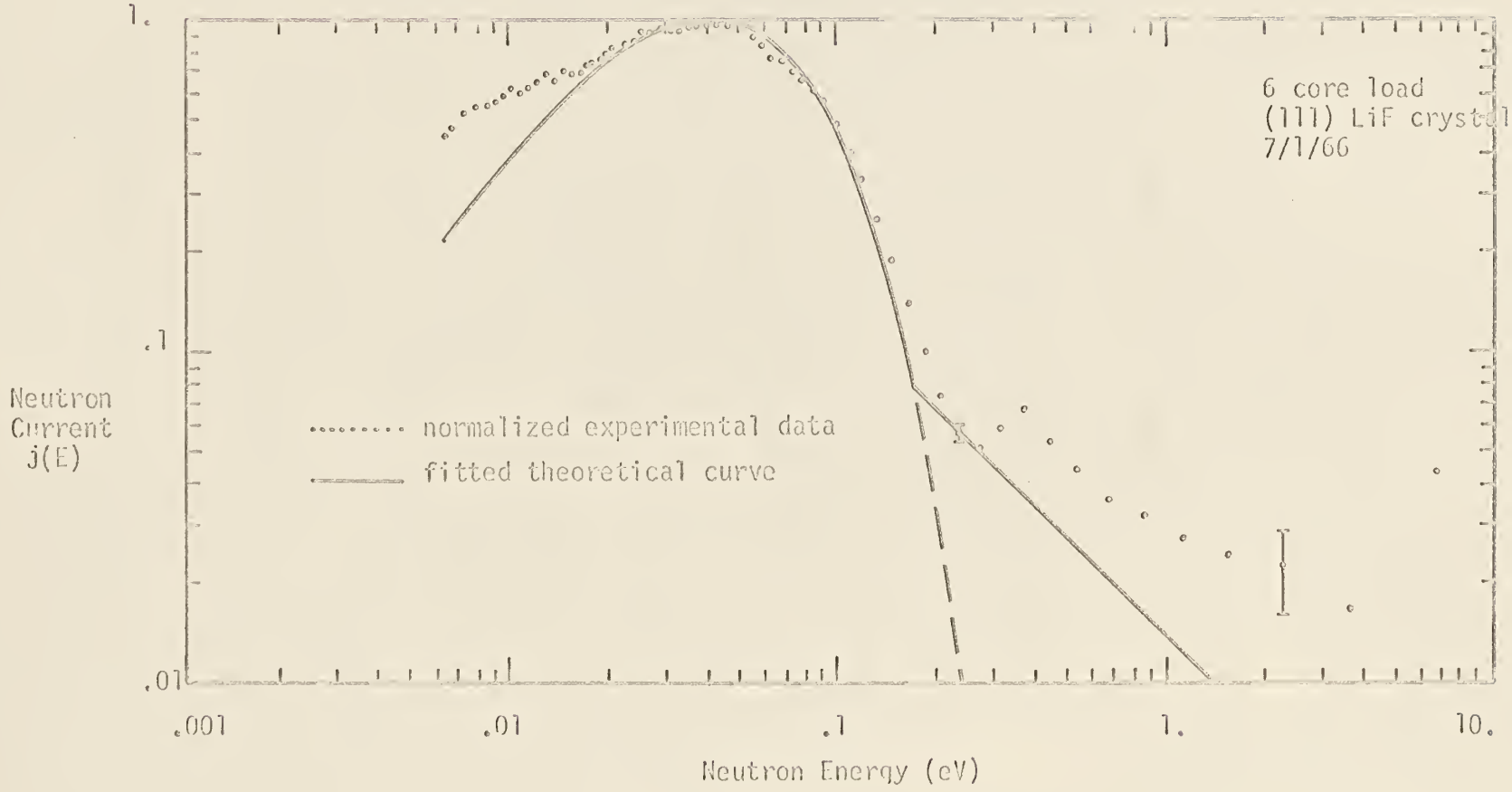

Fig. 31. Neutron spectrum from N.W. beamport

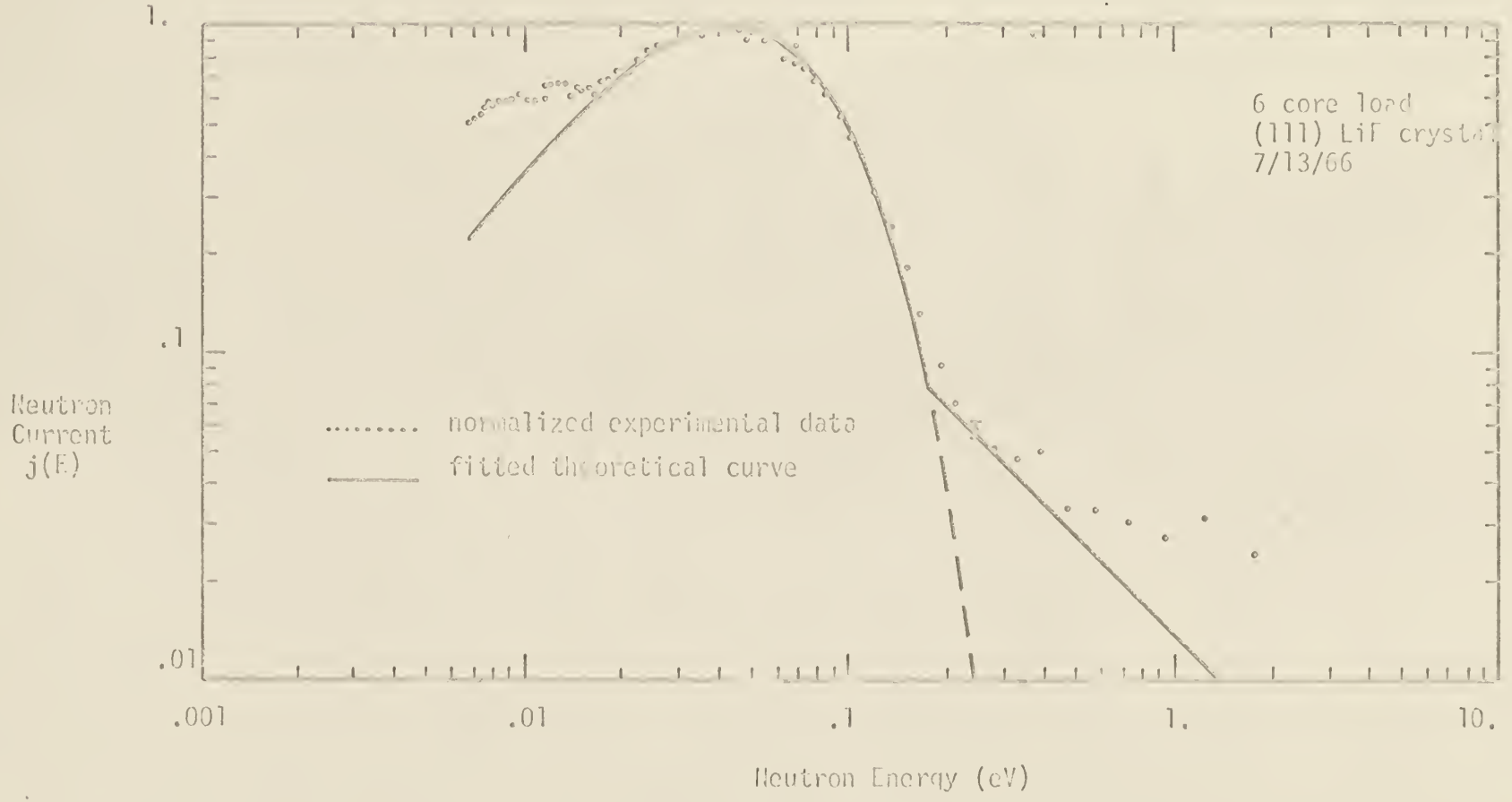

Fig. 32. Neutron spectrum from M.M. beamport

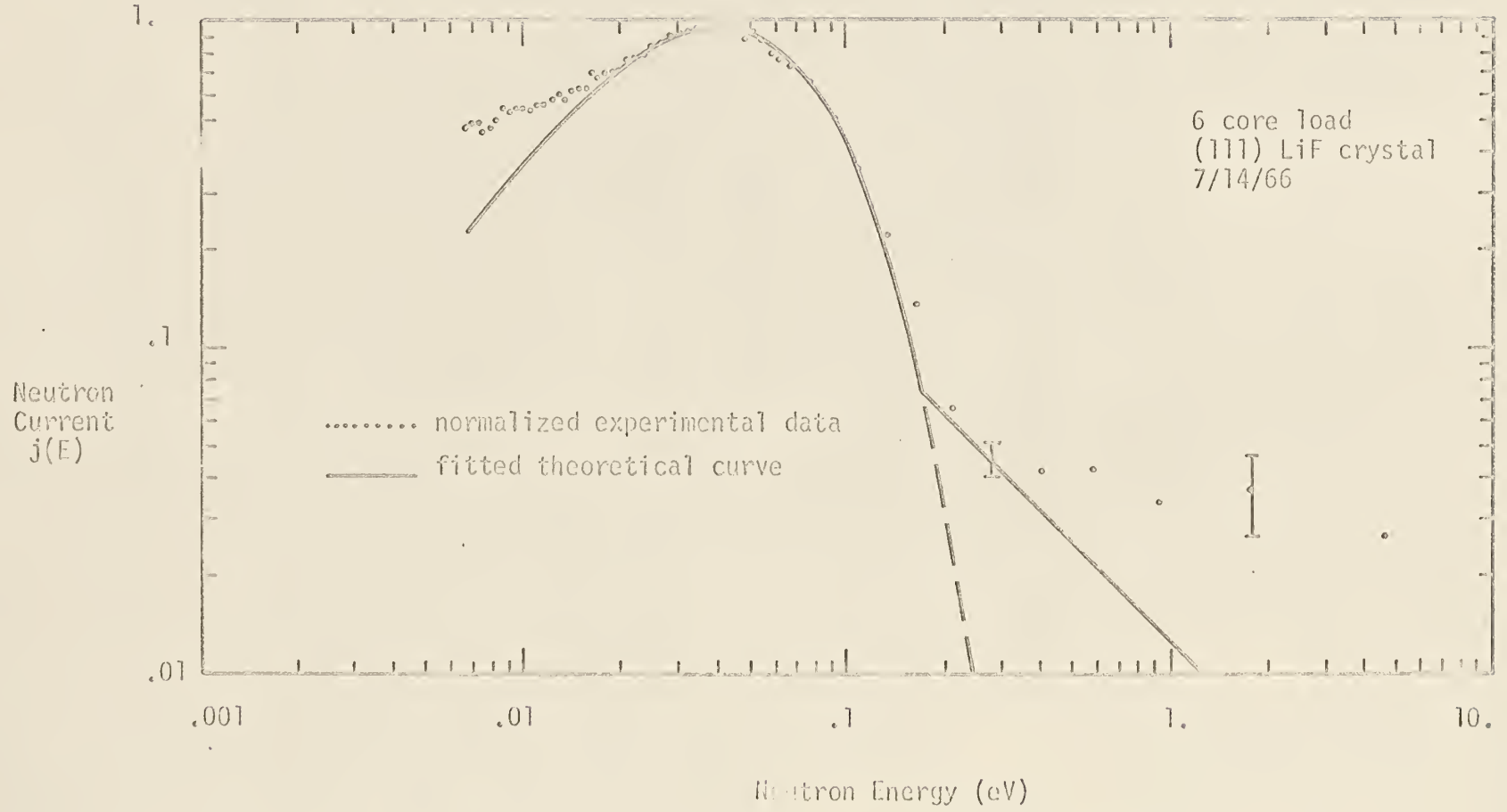

Fig. 33. Neutron spectrum from N.W. beamport

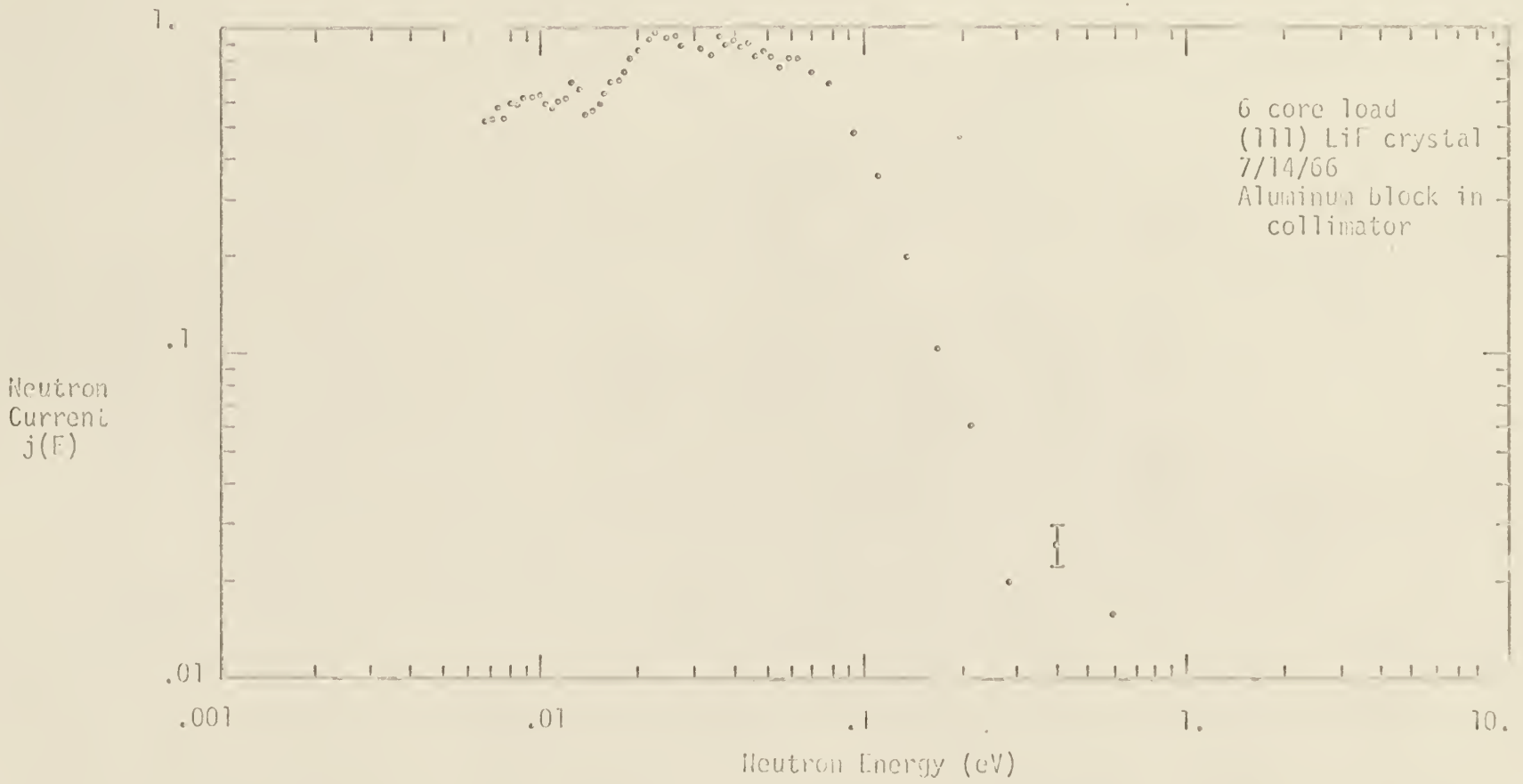

Fig. 34. Neutron spectrum from H.W. beamport

Table III. Pertinent Values from Theoretical Curves Fitted to the Beamport Leakage Spectra

Beam-port	Date	Crystal	Fuel loading	K_1[a] ($\frac{n\text{-}sec^2}{cm^3} \times 10^{-9}$)	v_{mp}[b] ($m/sec \times 10^3$)	v_c ($m/sec \times 10^3$)
S.E.	6/16/66	(111)	6	.1416	3.098	6.34
	6/17/66	(200)	6	.1007	3.342	---[c]
	6/29/66	(111)	6'	.1416	3.161	6.11
	7/5/66	(111)	6	.1332	3.165	5.88
	7/6/66	(111)	6"'	.1332	3.177	6.11
	7/6/66	(111)	6"	.1308	3.228	5.79
	7/1/66	(111)	6	.2125	2.774	5.63
	7/13/66	(111)	6	.1928	2.841	5.71
	7/14/66	(111)	6	.1988	2.971	5.71

[a] Maximum value in corrected experimental data has been normalized to unity.

[b] To obtain v_o, multiply these values by $\sqrt{2/3}$.

[c] No interception point could be accurately determined.

4.4 Measurement of the Energy Dependence of the Total Neutron Cross Section for Beryllium

The total neutron cross section for beryllium metal is shown in Fig. 35. There is fair agreement for the two different runs with the published values (25) above .01 eV. The peak at .02 eV is even better defined than the published value. Below .01 eV, the agreement is not so good. This may be readily attributed to the predominance of the third order diffraction pattern in this region.

Fig. 36 shows the variation of countrate versus varying thickness of beryllium for different neutron energies. The nonlinearity of these curves also points out the effect of the higher order diffraction patterns.

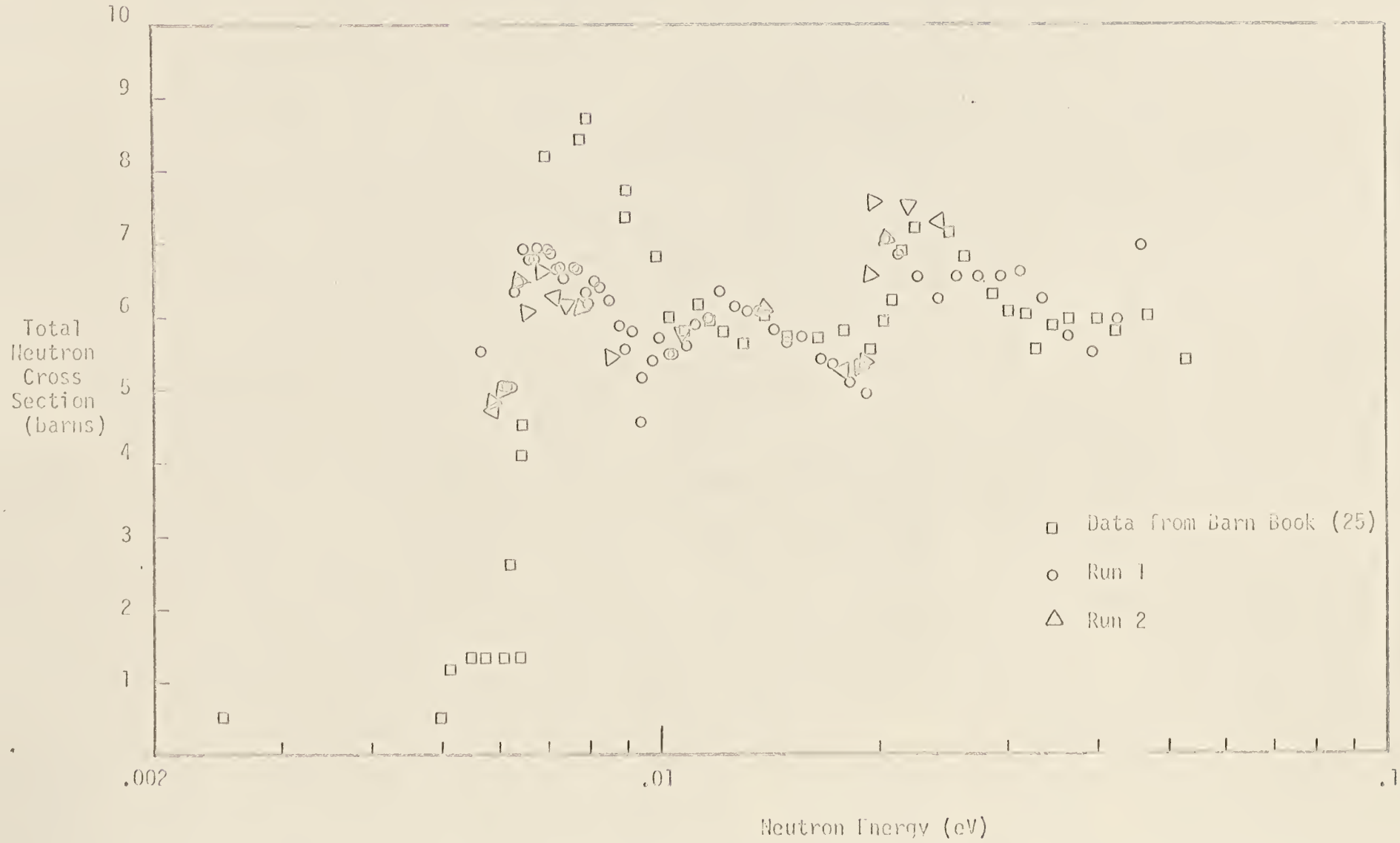

Fig. 35. Total neutron cross section ryllium

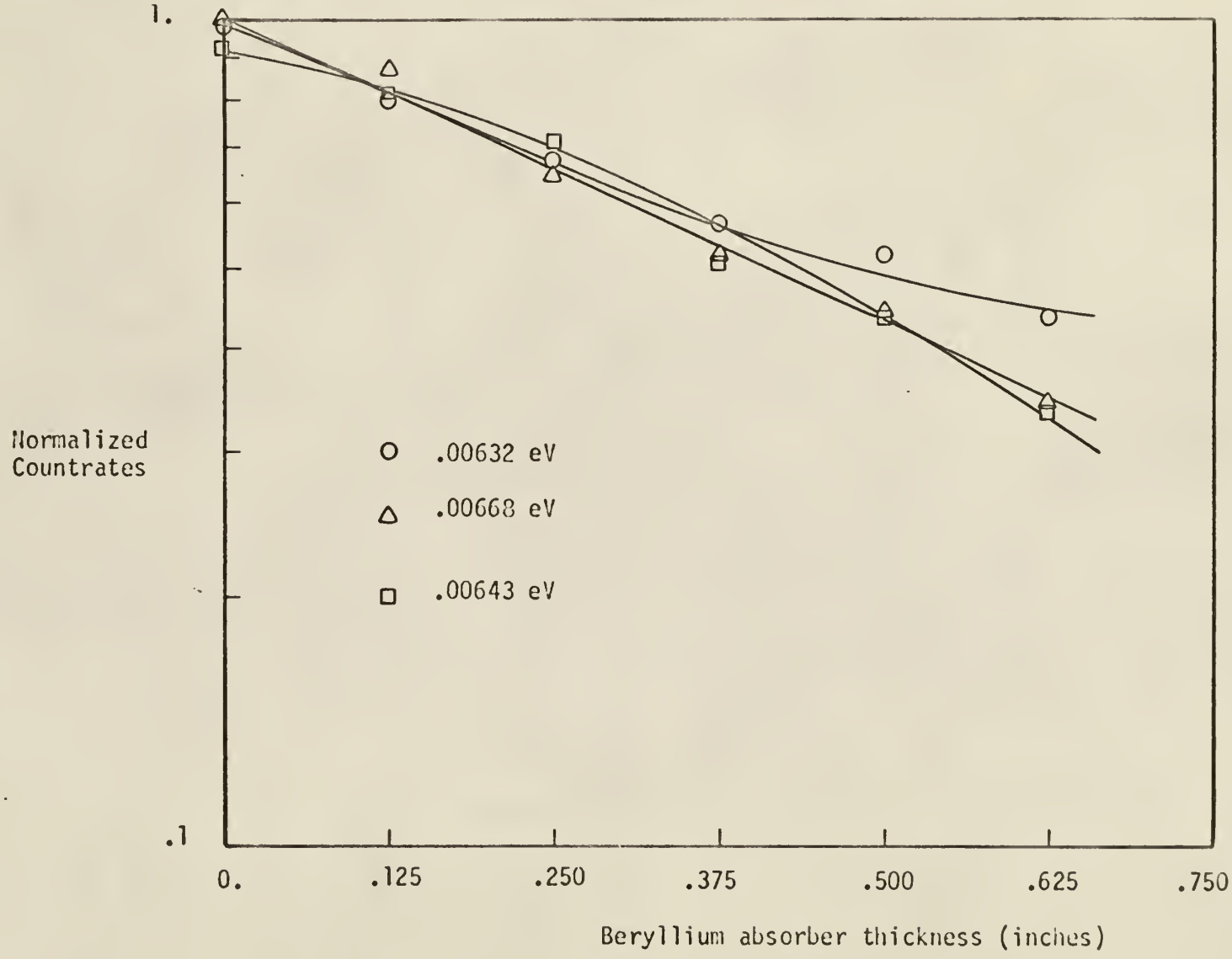

Fig. 36. Normalized countrates vs. beryllium absorber thickness

5.0 CONCLUSIONS

The measurements contained within this work have shown that:

1. The KSU neutron spectrometer may be operated safely, provided it is operated according to the instructions contained in section 3.4. If these instructions are faithfully followed, the maximum permissable exposures contained in 10CFR20 will not be exceeded.
2. Core configurations may be chosen for beamport experiments in such a way so as to yield the maximum possible signal to noise ratio.
3. The total neutron cross section for Be has been measured and found to be in reasonable agreement with published values. Measurement of this cross section has shown the KSU neutron spectrometer to possess very good resolution.
4. An instrument has been constructed which will allow undergraduate students at the senior level to measure the thermal neutron spectrum from the KSUTMII and obtain reasonable results within an afternoon. Provided the instrument has been previously aligned, these results will be reasonably accurate.
5. There is a definite perturbation of the thermal neutron spectrum caused by the presence of a considerable thickness of aluminum near the entrance of the beam tubes. At the N.E. beam port, a certain perturbation may also be noticed from the graphite dummy elements for certain core configurations.

6. The slits which define the collimated neutron beam should be constructed of material other than cadmium in order to better collimate the neutron beam in the epicadmium region and to reduce the background.
7. Improvements should be made on the crystal table assembly, especially in that portion which provides for rotation of the crystal about a vertical axis.
8. Measurement of the total neutron cross section for beryllium indicates that the energy calibration of the instrument is in error by 7% at .021 eV. Further studies should be made to determine the calibration error as a function of position.

6.0 SUGGESTIONS FOR FURTHER WORK

There are a number of improvements which may be made in the present system. One of the most important of these is the design and construction of better collimating slits. A rough measurement showed that nearly 90% of the background consisted of epicadmium neutrons. A better slit system could reduce the background by at least a factor of two.

If much work is to be done in the lower energy region, a Soller slit system inserted into the collimator could more than double the present countrate without reducing the resolution.

The start of a second axis has been provided. Because of lack of time, it was not completed. The experience obtained with the main support ring indicated that the secondary support ring may have to be removed and another means of support found. This procedure would also remove a great deal of weight as well as gain some extra height for the second gearbox.

Another improvement would be the substitution of a very thin ion chamber placed directly in the neutron beam in place of the present monitor probe. This would guard against flux tilts within the core.

The above improvements would allow more work to be done on the higher order diffraction patterns and refinement of the Be cross section measurements. Also, they would greatly increase the versatility of the instrument.

Another interesting experiment which is suggested is the study of the thermal neutron spectrum as a function of time during a reactor pulse. Obviously, this would have to await a pulsing license. It is suggested that if this experiment is performed, a stepped hole be cut in the wall of the

neutron generator room directly opposite the fast beam port in order to use the entire room as a beam catcher. Naturally, this hole could be plugged during operation of the neutron generator.

7.0 ACKNOWLEDGMENT

The author wishes to express his sincere appreciation for the help and guidance given by Dr. Milan Copic and Dr. Johannes G. Koen. Much gratitude is also extended to Mr. Kenneth M. Watts and Professor Robert W. Clack for their helpful suggestions and constructive criticism. The author is also very grateful for the help given by various members of the KSU Physics Department as well as several students enrolled in the Department of Nuclear Engineering. Thanks must also be extended to Mr. John P. Lambert for his help in making many of the radiation survey measurements included in this work.

Last, but not least, special thanks go to Dr. William R. Kimel for obtaining what must have seemed a never ending source of funds for this project.

8.0 REFERENCES

1. Sturm, William J.
   Measurement of Neutron Cross Sections with a Crystal Spectrometer, Phys. Rev., 71, 762 (1947).

2. Zinn, W. H.
   Diffraction of Neutrons by a Single Crystal, Phys. Rev., 71, 752 (1947).

3. Atoji, M.
   A Multipurpose Neutron Diffractometer, ANL-6920 (1964).

4. Gould, F. T.
   The Neutron Spectrometer for Subthermal Neutrons and the Cross Sections of Gold and Metallic Hydrides in the 4-11.5 Å Range, CU-179, Columbia Univ. (1958).

5. Egelstaff, P. A., ed.
   Thermal Neutron Scattering, Academic Press, New York, 109 (1965).

6. Egelstaff, P. A., ed.
   Thermal Neutron Scattering, Academic Press, New York, 93 (1965).

7. Bacon, G. E.
   Neutron Diffraction, 2nd ed., Clarendon Press, Oxford, 207 (1962).

8. Daavettila, D. A., et al.
   A Manual of Reactor Laboratory Experiments, ANL-6990, 29.5 (1965).

9. Anderson, C. A. and T. J. Thompson
   Measurements of Leakage-Neutron Energy Spectra, Nuc. Sci. and Engg., 18, 478 (1964).

10. Beyster, J. R. et al.
    Spatially Dependent Neutron Spectra, GA-2036 (1961).

11. Bacon, G. E.
    Neutron Diffraction, 2nd ed., Clarendon Press, Oxford, 65 (1962).

12. Bacon, G. E.
    Neutron Diffraction, 2nd ed., Clarendon Press, Oxford, 69 (1962).

13. Egelstaff, P. A., ed.
    Thermal Neutron Scattering, Academic Press, New York, 105 (1965).

14. Price, W. J.
    Nuclear Radiation Detection, 2nd ed., McGraw-Hill, New York, 317 (1964).

15. Allen, R. G.
Measurement of the Thermal Neutron Cross Sections of Au, Ag, In, Ni, and NiO using a Crystal Spectrometer, Univ. of Texas, Austin (1953).

16. Sturm, William J.
Measurement of Neutron Cross Sections with a Crystal Spectrometer, Phys. Rev., 71, 767 (1947).

17. Hughes, D. J.
Pile Neutron Research, Addison-Wesley, Cambridge, 241 (1953).

18. TRIGA Mark II Reactor General Specifications and Description, GA-2627, 69 (1961).

19. 250-kw TRIGA Mark II Pulsing Reactor Mechanical Maintenance and Operating Manual, GA-3399 (1962).

20. Fermi, E. and L. Marshall
Interference Phenomena of Slow Neutrons, Phys. Rev. 71, 666 (1947).

21. Sturm, William J.
Measurement of Neutron Cross Sections with a Crystal Spectrometer, Phys. Rev., 71, 764 (1947).

22. Ihde, Robert H.
Personal Communication, August 8, 1966.

23. Hughes, D. J. and R. B. Schwartz
Neutron Cross Sections, 2nd ed., 217 (1958).

24. Hughes, D. J. and R. B. Schwartz
Neutron Cross Sections, 2nd ed., 117 (1958).

25. Hughes, D. J. and R. B. Schwartz
Neutron Cross Sections, 2nd ed., 87 (1958).

26. Kapitzke, Capt. James
Personal Communication, May 28, 1966.

27. Kapitzke, Capt. James
Personal Communication, May 28, 1966.

9.0 APPENDICES

9.1 Appendix A: Beam Tube Measurements

9.1.1 Physical Dimensions of Beam Tubes

The physical dimensions of the beam tubes which were required for the collimator design are given in Tables IV and V. These dimensions may be used in the design of other collimators or for determining the clearance between the end of the present collimator and the end of the beam tube for use in future experiments.

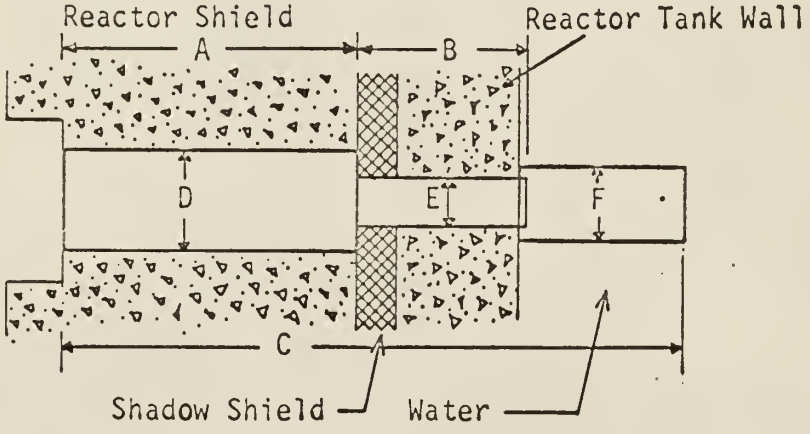

Fig. 37. Cross section of typical beam tube

Table IV. Longitudinal Dimensions of Beam Tubes

Beam tube	Dimension (in inches)		
	A	B	C
S.E.	64	30-1/4	112-1/8
N.E.	64-1/4	29-7/8	110-15/16
N.W.	64-1/4	30-1/4	111-1/4
S.W.	64-1/4	29-7/8	110-15/16

General Atomic (19) gives the inside diameters for all four beam tubes as follows.

Table V. Inside Diameters of Beam Tubes

Dimension	Value in inches
D	8 (nominal)
E	6.065
F	6.315

9.1.2 Summary of Radiation Survey Measurements from Open Beam Ports

9.1.2.1 Direct Beam

These measurements are included to allow the reader to gain an idea of the radiation hazard involved with the direct beam from a reactor beam port. Measurements are given for a completely open beam port as well as a collimated beam.

Dose rate measurements taken by placing dosimeters in the collimated radiation beam yield results which are in reasonable agreement with those in Table VI. For this series of measurements, two neutron and gamma sensitive dosimeters and two gamma sensitive dosimeters were held with tongs in the collimated radiation beam. An attempt was made to time the irradiation so that the dosimeters would reach mid-scale regardless of reactor power level. Two additional neutron and gamma sensitive dosimeters were irradiated at the maximum power level. These

Table VI. Measurements of Direct Radiation Beams from Completely Open Beam Ports

Beam tube	Power level (watts)	Neutrons			Gamma (mr/hr)
		Hurst detector		Nemo (mrem/hr)	
		Fast* (cps)	Slow** (cps)		
S.E.	1			5.6	3
	5			25	10
	15			77	30
	50			280	100
	150			860	300
	500			---	800
N.E.	1	13	400	75	24
	5	160	1000	380	70
	10			780	100
N.W.	1			11	10
	5			52	30
	15			130	70

*Multiply by 1 to obtain mrem/hr.

**Multiply by .08 to obtain mrem/hr.

measurements are shown in Fig. 38. It would appear that the two gamma sensitive dosimeters were not irradiated for the proper length of time at 96 kw.

In order to compare the dosimeter measurements with those in Table VI, a correction must be made for the radiating area as seen by the detector. The magnitude of this correction has been calculated to be 40 (26). If the total dose rate from the three beamports as given in Table VI is extrapolated to a reactor power level of 100 kw and then divided by the radiating area correction factor, the dose rates shown in Table VII are obtained.

Table VII. Collimated Beam Total Dose Rates for a Reactor Power Level of 100 kw

Beamport	Dose rate (rem/hr)
S.E.	19
N.E.	220
N.W.	30

If calculations are made of the separate contributions to the dose rate from both the gammas and the neutrons, it is seen that while the gamma dose rate agrees to within 50% of the dosimeter data, the corresponding value for the neutron dose rate does not. This is rather easily explained since the dosimeters which were used are only sensitive to thermal neutrons while the NEMO measures dose rates for all energy neutrons.

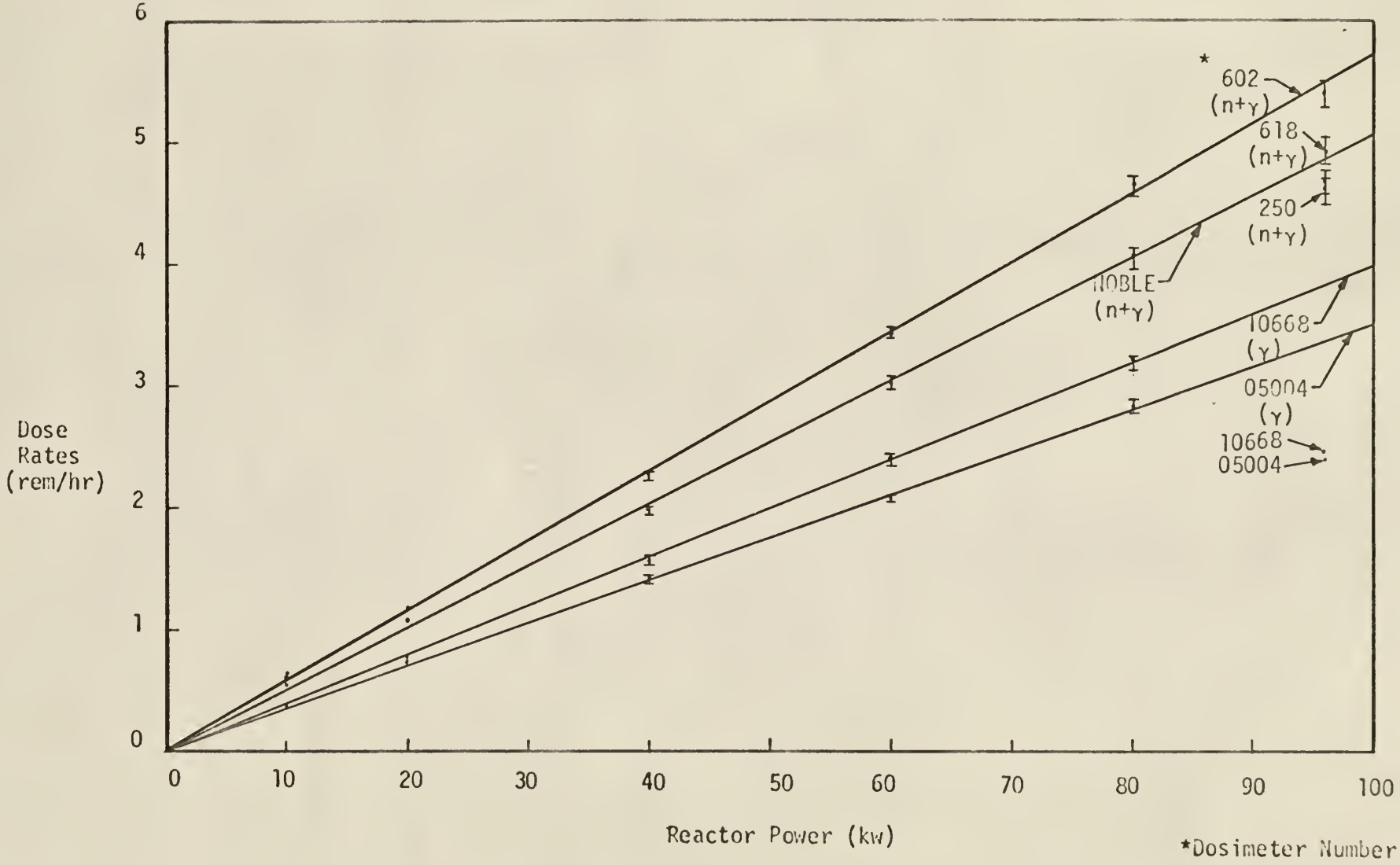

Fig. 38. Dose rates from collimated beam at S.E. beamport

9.1.2.2 Scattered Radiation Dose Rates

Positive control procedures make the possibility of operating the KSUTMII reactor with accidentally opened beam tubes vanishingly small. In order to gain an idea of the order of magnitude of the radiation levels involved in such an occurence, it was deemed desirable to operate the reactor in such a condition. The shielding plugs were completely removed from the N.E. beam tube and the reactor bay evacuated. The power level was raised in steps as determined by the radiation safety officer and the reactor supervisor. Measurements were then carefully taken at selected points within the reactor bay. These measurements are given in Table VIII.

Because of the limited space between the N.E. beam port and the shielding wall for the neutron generator room, it was decided to investigate the possibility of using this wall for a beam catcher. Since a fast neutron scattering experiment was already in progress at this beam port, the graduate student involved was prevailed upon to calculate a dose rate from his data. The particular geometry for his experiment is given in Fig. 39.

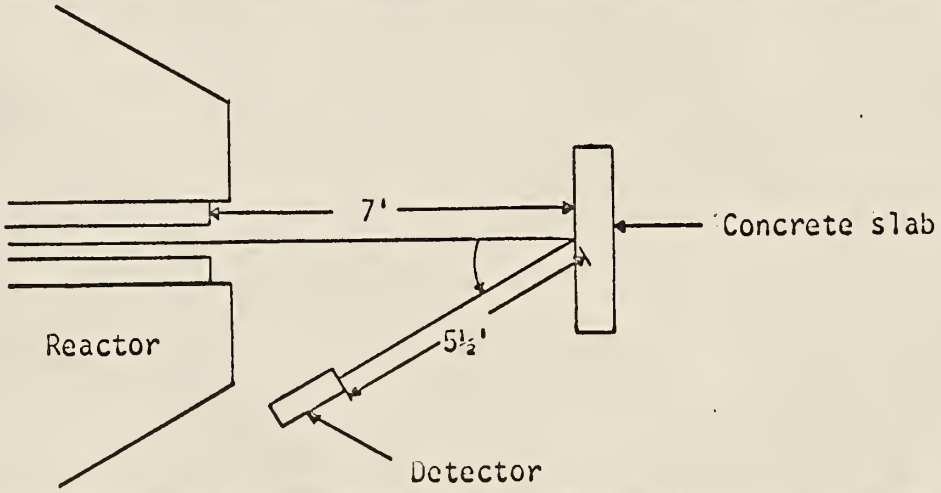

Fig. 39. Experimental arrangement for the determination of the dose rate from fast neutrons backscattered from a concrete slab

Table VIII. Radiation Levels in Reactor Bay with Unplugged Collimator in N.E. Beamport

Position	Power (kw)			
	.1	1.	10.	25.
Gamma dose in[a] direct beam	- 2.	- 10.	- 40.	- -
2 feet north of beam	12. 1.5[b]	64. 100.	600. -	- -
neutron generator console	3.5 .75	50. 10.	400. 200.	- -
east corner of loading dock	.46 .1	3.8 .12	50. .9	100. 16.
desks in N.W. corner	.7 .025	5.5 .08	30. 1.9	94. 13.
control room wall	.17 .08	.55 .06	25. .9	40. 5.5
22 foot level N.E. corner	.32 .1	3. .13	180. 1.15	140. 65.
Secondary water tank	1. .025	3. .05	18. 3.5	52. 8.5
Barnstead still	.6 .025	.5 .025	1.8 .13	4.8 .9
N.E. corner of bay, at wall	- -	- 1.2	- 110.	500. -

[a]These readings only in R/hr.

[b]Top reading is neutron dose rate in mrem/hr.
Bottom reading is gamma dose rate in mr/hr.

The results thus obtained (27) are given in Table IX. One of these positions was checked with a film badge. The low dose obtained yielded inconclusive results. As a result of the values obtained in Table IX, it was decided to use a beam catcher. The beam catcher finally used for this beam port consisted of the detector shield used to obtain the results in Fig. 39.

Table IX. Fast Neutron Dose Rate Measurements of Radiation Scattered from a Concrete Slab (Reactor Power is 10 kw)

α	Fast neutron dose rate (mrem/hr)
19	21.6
33	20.4
44	15.4
52	13.4
60	11.8
67	10.4
73	8.28
80	4.60

Table X shows a survey taken in the vicinity of the neutron spectrometer at the S.E. beam port. Surveys have been carried out for the operation at N.E. and N.W. beam ports as well. Since they all yield nearly the same results, only the one is included here.

Table X. Survey around Neutron Spectrometer at S.E. Beamport

Power level	Gamma (mr/hr)	Fast neutrons (cps)	Slow neutrons (cps)	Location
10 kw	.5-4			at crystal and beam exit
	15	20	600	front of beam catcher (20' from port)
	2	< 1	< 1	back of beam catcher
	< 1	< 1	< 1	periphery, at rope
50 kw	3-5	2	20	at face of beamport
	3-5	2	40	Rowland's position[a]
	70	30	1000	front of beam catcher
	7	< 1	< 1	back of beam catcher
100 kw	110	40	off scale	front of beam catcher
	13	2	7	back of beam catcher
	5	3	40	Rowland's position[a]
	2	-	10	periphery
	1	2	10	at instrumentation table

[a]This position is that occupied by the experimenter when making adjustments to the crystal as per section 3.4.

Nuclear Chicago Ion Chamber was used for gamma detection. The n, γ reaction may have helped to increase the gamma dose rate level.

The RCL counter (N.E. No. 585) was used for neutron detection. To convert fast neutrons to mrem/hr, multiply by one (1); to convert slow neutrons to mrem/hr, multiply by .08.

John P. Lambert
Radiation Safety Officer
12/1/65

9.1.3 Cadmium Ratio

Very simple measurements of the cadmium ratio were made at the S.E. and N.E. beamports. The values obtained were 47 and 17, respectively. These measurements were taken only as a matter of curiousity, but should be accurate to within 30%.

9.2 Appendix B: Activation of Surplus Lead Samples

Two lead samples were obtained through State Surplus in Topeka. A one minute irradiation was found to be sufficient for the .6 gram samples used. The reactor power level was 100 kw and the flux at the point of irradiation (rotary specimen rack) was approximately 7×10^{11} n/cm^2-sec. The results are given in Table XI.

Two slightly larger samples (obtained from the same sources) were irradiated in the AECL GAMMA CELL for nearly 24 hours. No evidence of photoactivation was observed.

A saturation activity test was run on a .25 gram sample of the surplus lead. The power level was 100 kw and the irradiation took place first in the rabbit and then in the rotary specimen rack. Saturation seemed to occur after five minutes. This test was only continued for 40 minutes. The saturation activity without the beta shield was 75 mr/hr. This reading was taken within five minutes after the sample was removed from the reactor.

From the results shown in Table XI, it may be seen that there are at least two different isotopes involved. One of these is short lived (5-10 minute half life or less) and is probably a beta or a weak gamma emitter. One-eighth inch of aluminum plus 1-1/2 inches of air were sufficient to reduce the saturation activation reading of 75 mr/hr to 4 mr/hr.

The other isotope apparently has a half life of about 2 1/2 days and is also a beta or very weak gamma emitter.

From the half life data, it is obvious that the saturation activity test was not continued long enough to produce a complete result. It does tend to

indicate, however, that the half life of the short lived isotope is more on the order of 1-2 minutes than 5-10 minutes. Consultation of appropriate half life data indicates that the impurity is likely to be antimony.

Table XI. Decay History of Activated Surplus Lead Samples

Date	Time	Sample	Readings outside rabbit without beta shield	With beta[b] shield	Without beta[b] shield
8/2/65	2:10pm	surplus	50[a]	--	--
	2:12pm	site	>200	--	--
	3:15pm	surplus	11.5	6.5	130
	3:15pm	site	11.5	9	120
	7:15pm	surplus	10.5	6	125
	7:15pm	site	9	6	125
8/3/65	2:55pm	surplus	5.5	5	110
	2:55pm	site	6.5	5.5	100
8/4/65	3:50pm	surplus	5.5	4.5	105
	3:50pm	site	4.5	4	90
8/15/65	7:40pm	surplus	.5	.6	5.5
	7:40pm	site	.7	.6	5

[a]All readings in mr/hr taken with a standard geiger survey meter.

[b]Sample was placed next to the detector.

9.3 Appendix C: Collimator Effectiveness and Safety

The measurements contained within this appendix show that the collimator provides excellent collimation for thermal neutrons. They also prove that the collimator shielding plugs allow the reactor to be operated at full licensed power with a plugged collimator in place without producing any significant radiation hazard. It has also been demonstrated that the absence of shielding plugs in the collimator may readily be detected by the reactor operator even though the outer beamport door is closed, provided the RAM probes for the beamports are placed in the proper positions.

The effectiveness of the collimator for thermal neutrons was determined by moving a small vertical BF_3 probe horizontally across the collimated neutron beam at a constant velocity. The data were accumulated by a TMC GAMMA SCOPE operating in the multiscaler mode. The timing of the multiscaler was one channel per second and the traversing mechanism traveled at one inch per minute. Although the diameter of the BF_3 probe was .3 inch, no correction for this was made in the final data since only an estimation of the flux profile was desired. Fig. 40 gives results for probe to snout distances of two and six feet. These results agree quite well with values calculated using geometrical considerations.

Table XII shows radiation measurements indicating the effectiveness of the collimator shielding plugs. The collimator was placed in the N.E. beamport since this beamport provides the maximum gamma and fast neutron dose rates. With both collimator plugs in place and the safety shutter and the outer door closed, the maximum dose rate around the beamport is less than 2 mr/hr.

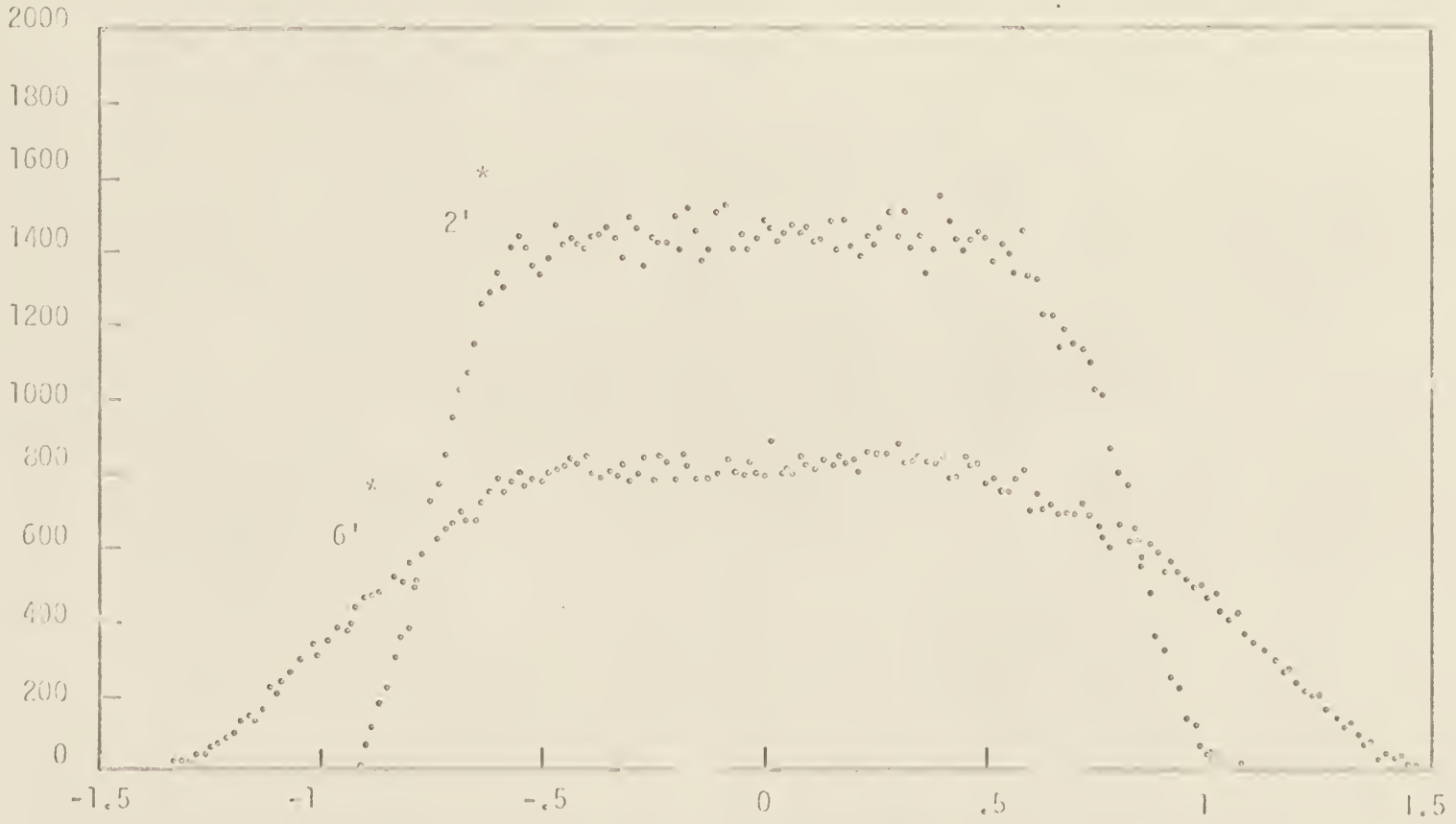

Fig. 40. Neutron profiles for collimated beam

Table XIII shows the RAM readings as a function of reactor power level. To obtain these measurements, the collimator was placed in the S.E. beamport without its internal shielding plugs and the outer door of the beamport locked. The RAM probe was hung on the outside of the door and the readings in the control room noted as the reactor was brought up to power. At the maximum power in each series, a rough survey was taken of the immediate area near the door. Two different series were taken, one with the safety shutter open and one with it closed. Also, the effect of placing the RAM probe in different positions on the door was noted. As a result of these measurements, it is suggested that all beamport RAM probes be hung on the beamport doors as indicated by position 1 in Fig. 41. This position placed the detector closest to the center of the beam tube.

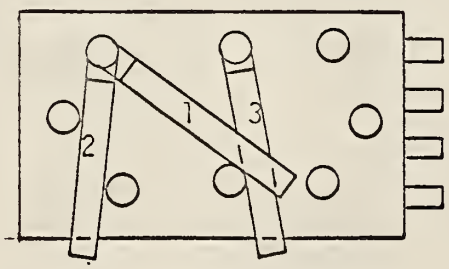

Fig. 41. Different positions for placing the RAM probe on beamport doors

Table XII. Radiation Measurements of Plugged Collimator

Condition of safety shutter and beamport door	NEMO neutron dose rate mrem/hr	Geiger survey meter gamma dose rate mr/hr
both open	4.0	8.5
both closed	.75	.15

Table XIII. RAM Readings for Unplugged Collimator in S.E. Beamport

RAM probe position[a]	Power level (kw)	RAM reading with safety shutter and door closed[b]	RAM reading with only door closed	Area survey results[c]
1	1	1		
	10	20		
	50	125		
	90	250		8
	.1		1.2	
	1		15	
	10		220	
	40		920	>100
2	40		500	
3	40		300	

[a]Refer to Fig. 41.
[b]Unless otherwise stated, all readings are in mr/hr.
[c]Combine neutron and gamma dose rates in mrem/hr.

9.4 Appendix D: Determination of the Mosaic Spread of the Diffracting Crystals

The mosaic spread of the diffracting crystals was determined by the conventional x-ray diffraction method. A calcite crystal was used to select the cobalt K_α line from a suitable x-ray tube. This monochromated beam was then directed upon the particular LiF crystal under investigation. A geiger counter was placed at the appropriate position and the LiF crystal was then slowly rotated through the Bragg angle at a constant angular velocity. The results obtained are summarized in Table XIV.

As one may see from Fig. 42, it is not surprising that there is such wide disagreement between the different values in Table XIV. The irregularities in the curve arise as a result of the small area actually being measured. It would have been more proper to use a neutron beam of large enough dimensions so that the entire face of the crystal would be illuminated. However, the equipment was not available to do this to the required accuracy.

Table XIV. Measured Mosaic Spreads and Peak Intensities of LiF Diffracting Crystals

Crystal	Surface	n(FWHM) (minutes)	Relative Peak Intensity (cpm)
(100) (#2)	cleaved	3-1/4	.78 x 200
(100) (#2)	ground	8-3/8	.83 x 500
(100) (#2)	ground	9-3/4	.70 x 500
(100) (#4)	cleaved	1-1/2	.67 x 500
(111) (#3)	sawed	12-3/4	.91 x 500
(111) (#1)	sawed	16-1/4	.76 x 500
(111) (#1)	sawed	12-1/2	.62 x 500
(111) (#1)	sawed	17-1/2	.80 x 500

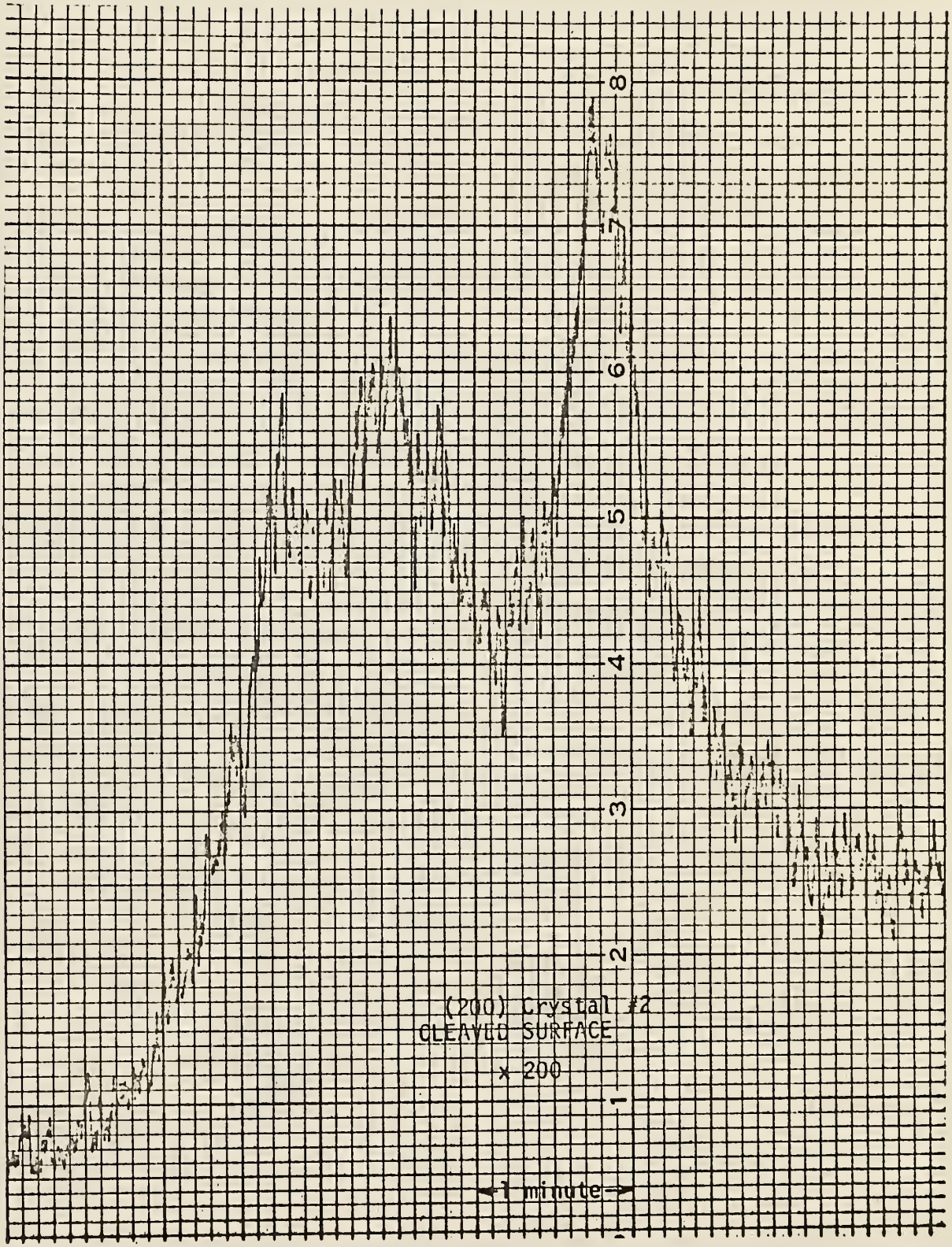

Fig. 42. Mosaic spread determination

9.5 Appendix E: Explanation of Computer Codes

9.5.1 REFLECTIVITY

The REFLECTIVITY computer code* was written to numerically integrate equation 15 as a function of diffraction angle and mosaic spread. Since this is a one-shot program, no input data is necessary. Instead, the values for the mosaic spread and the diffraction angle are contained within the program. The diffraction angle is determined in a DO loop which determines 12 different angles starting with five degrees.

The computer code consists of three parts. The first part, REFLECT, performs the following tasks:

1. computes the values of constants involving the mosaic spread and the diffraction angle,
2. computes the appropriate limits of integration,
3. sets the necessary internal switches for the subprograms, and
4. prints the final answers.** Each line of answers contains the mosaic spread, diffraction angle, and the associated integrated reflectivity.

Table XV describes the important variables contained in REFLECT. As shown, REFLECT contains the constants for a LiF (200) crystal. For a LiF (111) crystal, the following change in statement 1 + 13 should be made: V = .00604* (the rest is the same). Also, ETAA should be changed to reflect the different value of the mosaic spread.

---

*All computer codes in this work are written in FORTRAN IV for the PR-155 interpretive system on the IBM 1410 computer.

**For the proper input and output formats for all programs, refer to the appropriate program listing.

Table XV. Explanation of Selected Variables in REFLECT

Symbol	Explanation
A	A as defined in section 2.5.1
ANSWB	R as defined in equation 15
ETAA	mosaic spread in seconds
GA	lower limit of integration
GB	upper limit of integration
THETAA	diffraction angle in degrees
V	V as defined[a] in section 2.5.1

[a]The values for the structure factor used in calculating this variable are experimental values (28) rather than the theoretical values.

Table XVI. Explanation of Selected Variables in DUMMY

Symbol	Explanation
A	A as defined in section 2.5.1
T	T as defined in section 2.5.1
V	V as defined in section 2.5.1

The function subprogram, DUMMY, calculates the value of equation 15 at the points determined by the numerical integration subroutine. The important variables of DUMMY are explained in Table XVI.

GRAL is a numerical integration subroutine obtained from the KSU computing center. A complete explanation of the subroutine is available from this source.

As shown, the program requires about 40 minutes to run. The results obtained for the two different crystal planes are given in Appendix F.

```
      MON$$      JOB  REFLECTIVITY  JIM ROWLAND
      MON$$      COMT 15,5PAGES,ROWLAND,NUCLEAR ENGG
      MON$$      ASGN MJB,12
      MON$$      ASGN MGO,16
      MON$$      MODE GO,TEST
      MON$$      EXEQ FORTRAN,,,18,,,,REFLECT
       EXTERNAL DUMMY
       COMMON A,V
     1 FORMAT(3E18.8)
       IGUA=1
       GA=1.
       GAE=0.
       ETAA=9.
       ETA=ETAA*3.1415926/10800.
       THETAA=0.
       DO 10 L=1,10
       GRE=.0001
       THETAA=THETAA+5.
       THETA=THETAA*3.1415926/180.
       A=2.69/.3867
       F=SIN(THETA)
       V=.00256*.3867*F*F/(ETA*SIN(2.*THETA))
       GB=1.+2.*V
       ANS=GRAL(DUMMY,GA,GB,GAE,GRE,IGUA)
       ANSB=ETA*ANS*2.828
    10 WRITE(3,1)ETAA,THETAA,ANSB
       CALL EXIT
       END
      MON$$      EXEQ FORTRAN,,,18
       FUNCTION DUMMY(T)
       COMMON A,V
       HT=SQRT(T)
       TOP=EXP(2.*A*HT)-1.
C$$$$$ DENOM OF LOG CHANGED TO AVOID TAKING LOG(U/0)
       BOT=(T+1.)*TOP*ALOG(2.*V/(T-.999999))+4.*HT*(TOP+2.)
       DUMMY=TOP/BOT
       RETURN
       END
      MON$$      EXEQ FORTRAN,,,18
       FUNCTION GRAL(DUMMY,GA,GB,GAE,GRE,IGUA)
C      THIS FUNCTION COMPUTES THE INTEGRAL OF THE FUNCTION GIVEN
C     1AS A FUNCTION TYPE SUBPROGRAM IN THE CALLING STATEMENT
C     2FROM GA TO GB WITH AN ABSOLUTE ACCURACY OF GAE AND A
C     3RELATIVE ACCURACY OF GRE.
C      IGUA=0 FOR A NORMAL INTERGRATION, IGUA=1 FOR AN
C     1EXTENSION OF A PREVIOUS INTERGRATION.
       DIMENSION GW(5)
 1041 FORMAT(1X,44HB IS NOT GREATER THAN PRESENT VALUE OF GXMOM)
 1042 FORMAT(1X,23HB IS NOT GREATER THAN A)
 1043 FORMAT(1X,14HH IS TOO SMALL,5X,6HXMOM =,1PE18.7,5X,3
     2HH =,F18.7)
```

```
C       BEGIN
        GRAL = 0.0
 1000 IF(IGUA)1001, 1001, 1003
 1001 IF(GB-GXMOM)1002, 1002, 1009
 1002 WRITE(3,1041)
 1044 RETURN
 1003 IF(GB-GA)1004, 1004, 1005
 1004 WRITE(3,1042)
        GO TO 1044
 1005 GRAL = 0.0
        GXMOM = GA
        GMAMI = 0.0
        GXMAX = GA
        GHXMA = 0.0
        GSIGM = 0.0
        GFXMO = DUMMY(GA)
        GHSUG = 0.25*(GB-GA)
 1009 IGSWA = 0
        GHMMI=0.025*(GB-GXMOM)*GRE
C       STOP
 1012 IF(GHSUG-GHMMI)1013, 1014, 1014
 1013 GHSUG = GHMMI
 1014 GH = GHSUG
        IGSWB = 0
        IF(GXMOM+4.*GH-GB)1016, 1015, 1015
 1015 GH = 0.25*(GB-GXMOM)
        IGSWA = 1
C       YET ONE
 1016 GX = GXMOM
        GW(1) = GFXMO
        DO 1020  IGK=2,5
        IF(IGK-5)1019, 1017, 1017
 1017 IF(IGSWA)1019, 1019, 1018
 1018 GW(IGK) = DUMMY(GE)
        GO TO 1020
 1019 GX = GX+GH
        GW(IGK) = DUMMY(GX)
 1020 CONTINUE
        GMID = (14.*(GW(1)+GW(5))+64.*(GW(2)+GW(4))+24.*GW(3))/45.
        GDELT=ABS((2.*(GW(1)+GW(5))+8.*GW(3))/3.-GMID)
        GAMID = ABS(GMID)
        GEPS = GAMID*GRE+GAE
        IF(GDELT-GEPS)1026, 1027, 1027
 1026 IGSWB = 1
 1027 IF(IGSWA)1029, 1029, 1028
 1028 IF(IGSWB)1029, 1029, 1038
 1029 GHSUG = (GEPS/(GEPS+GDELT)+0.45)*GH
        IF(IGSWB)1030, 1030, 1038
 1030 IF(IGSWA)1033, 1033, 1031
 1031 IF(GH-GHMMI)1037, 1037, 1032
 1032 IGSWA = 0
 1033 IF(GHSUG-GHMMI)1035, 1034, 1034
 1034 GH = GHSUG
```

```
      GO TO 1016
 1035 IF(GH-GHMMI)1036, 1037, 1036
 1036 GH = GHMMI
      GO TO 1016
 1037 CONTINUE
 1038 IF(GAMID-GMAMI)1040, 1040, 1039
 1039 GMAMI = GAMID
      GXMAX = GXMOM
      GHXMA = GH
 1040 GRAL = GRAL+GH*GMID
      GXMOM = GX
      GFXMO = GW(5)
      GSIGM = GSIGM+GDELT*GH
      IF(IGSWA)1012, 1012, 1044
      END
     MON$$     EXEQ LINKLOAD
               CALL REFLECT
     MON$$     EXEQ REFLECT,MJB
     MON$$     JOB  ACT$$    JIM ROWLAND    NE          0093U4041
```

9.5.2 SPECTRUM

The SPECTRUM computer code was written to apply the necessary correction factors to the raw data obtained from the neutron spectrometer. After all corrections have been applied, the data is normalized so that the magnitude of the experimental point at the most probable velocity is unity. Equation 6 is then fitted to this normalized experimental data between selected points using a least-squares technique.

SPECTRUM consists of two parts, DATA and SUMSQ. SUMSQ calculates the squares of the deviations between a trial theoretical curve and the normalized experimental points. DATA computes everything else.

Data is read by the program in the following order:

1. A card giving the number of descriptive cards
2. Several descriptive cards
3. A card giving the number of data points
4. A card giving the number of the beginning point for the least-squares fit
5. A card giving the number of the ending point for the least-squares fit
6. Cards giving the arm positions for the data (as determined from the spectrometer calibration ring)
7. Cards giving the data channel counts
8. Cards giving the monitor channel counts
9. A card giving the number of background points

10. Cards giving the background arm angles
11. Cards giving the background data channel counts
12. Cards giving the background monitor channel counts, and
13. A card giving the time taken for some number of monitor counts, that number of monitor counts, and the resolving time of the counter.

Two different forms of output are obtained, i.e., punched cards and printed output. The punched cards are in a form to be used with a suitable plotting program.* This output is in the following form:

1. A card giving the number of descriptive cards
2. Several descriptive cards
3. A card giving the number of data points, and
4. Cards giving velocity, normalized experimental countrate, energy, and theoretical countrate.

The printed output consists of the following:

1. A listing of the descriptive cards
2. The value of the first guess at K_1 in equation 6
3. The value of the first guess at v_o as given in equation 6
4. A table containing many pertinent values, each of which is identified by an appropriate table heading, and
5. The least-squares fitted constants for K_1 and v_o above.

The important variables used in DATA are explained in Table XVII.

The execution times for SPECTRUM are highly variable, being between 5 and 20 minutes per data set. A long execution time generally indicates a poor initial guess at either v_o or K_1.

Table XVII. Important Variables in DATA

Symbol	Explanation
ACOUNT	an array containing the corrected normalized experimental data
AINC	the present value of the increment for changing K_1
AMAX	the normalizing value for K_1
ANTER	an array containing the geometrical correction factor as described in section 2.5.2
ARM	an array containing the arm positions for the data points
B	conversion factor from degrees to radians
BARM	an array containing the background arm positions
BCOUNT	an array containing the theoretical values for the leakage spectrum
BG	an array containing the data channel counts for the background
BGM	an array containing the monitor channel counts for the background
BINC	the present value of the increment in the v_o
CHECK	an array containing the monitor channel counts for the data
CONST	1.
CORR	C(v) as defined in section 2.7
DEAD	the resolving time of the data channel counting system in microseconds
EFF	an array containing the detector efficiency for the data channel BF_3 probe
ENERGY	neutron energy

Table XVII. (continued)

Symbol	Explanation
IZ	a counter for determining the number of iterations in the curve-fitting procedure
L	the first data point to be fitted to the theoretical curve
LA	the last data point to be fitted to the theoretical curve
MON	the monitor counts for the resolving time correction
N	the number of data points
NB	the number of background points
NR	the number of descriptive cards
REF	the crystal reflectivity as described in equation 16a
SAINC	the initial value of the K_1 increment
SBINC	the initial value of the v_o increment
SUM	the sum of the square of the deviations between the theoretical and experimental points
SUMA	the previous value for SUM
THEORY	an array containing the final theoretical points for the spectrum
THETA	an array containing the arm angles for the data
TIME	the resolving time of the data channel counting system
VEL	an array containing the neutron velocities for the corresponding arm angles
WAVE	an array containing the neutron wavelengths for the corresponding arm angles
XCOUNT	an array containing the data channel counts for the data
ZERO	the zero point of the spectrometer calibration ring

```
      MON$$       JOB  SPECTRUM
      MON$$       COMT SAVE PUNCHED CARDS
      MON$$       COMT 15 MINUTES,07 PAGES
      MON$$       ASGN MJB,12
      MON$$       MODE GO,TEST
      MON$$       ASGN MGO,16
      MON$$       EXEQ FORTRAN,,,,,,,,DATA
       REALMON
C      N SHOULD NOT EXCEED 75
C      THIS PROGRAM GOOD FOR 200 PLANE ONLY
       DIMENSIONARM(75),VEL(75),WAVE(75),ENERGY(75),REF(75),E
      1FF(75),ANTER(75),CORR(75),THEORY(75),BCOUNT(75),THETA(75),
      2ACOUNT(75),XCOUNT(75),CHECK(75)
       DIMENSIONBARM(75),BG(75),BGM(75)
       DIMENSIONCHI(21)
       DIMENSIONSUMSQA(2)
       COMMONVEL,BCOUNT,ACOUNT
       EQUIVALENCE(BCOUNT(1),THETA(1))
       EQUIVALENCE(CHECK(1),ANTER(1))
       EQUIVALENCE(BARM(1),VEL(1)),(BG(1),WAVE(1)),(BGM(1),ENE
      1RGY(1))
     1 FORMAT(I3)
     2 FORMAT(5F6.0)
     3 FORMAT(1H1,1X,9HARM ANGLE,2X,8HVELOCITY,2X,10HWAVELENGTH
      1,2X,6HENERGY,2X,12HREFLECTIVITY,3X,9HDET.EFF.,2X,12HINTE
      1RCEPTION,2X,10HCORRECTION,2X,12HEXPERIMENTAL,3
      1X,11HTHEORETICAL)
     4 FORMAT(3X,7HDEGREES,5X,5HM/SEC,4X,9HANGSTROMS,4X,2HEV,4X
      1,2HEV,4X,13H=1 AT2200M/S,3X,7HPERCENT,3X,12H1/2 IN.
      1BEAM,4X,6HFACTOR,4X,11HCOUNTS/M IN.,4X,11HCOUNTS/MIN./)
     5 FORMAT(F9.2,F12.0,F9.3,E11.4,F10.3,F13.3,2F14.5,F12.5,F1
      14.6)
     6 FORMAT(5F11.4)
     7 FORMAT(5F9.0)
     8 FORMAT(1H1,9HCONSTANT=,E14.7/1X,17HMAXIMUM VELOCITY=,F6.0)
     9 FORMAT(1X,79H
      1                                                    )
    10 FORMAT (1H1)
    11 FORMAT(I5)
    12 FORMAT(E14.7)
    13 FORMAT(4E14.8)
       J=0
       KA=0
C      N IS THE NUMBER OF OBSERVATIONS
C      L IS THE NUMBER OF THE FIRST POINT TO FIT
C      LA IS THE NUMBER OF THE LAST POINT TO FIT
       READ(1,1)NR
       WRITE(2,1)NR
       WRITE(3,10)
       DO22I=1,NR
       READ(1,9)
       WRITE(3,9)
    22 WRITE(2,9)
       READ(1,1)N,L,LA
       K=L
       WRITE(2,11)N
       READ(1,2)ZERO
       READ(1,2)(ARM(I),I=1,N)
       READ(1,2)(XCOUNT(I),I=1,N)
       READ(1,2)(CHECK(I),I=1,N)
       READ(1,1)NB
       READ(1,2)(BARM(I),I=1,NB)


       READ(1,2)(BG(I),I=1,NB)
       READ(1,2)(BGM(I),I=1,NB)
       READ(1,7)TIME,MON,DEAD
```

```
      DTIME=MON*DEAD/TIME
      DO37I=1,NB
   37 BG(I)=BG(I)/BGM(I)
      I=NB
      BARM(I+1)=BARM(I)+BARM(I)-BARM(I-1)
      BG(I+1)=BG(I)+(BG(I)-BG(I-1))*(BARM(I+1)-BARM(I))/(BARM(
     1I)-BARM(I-1))
      DO43I=1,N
      XCOUNT(I)=XCOUNT(I)/CHECK(I)
   43 XCOUNT(I)=XCOUNT(I)*(1.+XCOUNT(I)*DTIME)
      DO54I=1,N
      J=1
   46 IF(BARM(J)-ARM(I))51,47,49
   47 XCOUNT(I)=XCOUNT(I)-BG(J)
      GOTO54
   49 J=J+1
      GOTO46
   51 IF(J.EQ.1)GOTO47
      J=J-1
   53 XCOUNT(I)=XCOUNT(I)-(BG(J+1)-BG(J))*(ARM(I)-BARM(J))/(BA
     1RM(J+1)-BARM(J))-BG(J)
   54 CONTINUE
      AN=(6.02E23)*57.6/(76.0*22.4E03)
      B=3.1415926/180.
      DO70I=1,N
      THETA(I)=(ARM(I)-ZERO)/4.
      SAB=SIN((THETA(I))*B)
      WAVE(I)=4.01*SAB
      VEL(I)=982./SAB
      ENERGY(I)=5.04E-03/(SAB*SAB)
      A=(8.+13.*EXP(-2.6*.0081/(ENERGY(I)**4)))/8.
      REF(I)=(.50268+3.3083E-06*(THETA(I)**2.816))/VEL(I)
      EFF(I)=1.-EXP(-AN*(3840.E-24)*50.8*SQRT(.025/ENERGY(I)))
      ANTER(I)=1.
      IF(SAB.GE..25)GOTO69
      ANTER(I)=4.*SAB
   69 CORR(I)=REF(I)*EFF(I)*COS(THETA(I)*B)*ANTER(I)*VEL(I)*VE
     1L(I)*A
   70 ACOUNT(I)=XCOUNT(I)/CORR(I)
      AMAX=ACOUNT(L)
      DO76J=L,LA
      IF(AMAX-ACOUNT(J))74,76,76
   74 AMAX=ACOUNT(J)
      K=J
   76 CONTINUE
      DO78I=1,N
   78 ACOUNT(I)=ACOUNT(I)/AMAX
   79 CONST=ACOUNT(K)/((VEL(K)**3)*EXP(-(1.225)**2))
      WRITE(3,12)CONST,VEL(K)
      IK=0
      SBINC=2.
      CONSTA=CONST
      CONSTB=VEL(K)
   85 AINC=CONSTA/100.
      IZ=IZ+1
      IF(IZ.GE.6)GOTO114
      SAINC=AINC
      BINC=0.
      GOTO93



   91 BINC=SBINC
      AINC=0.
   93 JQ=0
   94 CALLSUMSQ(CONSTA,CONSTB,L,LA,SUM)
   95 CONSTA=CONSTA+AINC
      CONSTB=CONSTB+BINC
      SUMA=SUM
```

```
      CALLSUMSQ(CONSTA,CONSTB,L,LA,SUM)
      IF(SUMA.EQ.SUM)GOTO106
      IF(SUMA.GT.SUM)GOTO95
  101 IF(JQ.EQ.1)GOTO106
      AINC=-AINC
      BINC=-BINC
      JQ=1
      GOTO95
  106 IF(AINC.EQ.0.)GOTO108
      GOTO91
C     IF(ABS(AINC)-(SAINC/100.))37,37,48
  108 IF(BINC.EQ.0.)GOTO110
      GOTO85
C     IF(ABS(BINC)-(SBINC/100.))36,36,48
  110 AINC=-AINC/10.
      BINC=-BINC/10.
      JQ=0
      GOTO95
  114 I=1
  115 IF(I.EQ.1)GOTO123
      IF(I.EQ.72)GOTO123
  117 THEORY(I)=CONSTA*(VEL(I)**3)*EXP(-(1.225*VEL(I)/CONSTB)*
     1*2))
      IF(I.GT.N)GOTO126
      WRITE(2,13)VEL(I),ACOUNT(I),ENERGY(I),THEORY(I)
      WRITE(3,5)ARM(I),VEL(I),WAVE(I),ENERGY(I),REF(I),EFF(I),
     1ANTER(I),CORR(I),ACOUNT(I),THEORY(I)
      I=I+1
      GOTO115
  123 WRITE(3,3)
      WRITE(3,4)
      GOTO117
  126 CONTINUE
      WRITE(3,8)CONSTA,CONSTB
      CALLEXIT
      END
     MON$$      EXEQ FORTRAN,,,,,,,SUMSQ
      SUBROUTINESUMSQ(CONSTA,CONSTB,L,LA,SUM)
      COMMONVEL(75),BCOUNT(75),ACOUNT(75)
    1 FORMAT(3E14.7)
      SUM=0.
      DO5I=L,LA
      BCOUNT(I)=CONSTA*(VEL(I)**3)*EXP(-(1.225*(VEL(I))/CONSTB
     1)**2)
    5 SUM=SUM+(BCOUNT(I)-ACOUNT(I))**2/ACOUNT(I)
      RETURN
      END
     MON$$      EXEQ LINKLOAD
                CALL DATA
     MON$$      EXEQ DATA,MJB
```

9.5.3 CROSS SECTION

The CROSS SECTION computer code was written to process data obtained from beryllium total neutron cross section measurements. This program is written for measurements taken using beryllium discs and a LiF (111) crystal. In order to determine cross sections of other materials or to use other diffraction crystals, some of the internal constants in the program must be changed.

The program is rather straight forward. Down to, and including, statement 38, the data is merely read into the computer and the background subtracted.

The data input is similar in nature to that in the SPECTRUM computer code. The input is given in the following form:

1. A card giving the total number of data points
2. A card giving the location of the zero point as determined from the spectrometer calibration ring
3. Cards giving the arm positions for the data as indicated by the spectrometer calibration ring
4. Cards giving the data channel counts for the beryllium attenuated neutron beam
5. Cards giving the monitor channel counts for the beryllium attenuated neutron beam
6. Cards giving the data channel counts for the unattenuated beam
7. Cards giving the monitor channel counts for the unattenuated beam

8. Cards giving the thickness of the beryllium discs (in numbers signifying the total thickness in eighths of an inch) for each different arm position
9. A card giving the number of background data points
10. Cards giving the arm positions for the background as indicated on the spectrometer calibration ring
11. Cards giving the data channel counts for the background, and
12. Cards giving the monitor channel counts for the background.

The output consists of punched cards which are suitable for use with PLOT (see section 8.5.2) and a printed listing. The punched cards come out in the following form:

1. A card giving the number of data points, and
2. Cards giving the computed value for the total neutron cross section and the corresponding velocity.

The printed output consists of a table (with column headings) listing arm position, corresponding neutron velocity, wavelength, and energy, and the total neutron cross section.

The important variables contained within CROSS SECTION are summarized in Table XVIII.

Table XVIII. Important Variables Contained in CROSS SECTION

Symbol	Explanation
ACOUNT	an array containing normalized unattenuated beam data
ARM	an array containing arm positions for data
AZERO	the zero position of arm
BARM	an array containing arm positions for background
BG	an array containing data channel counts for background
BGM	an array containing monitor channel counts for background
DATA	an array containing data channel counts for Be attenuated beam
DMON	an array containing monitor channel counts for Be attenuated beam
ENER	neutron energy in eV
N	number of data points
NB	the number of background points
SIGMA	the total neutron cross section in barns
VEL	neutron velocity in meters per second
WAVE	neutron wavelength in angstroms
XCOUNT	an array containing normalized attenuated beam data

```
      MON$$      JOB  CROSS SECTION
      MON$$.     COMT 15,5,ROWLAND,NE
      MON$$      ASGN MGO,16
      MON$$      ASGN MJB,12
      MON$$      MODE GO
      MON$$      EXEQ FORTRAN,,,,,,,ROWLAND
       DIMENSIONDATA(100),DMON(100),RDATA(100),RDMON(100)
      1,THICK(100),ARM(100),XCOUNT(100),BG(100),BGM(100)
       DIMENSIONBARM(100),BG(100),BGM(100)
     4 FORMAT(I3)
     5 FORMAT(5F6.0)
     6 FORMAT(1H1,1X,9HARMANGLE,2X,8HVELOCITY,2X,10HWAVELENGTH
      1,2X,6HENERGY,5X,5HSIGMA)
     8 FORMAT(5X,3HCM.,7X,5HM/SEC,4X,9HANGSTROMS,4X,2HEV,8X,
      15HBARNS)
    10 FORMAT(F9.2,F12.0,F9.3,F11.4,F10.3)
     1 FORMAT(2E14.8)
C      TOTAL CROSS SECTION FOR BERYLLIUM USING LIF (111) CRYSTAL
       READ(1,4)N
       READ(1,5)AZERO
       READ(1,5)(ARM(I),I=1,N)
       READ(1,5)(DATA(I),I=1,N)
       READ(1,5)(DMON(I),I=1,N)
       READ(1,5)(RDATA(I),I=1,N)
       READ(1,5)(RDMON(I),I=1,N)
       READ(1,5)(THICK(I),I=1,N)
       READ(1,4)NB
       READ(1,5)(BARM(I),I=1,NB)
       READ(1,5)(BG(I),I=1,NB)
       READ(1,5)(BGM(I),I=1,NB)
       DO16I=1,N
       XCOUNT(I)=DATA(I)/DMON(I)
    16 ACOUNT(I)=RDATA(I)/RDMON(I)
       DO18I=1,NB
    18 BG(I)=BG(I)/BGM(I)
       CONST=8./(.1236*2.54)
       B=3.1415926/180.
       WRITE(3,6)
       WRITE(3,8)
       WRITE(2,4)N
       BARM(NB+1)=BARM(NB)*2.-BARM(NB-1)
       BG(NB+1)=BG(NB)+(BG(NB)-BG(NB-1))*(BARM(NB+1)-BARM(NB))/
      1(BARM(NB)-BARM(NB-1))
       DO38I=1,N
       J=1
    28 IF(BARM(J)-ARM(I))34,29,32
    29 XCOUNT(I)=XCOUNT(I)-BG(J)
       ACOUNT(I)=ACOUNT(I)-BG(J)
       GOTO38
    32 J=J+1
       GOTO28
    34 IF(J.EQ.1)GOTO29
       J=J-1
    36 XCOUNT(I)=XCOUNT(I)-(BG(J+1)-BG(J))*(ARM(I)-BARM(J))/
      1(BARM(J+1)-BARM(J))-BG(J)
       ACOUNT(I)=ACOUNT(I)-(BG(J+1)-BG(J))*(ARM(I)-BARM(J))/(
      1BARM(J+1)-BARM(J))-BG(J)
    38 CONTINUE
       DO46I=1,N
       SIGMA=(CONST/THICK(I))*ALOG(ACOUNT(I)/XCOUNT(I))
       SAB=SIN((ARM(I)-AZERO)*B/4.)
       WAVE=4.64*SAB
       VEL=851./SAB
       ENER=3.78E-03/(SAB*SAB)
       WRITE(2,1)VEL,SIGMA
```

```
46 WRITE(3,10)ARM(I),VEL,WAVE,ENER,SIGMA
   CALLEXIT
   END
MON$$,,    EXEQ LINKLOAD
           CALL ROWLAND
MON$$      EXEQ ROWLAND,MJB
```

9.0 Appendix F: Determination of an Empirical Equation for Integrated Reflectivity

The solutions to equation 15 as generated by the REFLECTIVITY computer program (see Appendix E for explanation of this program) are given in Table XIX.

As indicated in section 2.5.1, let us try to fit the above data in Table XIX with an empirical equation of the following form:

$$\frac{R^{\theta}}{\sin\theta} = D + H\theta^{k}. \tag{16a}$$

In order to evaluate the three empirical constants, D, H, and k, three different values of θ were chosen, i.e., 15^{o}, 35^{o}, and 50^{o}. Thus, three simultaneous equations in three unknowns were obtained which were then solved by conventional methods. The values for the constants found in this manner are given in Table XX.

The approximation is thus accurate to about 3% of the desired value for both planes and for the range of the tables, and accurate to about 1/2% within the range of the data taken in these experiments.

Table XIX. Summary of Results from REFLECTIVITY Computer Program

Diffraction angle	R^0 (minutes)x 10^3		$R^\theta/\sin\theta$ (minutes)x 10^3	
	111 plane	200 plane	111 plane	200 plane
5	.10304	.043841	1.1822	.50299
10	.20501	.087542	1.1806	.50413
15	.30754	.13179	1.1882	.50920
20	.41231	.17732	1.2055	.51845
25	.52115	.22494	1.2331	.53225
30	.63618	.27559	1.2724	.55118
35	.75997	.33047	1.3250	.57615
40	.89585	.39113	1.3937	.60849
45	1.0482	.45967	1.4824	.65007
50	1.2235	.53910	1.5972	.70375
55	1.4309	.63390	1.7468	.77385
60	1.6849	.75114	1.9456	.86736

Table XX. Summary of Empirical Constants for Equation 16a

Parameter	Crystal plane	
	111	200
D	1.1755×10^{-3} min.	$.50268 \times 10^{-3}$ min.
H	1.9898×10^{-9} min.	3.3083×10^{-9} min.
k	2.907	2.816

Table VI. Results of approximation for K^0

Diffuse [illegible] (minutes)	111 plane (minutes) x 10^3	200 plane (minutes) x 10^3
5	1.1755	.60215
10	1.179	.60486
15	1.190	.60976
20	1.204	.61796
25	1.237	.63167
30	1.270	.65048
35	1.315	.67042
40	1.359	.69005
45	1.405	.70202
50	1.596	.70401
55	1.701	.70599
60	1.801	.69910

CONSTRUCTION OF A NEUTRON SPECTROMETER AND DETERMINATION OF BEAMPORT SPECTRA OF THE KANSAS STATE UNIVERSITY TRIGA MARK II NUCLEAR REACTOR

by

JAMES WARREN ROWLAND, JR.

B.S., Kansas State University, 1964

AN ABSTRACT OF
A MASTER'S THESIS

submitted in partial fulfillment of the

requirements for the degree

MASTER OF SCIENCE

Department of Nuclear Engineering

KANSAS STATE UNIVERSITY
Manhattan, Kansas

1967

ABSTRACT

A neutron spectrometer and the associated collimator have been constructed by the author. This equipment has been used to study the neutron leakage spectra from the different types of beamports in the KSUTRII reactor. The effects upon these spectra of changing the fuel loading pattern have also been studied. It is shown that for certain types of experiments, proper selection of the beamport and fuel loading is important in obtaining the maximum possible signal to noise ratio.

Measurements have also been made of the total neutron cross section for metallic beryllium between the energies of .0057 and .046 eV. Higher order diffractions cause the results to be in error by as much as 300% below the break at .0063 eV. Above .015 eV, the results are generally within 20% of the published values. The break in the cross section at .021 eV is very sharp, indicating a resolution of .006 eV at this energy.

It has been demonstrated that this neutron spectrometer may be operated safely provided that the instructions in section 3.4 are closely followed. In this connection, the author's total maximum film badge reading during any calender quarter was 190 mrem.